UNIVERSITY OF BIRMINGHAM

AUTOMOTIVE RADAR TARGET DETECTION USING AMBIGUITY FUNCTION

BY

MAHVISH NAZIR

A thesis submitted to
the University of Birmingham
for the degree of
DOCTOR OF PHILOSOPHY

Department of Electronic, Electrical and Systems Engineering
School of Engineering
College of Engineering and Physical Sciences
University of Birmingham
March 2016

Abstract

The risk of collision increases, as the number of cars on the road increases. Automotive radar is an important way to improve road traffic safety and provide driver assistance. Adaptive cruise control, parking aid, pre-crash warning etc. are some of the applications of automotive radar which are already in use in many luxury cars today.

In automotive radar a commonly used modulation waveform is the linear frequency modulated continuous waveform (FMCW); the return signal contains the range and velocity information about the target related through the beat frequency equation. Existing techniques retrieve target information by applying a threshold to the Fourier power spectrum of the returned signal, to eliminate weak responses. This method has a risk of missing a target in a multi-target situation if its response falls below the threshold. It is also common to use multiple wide angle radar sensors to cover a wider angle of observation. This results in detecting a large number of targets. The ranges and velocities of targets in automotive applications create ambiguity which is heightened by the large number of responses received from wide angle set of sensors.

This thesis reports a novel strategy to resolve the range-velocity ambiguity in the interpretation of FMCW radar returns that is suitable for use in automotive radar. The radar ambiguity function is used in a novel way with the beat frequency equation relating range and velocity to interpret radar responses. This strategy avoids applying a threshold to the amplitude of the Fourier spectrum of the radar return.

This novel radar interpretation strategy is assessed by a simulation which demonstrates that targets can be detected and their range and velocity estimated without ambiguity

using the combined information from the radar returns and existing radar ambiguity function.

Dedicated to Haaziq and Hashim

Acknowledgements

I would like to express my immense and sincerest gratitude to my supervisor; Mr. David Pycock for without his continuous support and careful guidance, this thesis would not have been possible. His vast knowledge has enabled me to develop a thorough understanding in the subject matter. His kindness and strong motivation, on the other hand, have helped me to overcome multiple obstacles and low periods during the whole research process until completion. The whole experience has taught me to have patience and keep moving forward.

I would also like to thank my internal assessor, Professor Mike Cherniakov who gave me valuable suggestions regarding my research work whenever I had the chance to present my work to him.

I owe my deepest appreciation to my loving and caring family especially my parents who always believed in me and encouraged me throughout the journey of my PhD. Without their support this thesis would not have been a success. A special thank you reaches to my husband who has always pushed me to achieve greater heights in academics. The presence of my two little boys has always helped me come out of the blues.

I am indebted to my wonderful colleagues and friends who have tremendously instilled my confidence and uplifted the positive vibes.

Last but not least, my heartfelt gratitude goes to our school postgraduate secretary Mrs. Mary Winkles for she has always been so helpful with all the admin work.

Table of Contents

List of Figures

List of Tables

List of Abbreviations

ACC	Adaptive cruise control
ADC	Analog-digital converter
AF	Ambiguity function
AR	Auto regressive
CFAR	Constant false alarm rate
CPI	Coherent processing interval
CW	Continuous waveform
DMFT	Discrete match Fourier transform
FFT	Fast Fourier Transform
FMCW	Frequency modulated continuous wave
FSCW	Frequency shift continuous wave
FSK	Frequency shift keying
LFM	Linear frequency modulated
LFM-CW	Linear frequency modulated continuous wave
LPF	Low pass filter
MTD	Moving target detection

OS	Ordered statistics
PAP	Position ambiguity plot
PPI	Plan position indicator
PRI	Pulse repetition interval
PRF	Pulse repetition frequency
RF	Radio frequency
R-V	Range-Velocity
SF	Stepped frequency
TFA	Time frequency analysis
TPS-LFM	Transformable periods and symmetrical – Linear frequency modulation
VAP	Velocity ambiguity plot

Chapter 1

1 Introduction

1.1 Introduction to automotive radars

Vehicle safety is a key research area for a large number of automobile manufacturers seeking to differentiate their products with additional safety features and seeking to meet new or expected regulations regarding pedestrian safety. The need for improved driver assistance to avoid accidents increases as the number of vehicles on the road increases. Some modern vehicles have Adaptive Cruise Control (ACC) systems, which can actuate the brakes of a vehicle to control its distance behind another vehicle. Commonly, radar or laser systems are used to measure the distance of a vehicle behind another and to keep pace with the car that is followed. Some systems also feature forward collision warning to alert the driver if the vehicle is less than the braking distance from the car in front. In an urban environment, common, additional hazards include cars cutting in from adjacent lanes, pedestrians crossing the roads and cyclists weaving through traffic. Automating warnings for the hazards that arise in urban driving has the potential to substantially reduce accident rates.

Radar can precisely measure the distance and velocity of remote objects. With the use of multiple sensors angular information can also be retrieved. Radar is not affected by environmental influences such as extreme temperatures, weather conditions or variation in lighting. Therefore, radar is commonly identified as the most appropriate technology for assisting with collision warning, parking and urban stop & go driving [1], [2].

Moreover, radar can readily be combined with other sensing technologies to improve system accuracy, reliability and adaptability [3].

1.2 Automotive radar applications

Whilst automotive radar is a relatively common feature of many luxury motor vehicles sold in Europe and the United States of America (USA) research continues to further develop automotive radar to improve precision and avoid ambiguity. There is a high demand on sensor specification and signal processing to resolve the targets accurately at close ranges for new safety applications. An overview of the automotive radar applications are given in [4]. The important applications of automotive radar, as described below, are adaptive cruise control, pre-crash warning, blind spot detection, collision avoidance and as a parking aid.

1.2.1 Adaptive cruise control

A vehicle is kept at a constant, preselected speed in a standard cruise control system. An adaptive cruise control (ACC) system offers extended functionality as compared to the standard, fixed speed, cruise control system to automatically maintain a safe distance behind vehicles moving at a lower speed. When the path is clear the ACC increases the speed of the vehicle to reach its preselected maximum.

Although some ACC systems alert the driver of a potential collision with the car ahead, it is more of a comfort system allowing the driver to select a speed for relaxed driving. An extended functionality called ‘stop & go’ is used when the traffic ahead comes to a halt.

1.2.2 Pre-crash warning

Air bags and seat-belt tensioners have proved to be effective lifesaving safety systems. However, they require some time before they reach their maximum effectiveness. Pre-crash systems are being investigated to detect impacts earlier than the conventional mechanical systems and alert the driver of a potential crash. As part of the collision avoidance system some advanced vehicles can take evasive measures to prevent the collision from happening or reduce the impact of the collision.

1.2.3 Blind spot detection

This application of automotive radar is used before turning or changing lanes when there is a danger that other road users approaching in a neighbouring lane could be overlooked. This driver assistance technology senses cars coming up in drivers' blind spot behind or alongside his vehicle and alerts the driver not to change lanes.

1.2.4 Collision avoidance

This automobile safety system is designed to reduce the severity of a collision. For such systems, the likely collision has to be detected early enough to initiate countermeasures. This could include automatic braking or steering to minimise the effect of the potential crash. While pre-crash warning and blind spot detection aim at very specific situations, collision avoidance requires a detailed prediction of the traffic scene. Moreover, it requires a high target detection rate and very low false alarm rate. This requirement is a challenge in the system design.

1.2.5 Parking aid

This application of automotive radar uses very short range radar sensors for road vehicles designed to alert the driver to obstacles while parking. Many modern cars equipped with parking sensors are already in the market. Sonar is also commonly used as a parking aid and is often preferred as it is much cheaper.

Figure 1.1 illustrates various automotive radar applications.

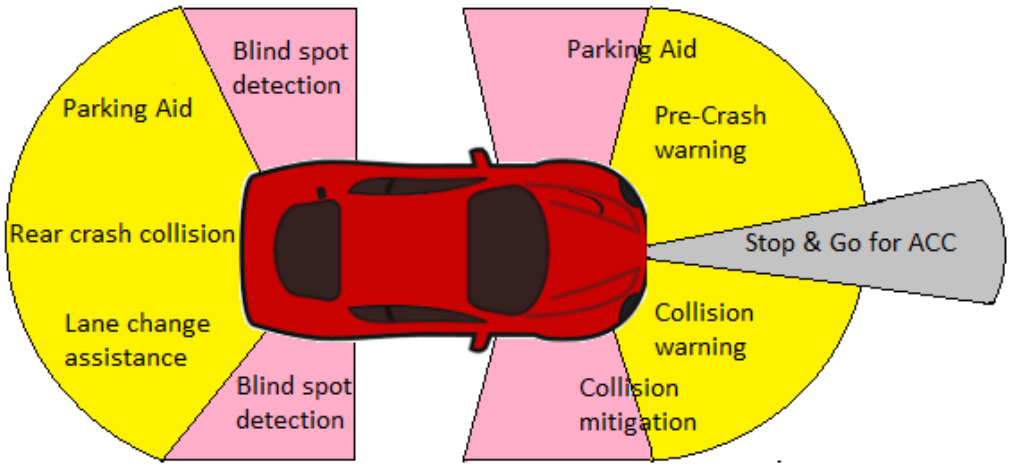

Figure 1.1: Automotive radar applications.

1.3 Research in various areas of applications

The general concept of a radar sensor used in car applications was described in [5]. For ACC applications, a single 77-GHz far-distance radar sensor with a range of 200 m and a narrow azimuth angle of 15°, is commonly used. With such systems all targets within the observation area will be detected [6]. Additional ultrasonic sensors with a maximum range of 2 m are used for parking aid applications which have limited potential to extend their functionality to other applications like stop & go. For this reason 24 GHz radar systems which have good performance in range and azimuth angle measurement

are used in some automotive applications such as parking aids [7], blind spot detection and pre-crash detection [8]. A detailed technical description of 24 GHz radar sensors is given in [9].

In the urban context, applications to assist with Stop & Go, blind spot detection and more complex crash prevention a range of at least 50 m is needed. Such systems also require a wide azimuth angle to detect significant targets in adjacent lanes. A network of sensors can be used to cover a wide area and the possibility of use of multilateration technique [10].

For current research into automotive applications like pedestrian safety systems, collision avoidance and lane-changing assistance, more detailed information of the target type is needed. In [11] a target classification technique based on the range profile measured by near distance radar was presented. It was shown that the classification system was able to successfully distinguish between the radar echo signals originating from different object classes.

A very important parameter to be estimated in collision warning radar is acceleration. A method to estimate target acceleration along with range and velocity was given by [12].

In order to improve driver assistance systems, in addition to the radial target velocity, a technique to estimate the lateral velocity of the target inside the observation area was presented by [13]. The angular dependency of the radial velocity components form the basis of the method presented. The measurements were performed using a monopulse radar sensor. The accuracy of the estimated lateral velocity was improved by the fusion of multiple radar sensors [14].

1.4 Aim and objective of this thesis

Frequency Modulated Continuous Wave (FMCW) radars are popular in military and automotive applications because they readily accommodate complex scenarios and are reliable. Radar sensors for automotive applications require high accuracy and good target resolution. A considerable challenge here is the simultaneous measurement of range, azimuth angle and velocity, which is especially demanding when multiple targets are present. Traditionally a threshold is applied to the power spectrum to eliminate weaker responses. Application of the threshold is not an ideal solution. It has the risk of eliminating responses from close critical targets with low radar cross-section which result in low power spectrum. This thesis investigates a novel strategy to simulate a network of FMCW radar systems and use the knowledge of ambiguity functions to progressively eliminate false responses and select valid responses.

1.5 Thesis outline

This thesis comprises of five chapters. The outline of each chapter is as follows.

Chapter 1 is an introduction to automotive radar. It explains briefly the aim of automotive radar and various particular applications in more detail. The recent and current research in automotive applications that is taking place is introduced.

Chapter 2 contains an explanation of radar operation, the behaviour of radar, various frequencies and the nature of common radar waveforms used. A more detailed description of the radar ambiguity function for alternative waveforms is given and the benefit of multistatic radar explained. There is a review of recent research in automotive radar and the limitation of key methods is described.

Chapter 3 presents a novel strategy to detect targets in an automotive application of radar. It explains the various steps used in the novel strategy of using ambiguity function of radar in two stages. Initially the velocity of the target is assumed to be known and constant. This allows simplifying computation and be more focussed in finding the range to the target. In the second stage of computation the velocity is allowed to change and allows estimating target range and velocity.

Chapter 4 presents the results obtained during each step of processing using this novel strategy. The results obtained are from simulation only. Sources of error in the position and velocity of targets is identified.

Chapter 5 provides a conclusion and identifies the further research that is required.

Chapter 2

2 Target Detection Theory

2.1 Introduction

In a radar system an electromagnetic wave is transmitted and the reflected signal is analysed to identify the presence and character of that object. Radar can be used to detect the position and velocity of targets with a high accuracy that depends on the frequency and other properties of the transmitted signal. The radar principle has been applied to a wide range of frequencies ranging from few megahertz to the ultraviolet. The method of implementation varies within this wide frequency range but, in each case, the basic principles remain the same.

The form of the electromagnetic signal radiated by a radar system and the processing performed on the reflected signal determines what can be measured about the target object. For instance, pulse radar for aircraft surveillance will generate a repetitive train of short pulses. The shorter the pulse, greater is the spectral bandwidth and better is the range resolution. Whereas, to accurately determine the velocity of a moving target, through the Doppler frequency shift introduced in the reflected signal, the signal waveform must be of long duration, as in continuous wave Doppler radar. These and other signal waveforms are discussed in this chapter.

Target range is the fundamental quantity measured by most radars. It is estimated by the delay from the transmitted to the received signal. The radar equation in terms of power, P_r returning to the receiving antenna is given by:

$$P_r = \frac{P_t G_t}{4\pi R^2} \times \frac{\sigma}{4\pi R^2} \times A_r \quad (2.1)$$

The right hand side is a product of three factors, which, from left to right are:

(i) The reflected power density at a distance of R metres from radar that radiates a power of P_t watts from an antenna of gain G_t. The denominator accounts for the divergence of electromagnetic radiation with range in the transmitting path. (ii) The numerator of the second factor is the target cross section σ in square metres. The denominator is the same as in the first term but accounts for the divergence of the return path. The product of the first two terms represents the power per square metre returned to the radar. (iii) An antenna with an effective aperture area A_r intercepts a portion of the net radiated power [15].

2.2 Information available from the radar echo

A radar system is capable of providing more information about the target than is implied by the acronym, *ra*dio *d*etection *a*nd *r*anging. The first radar systems were designed to detect a target and determine its range, hence the acronym. The key parameters that a radar system is capable of estimating are stated below:

Range: The most important and distinguishing characteristic of the radar is its ability to determine range. Range is estimated from the time taken for the radar signal to travel from the transmitter to the target and back to the receiver.

The conventional radar waveform for measuring range is a short pulse. The shorter the pulse, the better is the range resolution. However, very short pulses with high energy are not easy to generate as they require high peak power and high bandwidth. To overcome

this limitation of high peak power in a short pulse, a pulse compression waveform is used which is discussed later in this chapter.

Radial velocity: There are two ways to determine target velocity. Successive measurements of range give the rate of change of range with time and hence radial velocity. However, this method takes comparatively a longer time to estimate radial velocity and provides discrete estimates of velocity and not a continuous measurement. Another way to measure radial velocity is to use the Doppler shift. The Doppler frequency shift produced by a moving target provides a measure of the radial velocity in a shorter time as compared to successively measure range to estimate velocity. It can also be used to differentiate moving targets from stationary clutter.

Angular direction: The direction in which the antenna points when the received signal is of maximum strength indicates the direction to the target. The orientation of the target from the radar can also be estimated using range information from multiple radar sensors and performing lateration technique, which is discussed in Section 2.7.

Target size: The magnitude of the radar return depends on the range to the target, the size and radar cross-section of the target. Target size can be determined if the range and radar cross-section of the target can be assumed to be constant. However, the relation is not so simple and a good estimate of size cannot be obtained from a single echo return. The radar cross-section depends on the shape of the target and the material that it is constructed from.

Shape: Measuring the scattered field in all directions can be used to determine the shape of a target. It is seldom practical to measure the scattered field in all directions.

However, the scattered field can be measured over a finite region. The larger the region over which the scattered field is measured, the truer will be the shape determination.

2.3 Radar frequencies

Commonly radars have been operated at frequencies extending from about 220 MHz to 35 GHz, but these are not the limits. Radar can be operated at frequencies below and above this range as discussed below. The basic principle of operation remains the same for different frequencies but the implementation differs widely. The choice of a suitable operating frequency depends on the application, as described below [15].

Lower than HF (below 3MHz): Radar signals at these frequencies are sometimes called ground waves as they follow the curvature of the earth. A significant portion of the radiated energy can be propagated beyond the radar horizon through diffraction. However, large antennas are required to direct the beam; the RF noise level is high due to clutter from the ground and other signals such as radio transmission. This frequency band is not suitable for most radar applications because of these factors.

HF (3 to 30 MHz): The reflection of the sky wave from the ionosphere can result in unwanted echoes which can be a problem. The upper portion of this frequency band has been used for radar astronomy after receiving echoes from sun's ionized atmosphere. Again this band is not suitable for most radar applications.

VHF (30 to 300MHz): Because of the present crowded spectrum at VHF, modern radars are not extensively found in this band. It is however, the most economical band in which to build large radars.

UHF (300 to 1,000 MHz): It is easier to construct narrow antenna beams at this frequency making it suitable for reliable, long range surveillance radar.

L band (1 to 2 GHz): This is a popular frequency band in the United States for aircraft surveillance radar. It is typically used in long-range surveillance, enroute traffic control.

S band (2 to 4 GHz): Most radar applications in the S band and at higher frequencies are used for precise target location and tracking. Good angular resolution is possible because relatively narrow beams can be constructed and the RF noise level is also low. The S band is of interest for medium range aircraft detection and tracking. It is also used in moderate-range surveillance, terminal traffic control and long-range weather monitoring.

C band (4 to 8 GHz): This band has been successfully used for intermediate range surveillance applications as in ship navigation radar where precise information is necessary. It is also commonly used in satellite communication systems, air traffic control and airborne altimetry.

X band (8 to 12.5 GHz): This is a popular frequency band for military weapons control and for short-range tracking, missile guidance, mapping, marine radar, airborne intercept. At X-band the radar can be small enough for mobile applications.

K_u, K, and K_a bands (12.5 to 40 GHz): The K band was originally adopted during World War II and was centred at 24 GHz, which soon proved not to be a good choice as it was too close to the water- absorption frequency of 22.2 GHz. Later it was divided into sub bands on either side of the water absorption frequency. The lower frequency band, K_u, extends from 12.5 GHz to 18 GHz and the upper frequency band, K_a, extends

from 26.5 to 40 GHz. The K-band frequencies offer a good resolution in both range and angle. Whilst high power output is difficult to achieve at this frequency, small size antennas are readily achieved. However, there is an increased atmospheric attenuation in this frequency band.

V band (40 to 75 GHz): The V band is not commonly used, except in millimetre wave radar research and other kinds of scientific research. In the United States, the Federal Communications Commission allocated the frequency band from 57 to 64 GHz for unlicensed wireless systems.

W band (75 to 110 GHz): The W band is used for satellite communications, military radar applications, and some non-military applications.

For concealed weapons detection many millimetre-wave cameras operate at 94 GHz. Automotive cruise control radar uses a frequency around 77 GHz.

Each frequency region has its own particular characteristics that make it better for certain applications than other frequencies. Predominantly two different frequency bands have been used for automotive applications: the 24 GHz and 77 GHz band. The 77 GHz band offers the benefit of higher performance with small antenna for a given beam width requirement. This enables a good angular resolution for a small sensor size compared to 24 GHz where sensors must be about three times larger to achieve the same performance [16]. Moreover, the combinations of high transmit power and high bandwidth is not allowed at 24 GHz but is permitted at 77 GHz which allows for long range operation and high spatial resolution at the same time. 77 GHz short range sensors with high spatial resolution having a bandwidth of up to 4 GHz will be introduced in the

near future [16]. This accounts for a relative bandwidth of only 5% at 77 GHz compared to nearly 17% at 24 GHz. This makes the design of antenna and wavelength dependent components much easier at 77 GHz than at 24 GHz.

Selecting a frequency of operation for radar sensors is determined by both technical requirements and regulatory factors, which vary between countries. For the operation of automotive radar sensors in millimetre-waves, two frequency bands have been defined. One is 76-77 GHz which is available nearly worldwide. Another is the neighbouring band from 77-81 GHz which has been introduced in Europe to replace automotive radar sensors in the 24 GHz band. It provides a larger bandwidth of 4 GHz at reduced transmit power as compared to 76-77 GHz band. The status of the frequency regulation for short and long range radar is summarized in [17] based on its importance for car manufacturers and their sensor suppliers.

Automotive radar systems in the 77 GHz domain have been used in the automotive industry for security and driver comfort systems. These radar systems commonly have a maximum range of 150 metres [6]. An optimized signal processing architecture for one such radar sensor network is described by [18].

2.4 Radar waveform Design

The signal modulation is commonly described as a ‘waveform’ and its design is a key factor in determining the performance and application of a radar system [19]. Range resolution is an important parameter in many radar systems and is determined, in part, by the nature of the waveform. It needs to be high enough to distinguish targets from clutter. Doppler resolution enables stationary clutter to be distinguished from moving

targets and even higher Doppler resolution allows multiple targets to be distinguished from one another. Radar imaging depends on both high range and Doppler resolutions. The range and Doppler resolution for a specific radar waveform is given by the ambiguity function and its resulting ambiguity diagram [20]. For a given specific application, a radar waveform must be able to produce a radar signal that:

1. Provides sufficient energy to detect targets and estimate their parameters;
2. Can accurately resolve targets;
3. Can reject unwanted echoes.

Two fundamental waveforms are the pulse and the continuous waveform (CW) which can be modulated to produce a variety of more sophisticated waveforms suitable for a range of applications. The research presented here is focussed on automotive applications of radar. Commonly used radar waveforms, some of which are relevant to automotive radar are discussed below.

2.4.1 Pulse Radar

In this method when a short pulse is transmitted the receiver listens for a backscattered echo for a fixed time after the end of the transmission pulse. When multiple targets at different distances are present, multiple echoes are received. The distance to the target or *range* is calculated from the time delay between the transmission of the pulse and the radar return, Eq. (2.2) [21]. Successive measurement of range over a period of time gives rate of change of target range and hence target velocity.

$$R = {}^{c\tau}/_{2} \tag{2.2}$$

Where, R is the range to the target, τ is the time delay between the transmission of the pulse and radar return and c is the velocity of light.

Target radial velocity can be extracted from the range rate which is given by Eq. (2.3) [22].

$$\dot{R} = {}^{\Delta R}/_{\Delta t} \tag{2.3}$$

Where, ΔR is the change in range and Δt is the change in time. Figure 2.1 shows the pulse radar operation.

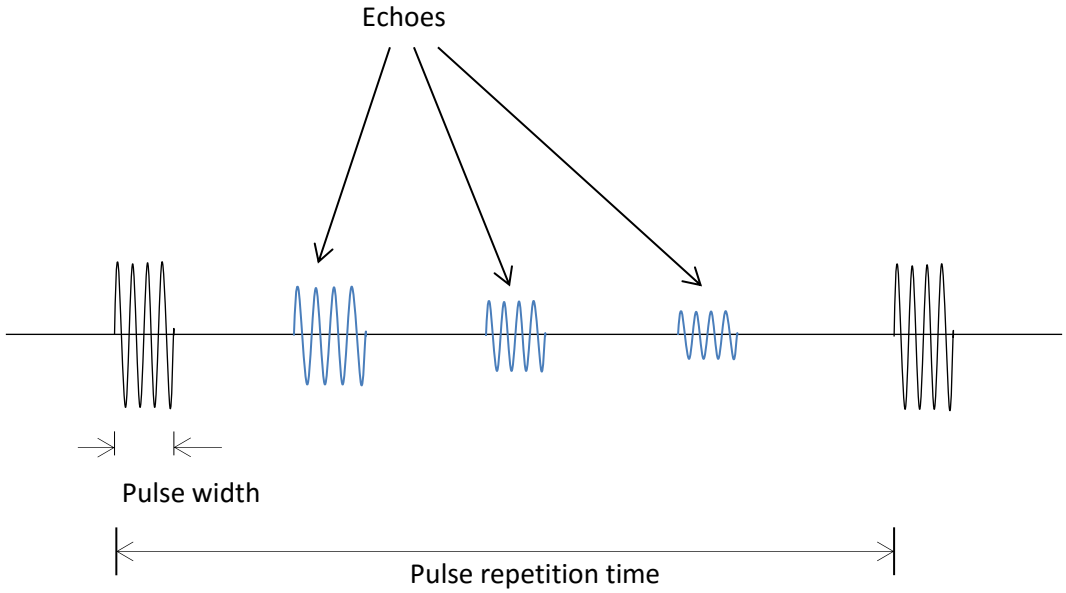

Figure 2.1: Radar pulse and return echo.

The pulse width needs to be sufficiently long that the scattered signal can be detected by the radar receiver. The energy of the transmitted pulse determines the maximum target range that can be detected and the width of the pulse determines the range resolution available to distinguish adjacent targets. The width of the transmitted pulse also determines the dead zone, at close ranges, when the receiver is blanked and the returned signal cannot be detected. The receiver input is blanked to avoid the amplifiers being saturated or damaged by the transmission pulse. The selection of the pulse width is a compromise between these various factors.

The pulse repetition frequency (PRF) can be set in accordance to the role of the system. A high PRF is used to build up a distinguishable echo by accumulating responses. However, a high PRF reduces the time for the echo to be received and thereby the maximum range that can be detected [23].

2.4.2 Continuous wave Radar

With continuous wave (CW) radar a continuous fixed frequency signal is transmitted and received with the reflections from multiple targets being superimposed. If the target is in motion, the received signal will be shifted in frequency in accordance to the Doppler effect. This shift in the frequency can be used to estimate the velocity of the target. This type of radar is unable to estimate target range because it operates continuously at a single frequency and is unable to measure the time delay between transmitted and received signal. A modulation of the carrier wave in amplitude, frequency or phase is designed so that the time for the return of the radar signal and the Doppler frequency shift can both be estimated. This will allow the measurement of range in CW radars. Common forms of modulation are described in the following sections.

2.4.2.1 Frequency modulated continuous wave radar

Frequency modulated continuous wave (FMCW) radar has a long history [24]. A relatively recent and a very good description of the FMCW radar is given in [25]. In this scheme a continuous carrier, modulated by a periodic function such as a sinusoid or sawtooth wave, is transmitted and the received echo analysed to provide range data [26]. The ‘modulation’ adds the range estimation capability to CW radar.

Frequency modulation can also overcome the short comings of pulse radar where short pulses with high peak power are required to yield good range accuracy and resolution. But short duration pulses result in poor Doppler resolution [21]. Frequency modulation uses long pulses and moderate peak power levels to obtain good Doppler and range resolution.

A linear frequency modulated (LFM) waveform is the simplest form of frequency modulation where the frequency is repeatedly swept linearly between frequencies f_1 and f_2, as shown in Figure 2.2. Each frequency sweep is commonly known as a chirp because of the sound made by a signal of this type at audio frequencies. For a stationary target the range is found from the difference in frequency between the transmitted and the received signal. If the target is moving, a velocity dependent Doppler frequency shift is superimposed on the range frequency shift [27].

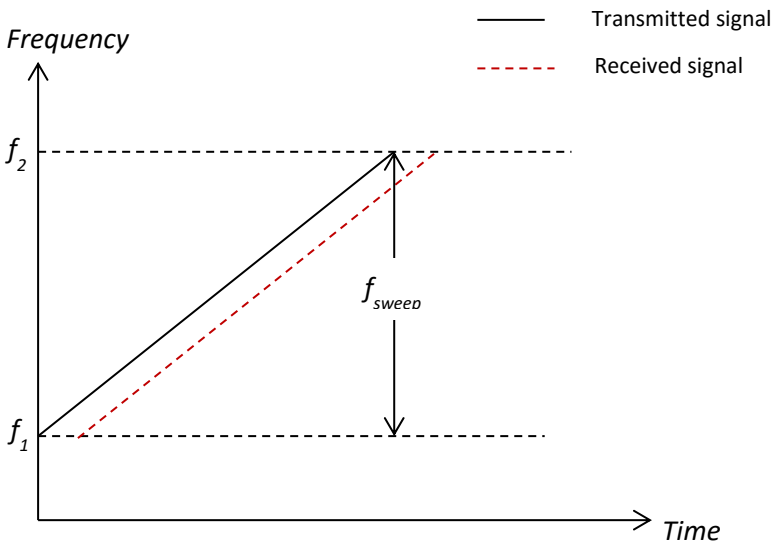

Figure 2.2: Linear Frequency modulated continuous wave.

In the presence of multiple targets, with an LFM waveform the detected range and velocity of the targets is ambiguous giving rise to ghost target positions. A simple way to address this issue in part, is to use multiple chirp signals with different slopes.

LFM waveform can take various forms. The most commonly used waveforms are the sawtooth and triangular patterns of modulation [23]. In a sawtooth arrangement the frequency of the transmitted wave is ramped linearly between two frequencies. The transmitted waveform has fixed amplitude but a linear sawtooth variation with time. The waveform is transmitted only as a single slope. In a triangular waveform there are two frequency slew rates or slopes. The triangular waveform with an equal up-slope and down-slope linear sweeps is a common choice because a sawtooth with a rapid switch back is difficult to achieve. The up and down slope that have the same gradient offers scope to disambiguate responses. Using a variation in slope is more effective as discussed in Section 2.5.1.

2.4.2.2 Frequency shift keying continuous waveform

Two discrete frequencies f_A and f_B are used in the transmit signal in a pure frequency shift keying (FSK) modulation [28]. Each frequency is transmitted within a coherent processing interval (CPI) of length T_{CPI}, as shown in Figure 2.3. The echo signal is down converted to the base band using a homodyne receiver, and then sampled. The frequency step $f_{step} = f_B - f_A$ is chosen to accommodate the maximum unambiguous target range required. Switching from f_A to f_B, the signal wavelength is changed, so the phase of the received signal is shifted from φ_A to φ_B. The phase shift $\Delta\varphi = \varphi_B - \varphi_A$ in the receiver depends on the difference between the two frequencies f_A and f_B and the

target range parameter R, as described in Eq. (2.4). The phase difference is used to estimate target range.

$$R = -\frac{c.\Delta\varphi}{4\pi.f_{step}} \tag{2.4}$$

Since the echo signal frequency only depends on the target velocity, the FSK radar can only resolve targets by velocity and not by range. When a target can be resolved its range can be estimated by the phase shift between the two spectra. The main disadvantage of the FSK technique is that it does not resolve two or more targets with the same radial velocity in the range direction. In an automotive application where multiple fixed targets are more likely to occur, range resolution cannot be provided by the FSK waveform [29].

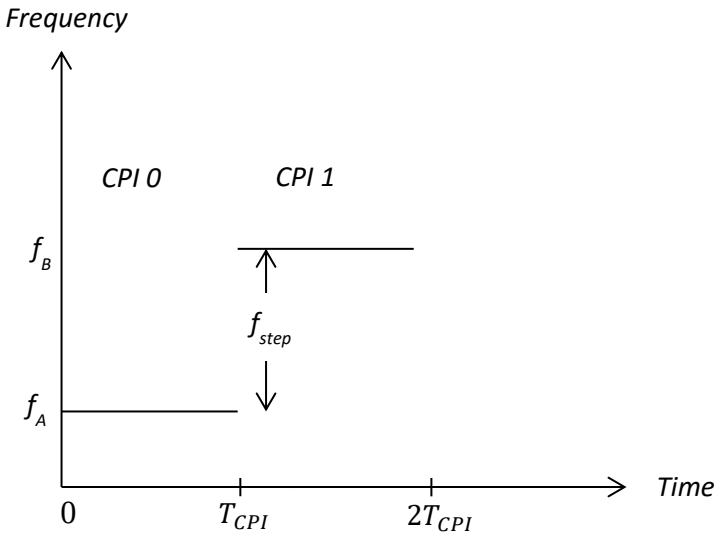

Figure 2.3: Frequency shift keying modulated continuous wave.

2.4.2.3 Combined LFM and FSK waveform

A combination between an FSK and LFM waveform design principles offers the possibility of unambiguous target range and radial velocity measurement

simultaneously [30]. In this technique the transmitted waveform consists of two linear frequency-modulated up-chirp signals A and B, transmitted in an intertwined sequence (ABABAB…), as shown in Figure 2.4. The two chirp signals have identical slope and bandwidth. Signal A is used as a reference and signal B is shifted in frequency $by\ f_{shift}$ [31]. The received signal is down converted into baseband and directly sampled at the end of each frequency step. A Fourier transform is performed on each sequence A and B. A single target with a specific range and velocity will be detected by each sequence. In each signal sequence A or B ambiguity in range and velocity will arise. This ambiguity can be resolved by combining the frequency and phase change from different sequences. The intersection point of these measurements in a range-velocity plot, as shown in Figure 2.5, allows the range and velocity of two targets to be computed [32]. This waveform is not processed by a classical matched filter procedure or analysed by an ambiguity function. It is processed in a non-matched filter form [33].

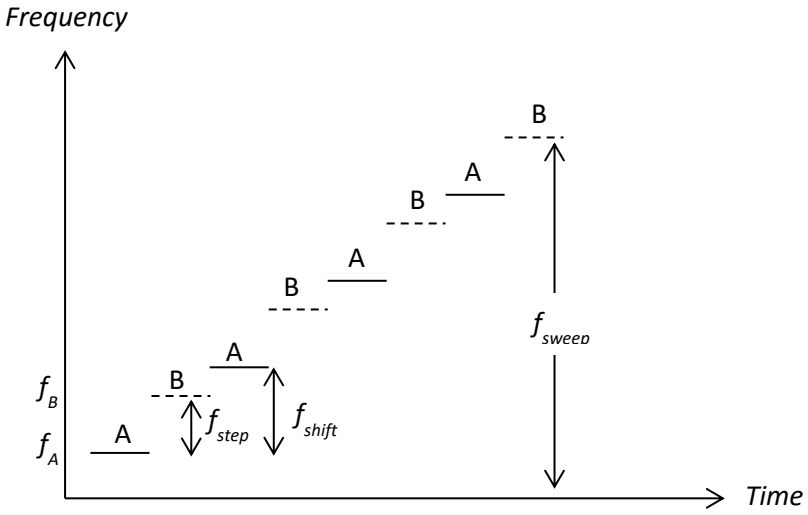

Figure 2.4: Combined LFM and FSK modulated wave.

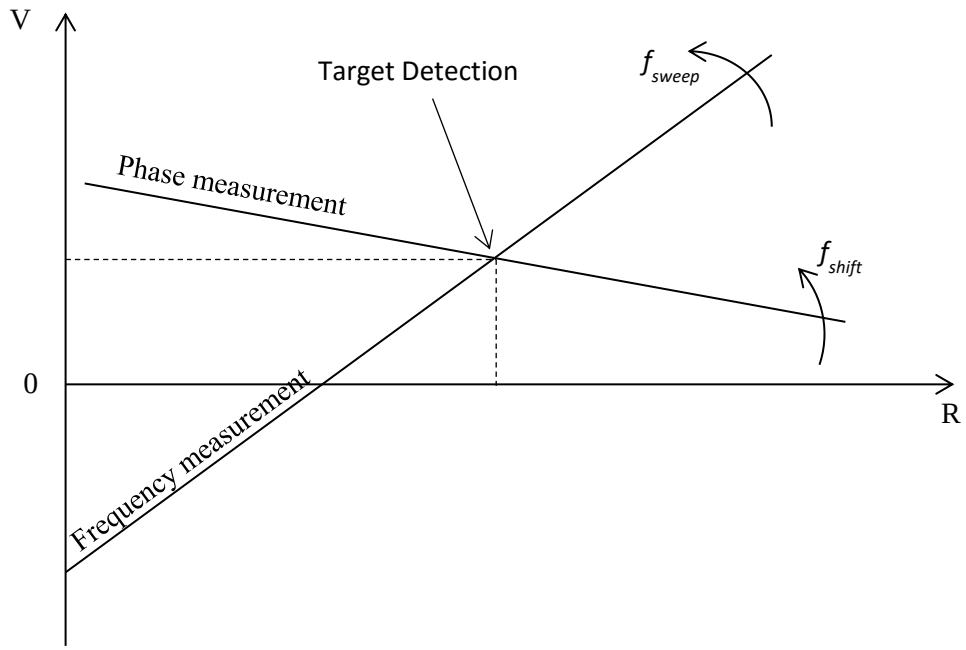

Figure 2.5: Graphical resolution principle of ambiguous frequency and phase measurements.

2.4.2.4 Stepped frequency CW waveform

When using a modulation to achieve high range resolution it is difficult to ensure that the acquired data can be received at the rate (or bandwidth) required. Stepped frequency (SF) waveform is a technique which addresses this problem by shifting the frequency from step-to-step [34]. The theory and practice of stepped frequency continuous radar units for target ranging and motion detection is explained in [35]. The frequency of each step is shifted from that of the previous step by a small amount, Δf as shown in Figure 2.6. For each transmitted step, the received echo corresponding to a particular range is coherently detected and its phase and amplitude stored. The phase of the received signals for transmit frequency f_1 and f_2, respectively, is given by the Eq. (2.5) and Eq.

(2.6).

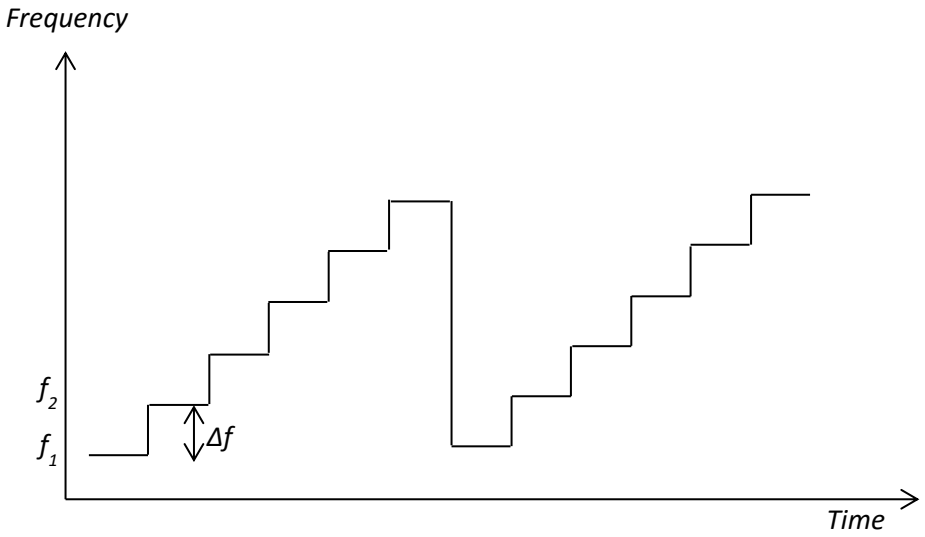

Figure 2.6: Stepped frequency continuous waveform

$$\varphi_1 = \frac{4\pi f_1 R}{c} \tag{2.5}$$

$$\varphi_2 = \frac{4\pi f_2 R}{c} \tag{2.6}$$

For equally spaced steps in frequency, a predictable step-to-step phase shift of $\Delta\varphi$ that is a function of the frequency difference $\Delta f = f_2 - f_1$ is given by the following equation:

$$\Delta\varphi = \frac{4\pi R \Delta f}{c} \tag{2.7}$$

This step-to-step shift appears as an apparent Doppler frequency, which is a function of target range. If multiple targets exist in the same range bin then each will produce a unique frequency that can be extracted from the FFT spectrum.

The authors of [36] described a stepped frequency modulated radar for vehicular collision avoidance which does not require wide-band signal processing as compared with conventional high resolution radars.

The problem with using a stepped frequency is the need to maintain the stability of the transmitter and local oscillators for the whole period for which the measurements are being made. A further problem in automotive applications is that when the target is a moving vehicle, there is a Doppler coupling in which the apparent range of each target is modified by the Doppler shift. Moreover, the time taken to process SF waveform results in Doppler smearing [37] wherein the target changes range bin by the time SF waveform has been transmitted.

2.4.2.5 Combined LFM and stepped frequency CW waveform

This waveform can be regarded as another variation of the combined LFM and FSK waveform. It is a combination of the stepped frequency continuous wave waveform (SF-CW) and the LFM-CW waveform. In this Chirp-SF-CW waveform the transmitted signal is a stepped frequency modulated signal. It consists of two linear frequency modulated up-chirps which are again transmitted in an intertwined sequence [38], as shown in Figure 2.7.

Using the Fourier transform each signal sequence A or B is separately processed. Targets are detected at peaks in the Fourier spectrum. The frequency of each spectral peak depends on the range and velocity of each target. The frequency measurements and signal phase information are used to calculate target range and velocity.

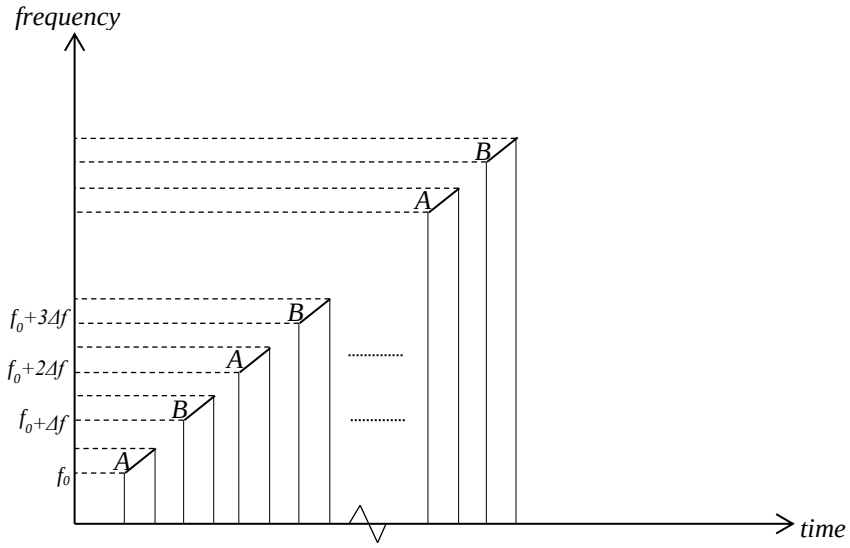

Figure 2.7: Chirp-SF radar waveform in the frequency domain.

2.4.2.6 Other waveforms

A coded step-form of frequency modulation of the transmitted signal for automotive radar was described by [39]. This waveform has four segments, an upchirp segment ‘A’, a downchirp segment ‘B’, a constant frequency modulation segment ‘C’ and finally a signal ‘D’ with a fixed number of bursts which are frequency-coded. The target detection and parameter estimation for the objects within the observation area was performed using the information received from the first three segments, ‘A-C’. The last signal segment ‘D’ was used only for target validation. The transmitted frequency does not change continuously but in discrete steps of short constant-frequency bursts. This allows simple digital generation of the modulation signal and since the reflected signal is mixed with constant transmitted signal, it can be sampled at steady-state phase at the end of each burst. The number of ghost targets detected increases with the number of

targets in the observation area making this waveform not suitable for multi-target scenarios.

In [40] a frequency stepped continuous wave-principle (FSCW) with two interleaved ramps was presented. The FFT for each ramp was calculated and the peaks from a single target appear at the same position. The target range and velocity were calculated using the information from the peak position and the phase difference between peaks. The peaks of two targets with different range and velocity can occur at the same position in unfavourable conditions. This can lead to wrong or missed detections. An extension to this principle uses multiple short ramps where the start frequency is continuously incremented [41] as shown in Figure 2.8. In this waveform the number of interleaved ramps is equal to the sampling points on one ramp. The bandwidth of a single ramp provides additional resolution as compared to FSCW, thus reducing the number of wrong and missed detections. This waveform migrates to FMCW 2D-FFT principle if the frequency increment is chosen to be zero.

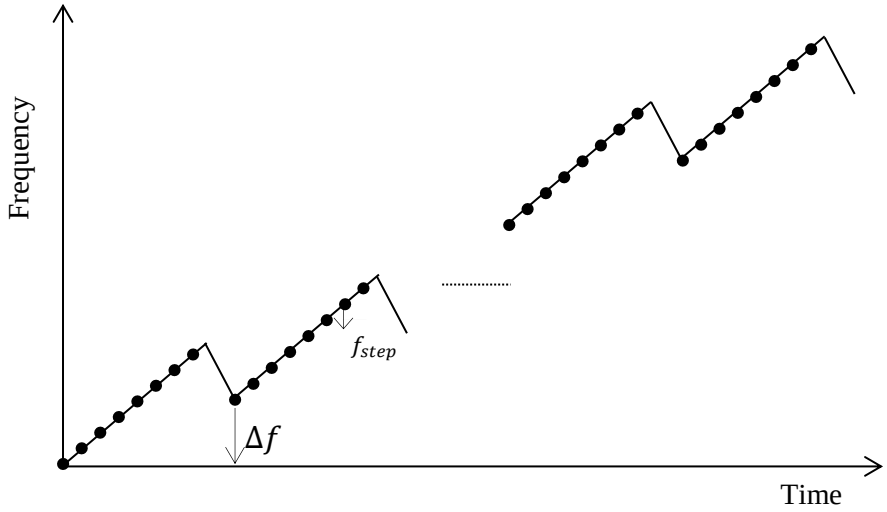

Figure 2.8: Ramp sequence.

2.4.3 Benefits of FMCW radar

Some of the waveforms that have been used, particularly in automotive radar, have been discussed. For shorter range detection, as in automotive radar, FMCW radar is commonly used [25] and [42]. FMCW radar techniques and applications are reviewed in [43]. The benefits of FMCW radar in automotive applications are: (i) The FMCW modulation is easy to generate, provides large bandwidth, a high average power, good short range performance, high accuracy, low cost due to low bandwidth processing and permits very good range resolution and allows the Doppler shift to be used to determine velocity, (ii) The FMCW radar can operate at short ranges, (iii) In addition, FMCW sensors can be made small having a single RF transmission source with an oscillator that is also used to down convert the received signal, (iv) Since the transmission is continuous, the modest output power of solid state components is sufficient. This would not be the case for pulse radar which requires a high instantaneous output power to achieve the same sensitivity and (v) The range resolution being a function of the bandwidth, it is easier to achieve a high range resolution with FMCW than with pulse radar.

Even though the FMCW principle has various benefits, there are certain issues determining its performance which are quite complex [44]. The design and implementation requires careful consideration to be effective at millimetre wavelengths.

2.5 LFM-CW radar

The FMCW waveform is the most widely used form of modulation for the reasons given in Section 2.4.3. In linear FMCW radar, the transmission frequency increases linearly with time. The echo signal from a target at a distance R will be returned at time

(propagation delay), $\tau = {}^{2R}/_{c}$. The beat frequency due to the range of the target is given in Eq. (2.8)

$$f_R = \frac{2Rf_h}{T_{chirp}c} \tag{2.8}$$

Where, R is the range to the target, f_h is the modulation frequency, T_{chirp}, is the duration of the modulation chirp and c is the velocity of light.

The Doppler frequency causes the frequency-time plot of the return signal to be shifted up or down. For a target approaching the radar, the received signal frequency is increased decreasing the up-sweep beat frequency and increasing the down-sweep beat frequency, as shown in Figure 2.9. The Doppler frequency is given in Eq. (2.9).

$$f_D = \frac{2V_r f_0}{c} \tag{2.9}$$

Where, V_r is the target radial velocity, f_0 is the carrier frequency and c is the velocity of light

Considering that the radar sensor operates at a frequency f_0, the up chirp modulation frequency $f_{hchirp1} = f_h$ and the down chirp modulation frequency $f_{hchirp2} = -f_h$. The beat frequency due to the range to a target and the Doppler shift, for both up and down chirps is given by Eq. (2.10) and Eq. (2.11).

$$f_b = f_D \pm f_R \tag{2.10}$$

$$f_b = \frac{2V_r f_0}{c} \pm \frac{2Rf_h}{T_{chirp}c} \tag{2.11}$$

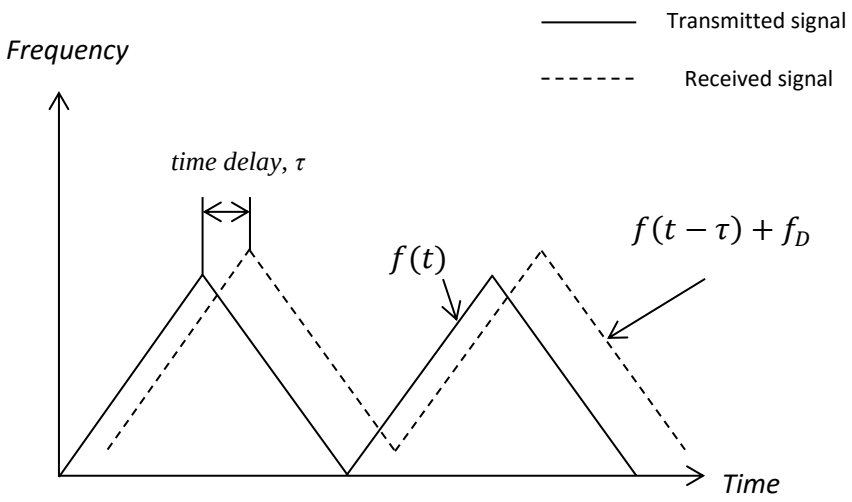

Figure 2.9: LFMCW waveform with a triangle shape for a single moving target.

2.5.1 Range-Velocity Graphs

A single chirp measurement gives the frequency shift for each target. This value is related to R and V_r through Eq. (2.11). Since many R and V_r combinations can satisfy the equation, the range and velocity estimates are ambiguous. This dependency between R and V_r for a single chirp measurement can be represented graphically by plotting Eq. (2.11) with velocity as a function of range, this is a straight line. The gradient of this line depends on chirp gradient.

The first step in processing the radar echo is to down convert it by the instantaneous carrier frequency. The base band signal is analysed to obtain the target range, R, and the radial velocity, V_r. Traditionally this is done using a Fourier transform of the sampled base band echo. For target detection an ordered statistic (OS) constant false alarm rate (CFAR) procedure with an adaptive amplitude threshold is applied for multi-target detection [45]. An ordered statistic is a sequence of amplitude values of echo signals

ordered according to increasing amplitude. The core idea of an OS CFAR procedure is to select one certain value from the ordered sequence and to use it as an estimate for the average clutter power.

With a moving target a single sweep of the LFM waveform gives an ambiguous measurement in range and radial velocity for a target. There will be a single spectral peak in the Fourier spectrum, say at index κ (normalized integer frequency). This corresponds to a line in a plot of target range and velocity described by Eq's. (2.12), (2.13) and (2.14).

$$\kappa = \frac{V_r}{\Delta V} - \frac{R}{\Delta R} \quad \Leftrightarrow \quad \frac{V_r}{\Delta V} = \frac{R}{\Delta R} + \kappa \tag{2.12}$$

Where, ΔR and ΔV are the range and velocity resolutions given by:

$$\Delta R = \frac{c}{2.f_h} \tag{2.13}$$

$$\Delta V = \frac{c}{2.f_0.T_{chirp}} \tag{2.14}$$

Figure 2.10 (a) shows this graphically with an example of the transmitted and received LFM signal and Figure 2.10 (b) shows the corresponding R-V diagram for a single target response to a single chirp. The line drawn corresponds to a measured spectral response at index κ indicating all solutions for Eq. (2.11) i.e. all possible combinations of target range and velocity.

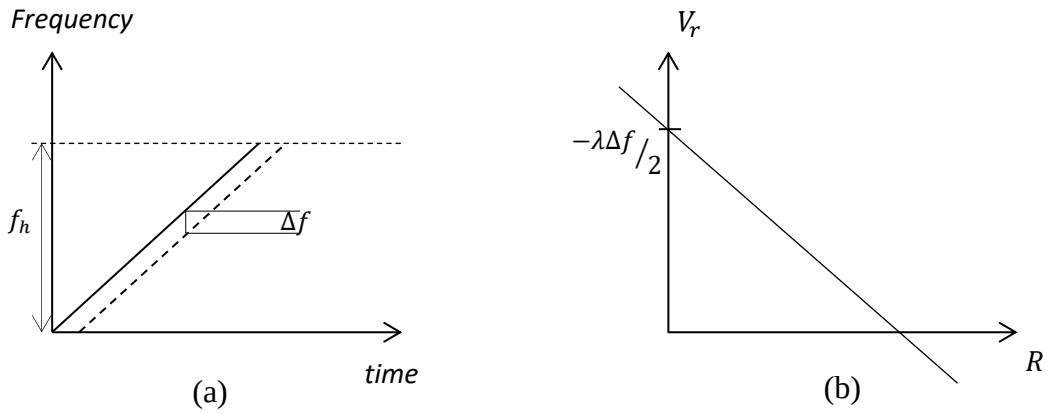

Figure 2.10: (a) Single chirp waveform with positive slope and (b) Range-Velocity diagram for single target measurement.

To resolve the resulting range-velocity ambiguities further measurements with different chirp gradients are used in the radar waveform. This is necessary in order to achieve an unambiguous range and velocity measurement for a single target because both the range and velocity contribute to a single frequency shift. Represented graphically, two measurements of a target, performed with different gradients, produce two lines which intersect at a point in the R-V diagram, defining a unique range and velocity as shown in Figure 2.11. The same solution could be found numerically.

Ghost targets result if only two chirps are used to detect two or more targets, as illustrated in Figure 2.12. The target pair A and C are ghost targets as they result from the intersection of wrong pair of R-V lines. To detect two targets without ambiguity four chirps with different slopes are required, as shown in Figure 2.13.

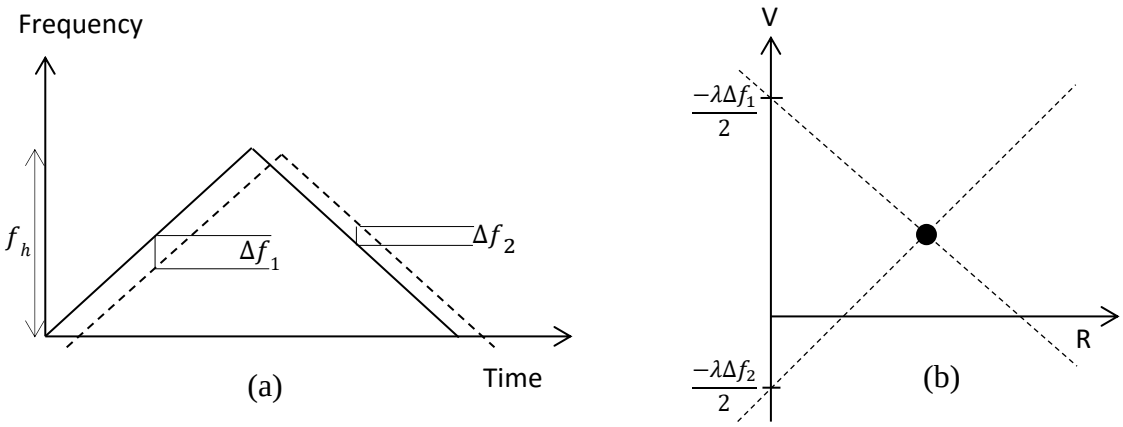

Figure 2.11: (a) Transmit and receive two chirp waveform and (b) Range-Velocity diagram for single target measurement.

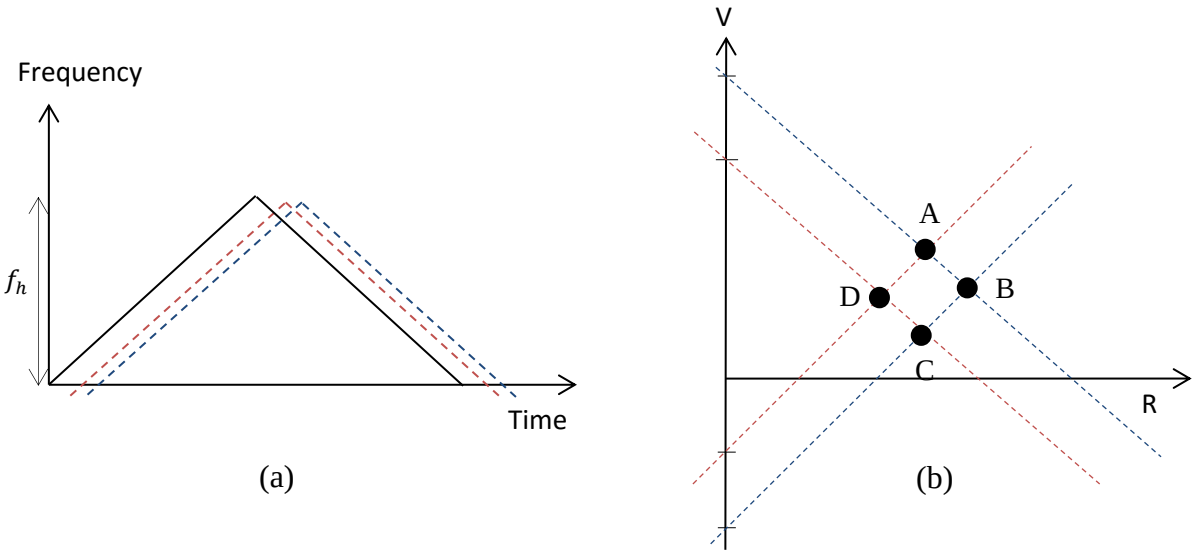

Figure 2.12: (a) Chirp waveform with up and down frequency gradients and return signals from two targets (blue and red dashed lines) and (b) Range-Velocity diagram showing true targets D and B with ghost targets A and C.

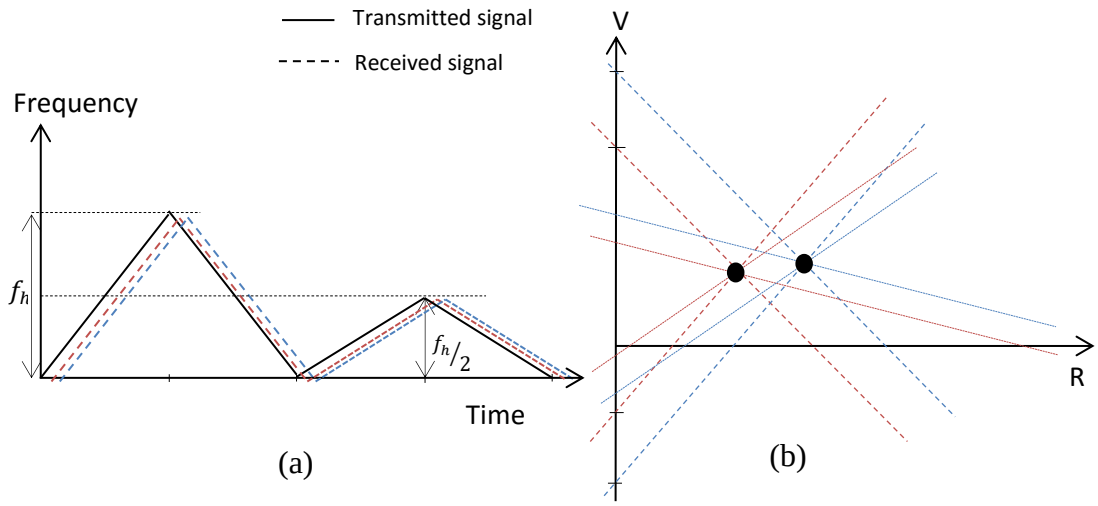

Figure 2.13: (a) Four chirp waveform with different frequency gradients and return signals from two targets and (b) Range-Velocity diagram for two targets which results in detection of only real targets.

In Figure 2.13 the frequency of modulation is different for each of the four chirp signals. Each chirp signal detects the target according to the radar equation. The detected spectral lines from all the four chirps are represented as the R-V lines in Figure 2.13 (b). The gradient or slope of each line depends on the chirp sweep rate. The intersections between the R-V lines corresponding to each chirp will identify up to 3 (or 4) targets. If any of those intersections does not have a physical representation of a reflecting object, it results in a ghost target. A real target is only considered when an intersection point results from the intersection of all the four chirps but not all such cases are real targets. An intersection point obtained from just two or three chirps will not be considered a target. The number of times that the intersection of four R-V lines will correspond to a ghost target will increase with the number of real targets that are present.

2.6 Signal processing for target detection

In analogue radar the echo signal was directly mapped to a commonly used radar display known as a Plan Position Indicator (PPI) where the antenna is usually represented in the centre. Target detection was performed manually even when the clutter and noise was strong. In digital radar the echo signal is down-converted to the baseband, sampled and numerically processed with a digital signal processor. Important target detection procedures that have been developed are reviewed in the following sections.

2.6.1 Traditional methods of LFM-CW target detection

In the preceding section the concept of LFM-CW radar was explained. A commonly used waveform sequence of four chirps, each with different gradients to aid the correct detection of multiple targets was introduced. This section describes the signal processing aspect for that waveform sequence.

The analog part of the processing consists of a mixer and an analog to digital converter. All further processing is performed digitally. Figure 2.14 shows an overview of this analog conversion process [46].

The analog processing of LFM-CW radar echo traditionally involves two stages. In the first stage a frequency shift to the baseband is achieved by removing the offset of the transmitted chirp and spectral analysis is perfomed to identify the frequency change in each echo using windowing and a Fast Fourier Transform (FFT). In the second stage an algorithm is used to estimate range and velocity of the target from the detected frequency changes.

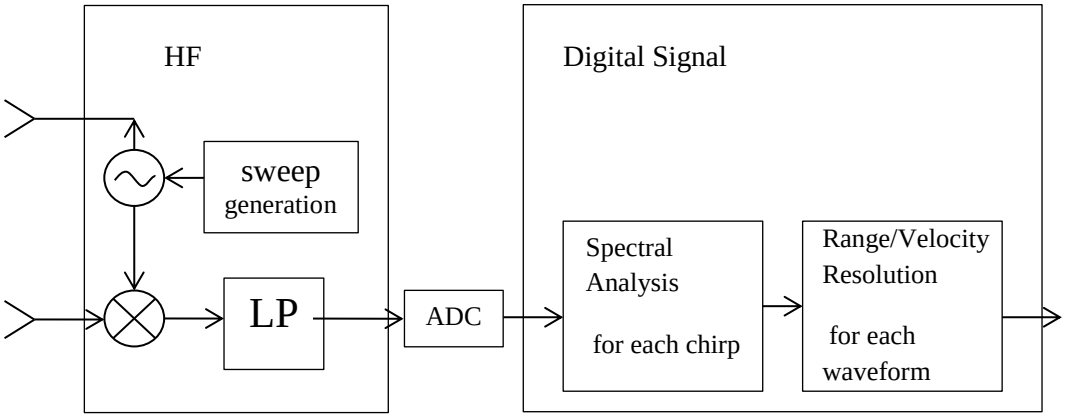

Figure 2.14: Overview of LFM-CW sensor.

The digitized echo is buffered, so that the complete chirp can be processed at one pass and each chirp processed in real-time, as shown in the block diagram of Figure 2.15.

In multiple target situations, there are multiple digitized and buffered signals which are superimposed target echoes with different frequency shifts. Thus, a sampled time domain signal is expected to consist of one or multiple target echoes, each adding a specific frequency component to the signal. The goal of the spectral analysis is to detect these frequency components.

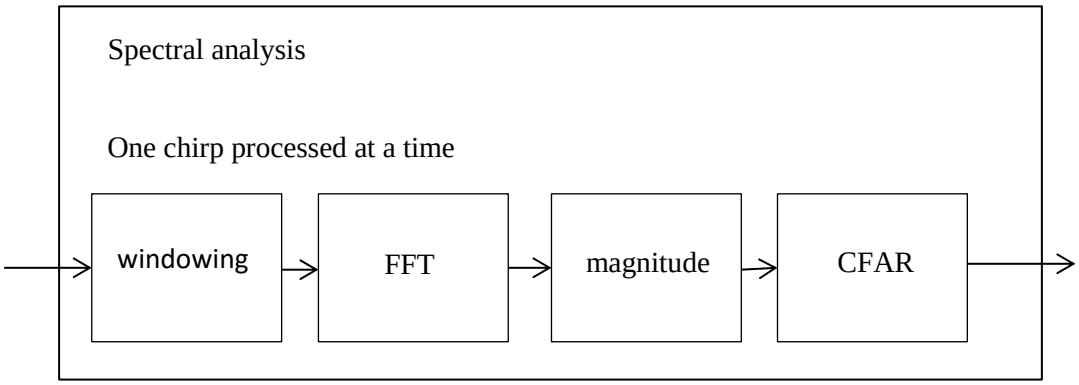

Figure 2.15: Overview of spectral analysis.

The time domain signal is windowed prior to the FFT processing to reduce the spectral peaks of the side lobes. The targets are peaks in the power spectrum.

The detection of peaks is performed using the constant false alarm rate (CFAR) algorithm [47]. The signal power in each bin is compared with an adaptive threshold. For each case where the signal value is above the threshold, a target is identified and the bin index recorded in a detection list with the frequency of the echo. A centre of gravity algorithm which precisely estimates the centre of an arbitrary but symmetric peak is used to compute a single frequency for each detected peak.

Finally the range and velocity are estimated using the equation, Eq. (2.11). Figure 2.16 describes the overall process of target detection.

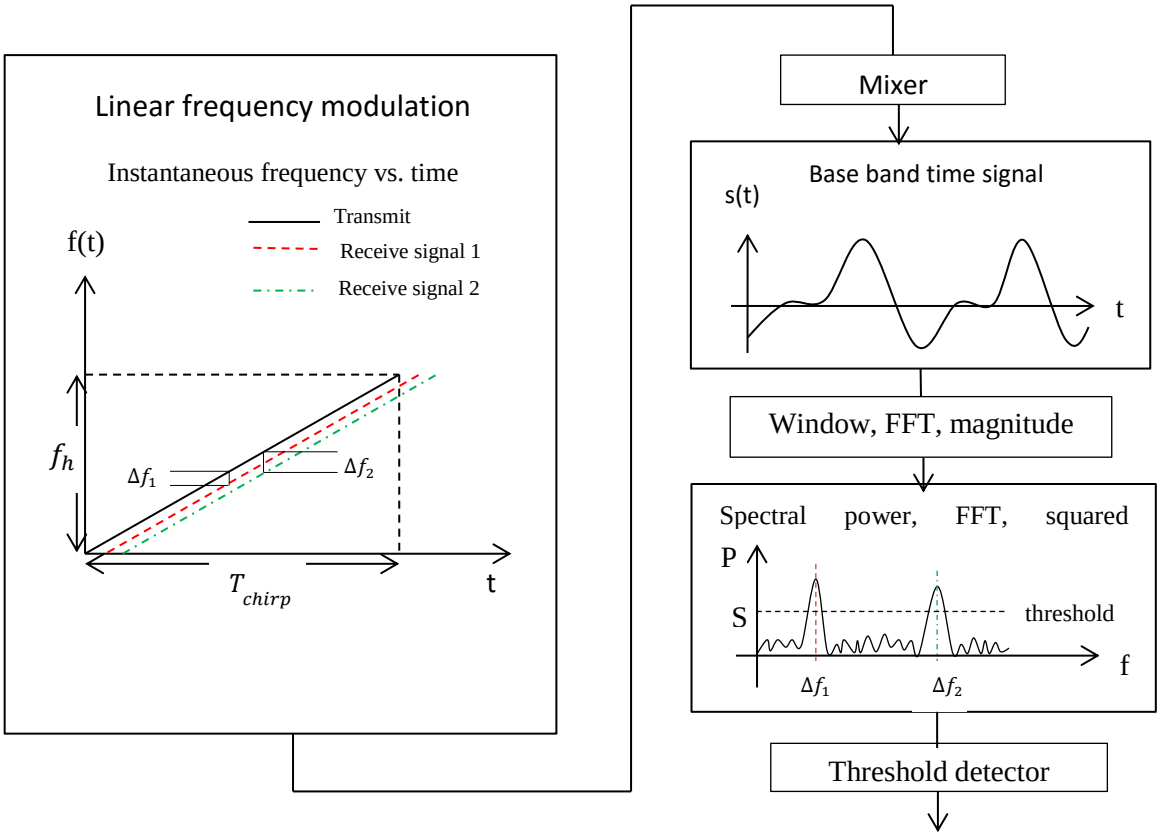

Figure 2.16: Single chirp, base band signal and its power spectrum.

The short coming of this traditional approach of target detection is that targets that fall below the threshold are ignored. The threshold is applied to the power spectrum to eliminate weak responses but a close target with a small radar cross-section would give a weak response, which within this strategy, would be ignored. Missed target situations also arise for small and very big targets within the observation area. A small target can be missed when its peak in the power spectrum is mistaken for side lobe due to a nearby very big target.

2.6.2 Improvements in target detection techniques

A significant amount of research has been carried out in the recent past to improve the accuracy of range and velocity estimation with multiple targets. Relevant methods of target detection are reviewed here.

In contrast to the traditional method of target range and velocity estimation in which the evaluation of FMCW data is based on FFT, [48] additionally evaluated its phase. This method enhanced measurement accuracy so that the sweep bandwidth could be reduced whilst maintaining the accuracy that can be achieved with the conventional FFT technique. Separate phase measurements are not required with the FMCW because it is already present in FMCW. The transfer phase of each reflection is used to estimate target range. The distance to the target is first determined from the time delay and refined using the phase. Ambiguity is resolved in the initial range estimation. Target velocity cannot be estimated with this method.

The authors of [49] addressed the problem of jointly estimating the range and velocity of moving targets using a 77 GHz FMCW radar for automotive applications. Their method was based on a high resolution method of spectral estimation to determine the

frequency of each echo in the baseband signal embedded in noise. The accuracy of this method depends on the accuracy of frequency estimation. Two frequency estimation methods are described: (i) FFT-based methods that are of interest because they have a low computational cost. However, these methods suffer from short and long range spectral leakage [50]. The first problem is the bias induced by the computation of the FFT in a grid of discrete frequencies. The second problem is long-range leakage caused by the interference between sinusoidal components; (ii) Auto-Regressive (AR) modelling, a high resolution method, is proposed for parametric spectral analysis and preceded by de-ramping and subband decomposition. This method demonstrated improvement in frequency resolution, however, the speed and range resolution remained unchanged.

In [51] a method was described to identify multiple targets with automotive radar which used transformable periods and a symmetrical LFM (TPS-LFM) waveform. This waveform improved target detection by reducing false target detection and reducing the rate at which targets were not detected. The false detection of targets was reduced by using three pairs of chirp with different slopes that were divided into eight segments, A-H, as shown in Figure 2.17.

For each target, an up frequency shift, f_{up}, and a down frequency shift, f_{dn} will be received respectively in segment A and B. For each target, combining f_{up} with f_{dn} for three slope pairs will identify more possible targets than are actually present. The real targets will appear in each slope pair. After all possible targets are listed, a comparison is done within them. Each possible target in the first slope pair is compared to the possible targets in the second slope pair to find data pairings having the same range and

velocity and are stored as suspects. The undesirable data pairings are eliminated. In the next step, the remaining data pairings are compared to the possible targets in the third slope pair. The data pairings that match all the slope pairs are stored as real targets. To

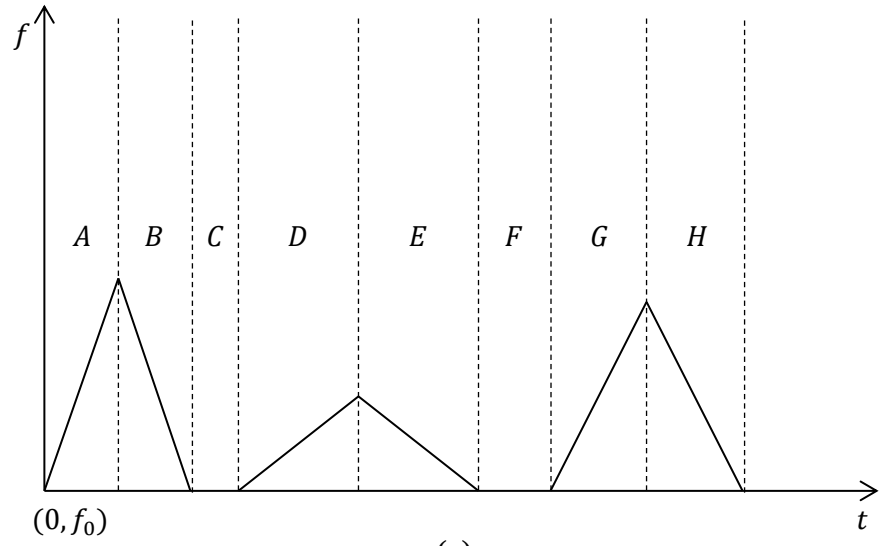

(a)

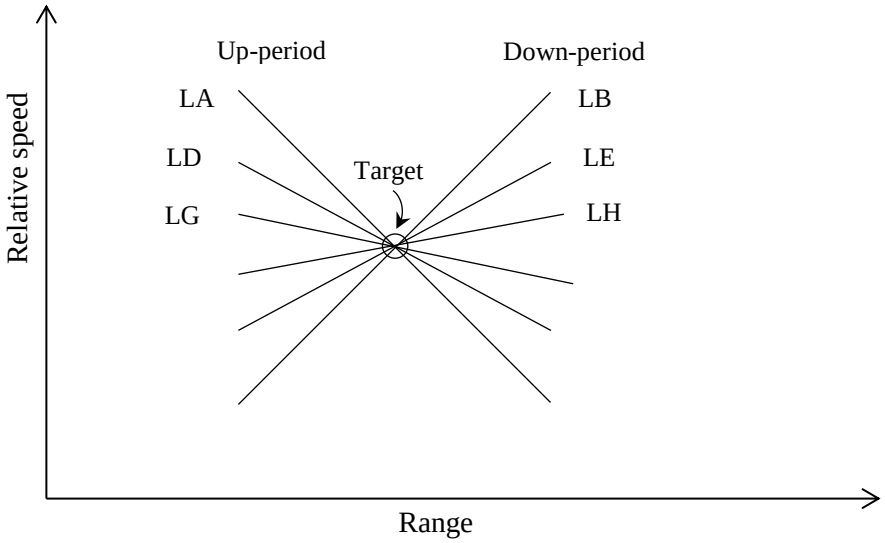

(b)

Figure 2.17: (a) TPS-LFM waveform in one cycle and (b) Intersection finder to detect target.

summarize this method, the detected targets are listed for the first pair of chirps and progressively compared with the responses for the remaining chirp pairs.

In the first slope pair (A, B) the frequency modulation is as wide as possible for a high distance resolution and in the second slope pair (D, E) the time period is made as long as possible for high speed resolution.

The greater complexity of this waveform over that with two pairs of chirps means that the signal processing is also more complex. [52] proposed an algorithm based on the discrete matching in the Fourier domain (DMFT) for chirp rate estimation.

If the transmitted LFM waveform is triangle, for slope A in Figure 2.17 it can be expressed as [53]

$$S_T(t) = a(t)\exp[j\pi(2f_0 t + \gamma t^2)] \tag{2.15}$$

Where, γ and $a(t)$ respectively are the chirp rate and transmitted signal envelope and f_0 is the carrier frequency. The return signal in baseband can be expressed as

$$S_f(n) = A(n)\exp[j\pi(2f_d nT_s + \gamma(nT_s)^2) + \varphi] \tag{2.16}$$

Where, T_s is analog-to-digital converter sampling period, n=1, 2,…., N, where N is the available sample points in each output signal, f_d is determined by chirp rate of transmitting signal and the time delay difference between the scatterer point and the reference point.

Eq. (2.16) indicates that the returned signal from each scatterer point of moving target is approximately a chirp signal and its chirp rate is determined by the chirp rate of transmitting chirp signal and the radial velocity of moving target.

For a LFM signal the situation is expressed in Eq. (2.17).

$$s(n) = a_1 e^{-j2\pi(k_{01} nT_s + k_{02}(nT_s)^2 + \varphi_0)} \tag{2.17}$$

For N samples, the DMFT is given by Eq. (2.18)

$$F(k_1, k_2) = a_1 e^{j2\pi\varphi_0 T_s} \sum_{n=0}^{N-1} n \tag{2.18}$$

Parameter estimation for multiple moving targets using the DMFT includes the following steps: (i) Compute the modulus of DMFT of the returned signal for multiple moving targets using Eq. (2.18); (ii) Search the peaks of the spectrum in the DMFT domain and obtain values for $k_1 = k_{01}, k_2 = k_{02}$ and the number of signals according to the positions of the peaks compared against a given threshold, and also separate each signal; (iii) Obtain range-velocity pairs using Eq. (2.11).

This technique is promising but the problem of thresholding is still present. Applying a threshold might result in a response from a significant target being eliminated from consideration because the amplitude in the Fourier spectrum is small. This can arise for a target close to the radar which has a small radar cross-section.

In order to detect range and velocity in FMCW radar, a single chirp is not sufficient. One or more subsequent chirps are required to eliminate the ambiguity between range and velocity. The ambiguity is greater with the greater number of targets that are present. Two different methods were given by [54] to process the LFM-CW radar return. Both methods involve computing the FFT, but the number of FFTs and their lengths differ. In the first method, fast ramps are generated with the same slope to fulfill the sampling theorem for the highest Doppler frequency. A two dimensional FFT was performed on each chirp radar return. For each range gate the Doppler spectrum was calculated and each target return detected with CFAR algorithm. This is practical when the number of targets being considered is small. The second method uses slow ramps with different slopes and the same bandwidth. The range resolution is determined by the

bandwidth and the velocity resolution by the duration of the shortest ramp. After the FFT, a CFAR is performed on the FFT spectrum for each ramp. Here the search is performed using the responses that were greater in magnitude in the Fourier spectrum than a selected threshold. The number of FFTs is low as compared to the two dimensional method and is the same as the number of ramps used. The drawback of this technique is also thresholding.

Further research into the precision of target detection using FMCW radar includes that reported in [55] where phase evaluation was used to estimate the range of a moving target with very high precision. The algorithm combines the beat frequency and phase estimations. The time varying phase caused by a relative movement between radar and transponder is used to set up a relative distance sensor. The combination of this relative distance measurement and the absolute distance measurements based on beat frequency allows a very precise distance measurement. However, as is obvious this technique cannot be used in automotive radar due to the need for a relative distance sensor. Another such approach which extends the FMCW radar with an additional phase evaluation for high accuracy range detection was proposed [56]. After a coarse target range detection using the frequency, a correction of the estimated position is achieved through the evaluated phase information. However, this has not been implemeted in the automotive application of target detection.

In [57] a method of range estimation with adaptive resolution was described. For long distance range estimation an FFT was computed and analysed. For targets that were close to the radar a zero-padding FFT was computed to obtain a high range resolution. This approach was extended in [58] to obtain the target range and velocity with

improved precision. Using FMCW radar the processing performed was varied depending on the distance to the target from the radar (classified as long, middle and short). When the target is close and the collision probability high, a de-interleaved time domain with frequency interpolation was used to enhance target range and velocity precision. For short range targets de-interleaving was employed to reduce the number of samples in the time domain without changing the ADC (Analog-to-Digital Converter) sampling rate. Frequency interpolation using a zero padded FFT was adopted to overcome the limitation of the reduced sampling rate. Zero padding is useful when the frequency sampling is considered to be too sparse to provide a good representation of continuous-frequency estimation spectrum [59].

Several methods have been proposed to resolve the problems of false or 'ghost targets' and 'missing targets' in the processing of FMCW radar to obtain target range and velocity. An FMCW waveform with an unmodulated continuous wave between up and down chirp was proposed [60]. The additional unmodulated wave helps combine the correct pair of beat frequencies in the up and down chirp for a target. Another waveform was proposed with dual down chirps having a small slope difference [61]. The small slope difference means that the correct pair of beat frequencies could be obtained. However, in multi target situation, these techniques are complex and the ghost targets are still detected, though with lower probability.

The number of combinations of range-velocity pairs must be considered in FMCW radar by extracting only the beat frequencies of the moving targets using the differential frequency power spectrum in the up- and down-chirps [62]. The number of incorrect pairs selected was reduced by separating stationary and moving targets. This method

was designed to reduce the number of false detections when multiple targets are present. Another method to identify the correct pairs of beat frequencies received from real targets was given in [63]. First the possible combinations were determined with beat frequencies to suppress the ghost targets. Then the power spectrum densities of the up and down beat frequencies were used to suppress ghost targets and detect missing targets. Results for possible pairs of beat frequencies were obtained after two step voting process. The strongest correlative beat frequencies were paired for real target. In the following year, [64] proposed a Moving Target Detection (MTD) algorithm to detect moving automobiles in two steps. The first step consisted of removal of clutter, including stationary targets and noise cancellation. Clutter cancellation was performed by DC filtering and using data from the previous FFT. High frequency noise was eliminated using a low pass filter (LPF). As a result the beat frequency for only the moving target was selected and extracted using the CFAR algorithm. Any remaining clutter was removed with a second application of the MTD algorithm. This method, however, did not detect multiple targets which is important in automotive applications. This method was later extended to detect multiple moving targets with clutter, including numerous stationary targets [65]. The up and down beat frequencies extracted were paired in order to detect range and velocity through combination processing. A combination method based on a voting table was proposed. The combination results of each beat frequency were voted in a range-Doppler table. The range-Doppler pairs with high scores in the table were considered as genuine moving targets.

A new transmit wave and detection algorithm was proposed for multi-target detection [66]. The FMCW transmitted waveform is shown in Figure 2.18. An approximate range was detected in the first, very short period where the Doppler shift is small. In this

period an approximate range was detected with error. The range bound, where the target existed was determined using the maximum Doppler shift. In the second period up and down beat frequencies were extracted and the possible range velocity combinations were determined. The ghost targets were eliminated using the range bound generated by the first period.

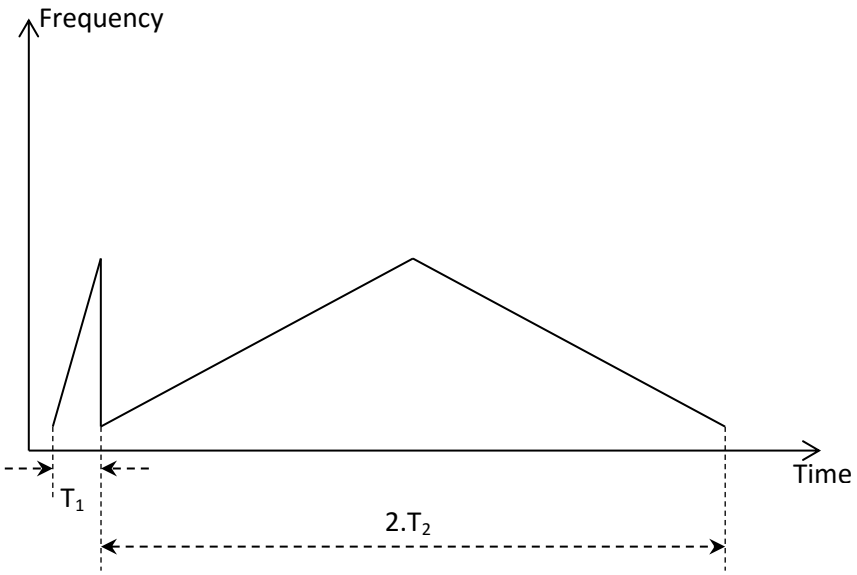

Figure 2.18: The proposed waveform with fast and slow ramps.

In another range-velocity detection method for automotive radar using a 2D-FFT [67], a fast-ramp train consisting of multiple linear FMCW signals was used as the transmission signal. A rough estimation of the target range was obtained after the first FFT. The velocity estimation and more accurate range estimation were obtained after the second FFT. The downside of the fast-ramp train method is the complex processing involved.

Other signal processing techniques using an FMCW radar have also been proposed for realistic situations where the frequency content changes over time [68]. The two-

dimensional FFT and time frequency analysis (TFA) are two techniques for FMCW radar analysis that have been reported [69]. In the 2-D FFT technique, the signal is digitized and represented in a two-dimensional array of velociy and range and a two-dimensional Fourier transform performed. The peaks of the 2-D spectrum were identified to determine the velocity and position of the target. The conventional 2-D FFT gives good results only when the targets are of nearly constant velocity which is not the case in automotive application. Better results are achieved for targets with changing velocity using the TFA in which the intermediate frequency is not arranged in a 2-D form but transformed into a time-frequency spectrogram. This spectrogram reveals the instantaneous frequency of the signal which is related to the range of the target as a function of time.

2.7 Multistatic radar for target detection

The earliest radars were bistatic and employed Continuous-Wave waveforms transmitted and received through separate apertures [70]. Most recent radar systems are monostatic having a co-located transmitter and receiver. The development of high resolution imaging radar, high speed digital processing and low sidelobe antennas have enhanced the performance of such radar systems. Multistatic radar extends the bistatic concept by having more than one transmitter or receiver. A system comprised of two receivers and one transmitter can be thought of as two connected bistatic radars.

When the transmitted signal is scattered from a target only a small part of the incident energy impinges on the receiver. The majority of the transmitted signal is lost. Multistatic radar topologies can overcome this limitation as more reflected signal is received by multiple sensors. The implementation of such systems has become feasible

due to the advent of high capacity transmission lines, wireless technology, multi-channel antennas, electronic beam steering, high speed digital processors and precise synchronisation systems [71]. Additionally, the use of more sensors enables more area to be surveyed and to be tailored according to the specific application of interest. Sensitivity is increased as more of the energy scattered in different directions can be collected, improving the signal-to-noise ratio. Target recognition and classification is enhanced as the target is being observed from different orientations. The accuracy of target location is enhanced by fusing data from multiple sensors that view from different directions. Reliability is enhanced because the system is tolerant to the loss of one or more sensors with a modest degradation of target detection performance [72]. The analysis of geometrical relationships and the accuracy in estimation of target position and velocity when data was combined from multiple radar systems was presented in [73].

For multistatic radar the possible modes of operation are:

1. Multiple monostatic operation is where each node has a co-located transmitter and receiver. Each node operates independently and in sequence, as shown in Figure 2.19 (b).
2. Multiple bistatic operation is where the receiver in each node receives signals originating from transmitting nodes only. A simple example of this type of network is the case where there is one common transmitter and N receivers or the case with one common receiver and M transmitters.

3. Full multistatic operation is where the nodes are spatially distributed and the receivers can choose which signals to accept. This might be a network containing either or both cases 1 and 2. One such case of operation is shown in Figure 2.19 (a).

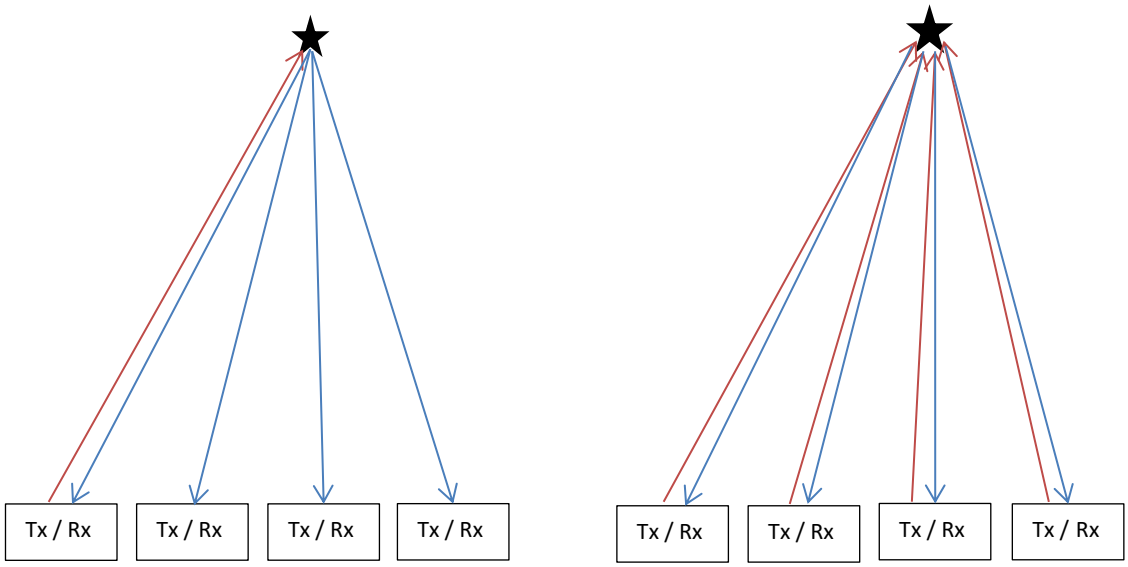

(b)

Figure 2.19: (a) Radar network topology with multistatic arrangement and (b) Radar network topology with monostatic arrangement.

If any radar system is to operate coherently then it must retain a phase reference usually derived from a clock signal. In distributed multistatic radar this requires the clock signal to be distributed to each node to precisely synchronize the transmitted waveform to a fraction of one period of the carrier wave, to achieve phase coherence. Information extraction and processing potential in coherent networks is enhanced significantly as compared to non-coherent systems [74]. In multistatic radar spatial coherence is required to maintain phase stability between the RF signals at each node. This leads to the classification of multistatic radar as: (i) Coherent or (ii) Non-coherent.

The relative merits of non-coherent and coherent networks and the balance between increased performance, complexity, and cost is discussed in [72]. In a multistatic radar system, multiple transmitters should use different transmissions for the receivers to uniquely identify different transmitters.

The sensor topology for collision avoidance and pre-crash warning services are explained in [75]. Commonly a group of short range radar sensors are mounted behind the front bumper. Each sensor measures target range and velocity with high accuracy and the target azimuth is measured by multilateration.

2.7.1 Trilateration and multilateration

The time delay between the transmission and reception of the signal reflected by a target leads to an estimate of the range at which the target is located. A single sensor is capable of estimating only the range measurement to the target and not its orientation. If multiple sensors are used, the different range measurements to the target by the sensors can then be combined to find the position of that target. This technique of combining information from different sources to determine the absolute or relative position is called trilateration. Trilateration can also be used to estimate the velocity of the target. Figure 2.20 shows the concept of trilateration procedure.

Multilateration can be thought as an extension of trilateration technique. It is based on a network of sensors which are capable of performing multistatic measurements. This means that one sensor is transmitting while other distributed sensors are receiving. This technique is well established in aeronautical and military applications [70].

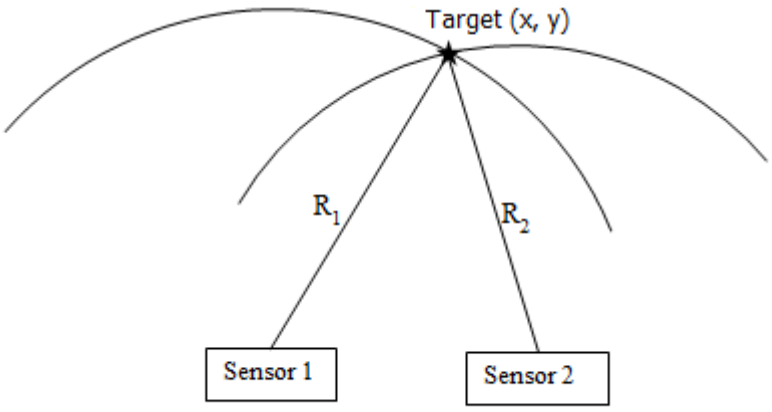

Figure 2.20: Concept of trilateration to find the target position using two sensors

In automotive applications with a network of four radar sensors, each sensor can be switched into transmit mode whilst the other four sensors are in receive mode. In such a network, a multistatic sensor receives and processes signals from all four sensors. The number of signal paths is greater in multistatic than a monostatic system. For example in a network of four sensors, a monostatic network where only one sensor is transmitting and others are receiving, the number of signal paths is only four. On the other hand, a multistatic system for the same number of sensors will have 16 signal paths with 10 unique signal paths, as illustrated in Figure 2.19.

Multilateration is thus an extension of the trilateration procedure to include the additional signal paths. With trilateration the range directly corresponds to the propagation delay of the signal from the sensor i to the target and back to the same sensor i and is given by

$$R_i = \frac{cT_{Ri}}{2} \tag{2.19}$$

On the other hand, multistatic interpretation measures the propagation delay not between the two same sensors but between the transmitting sensor i and receiving sensor j. The delay hence depends on the signal path given by:

$$D_{i,j} = R_i + R_j \tag{2.20}$$

The same applies to the sensor velocity measurements

$$V_{i,j} = V_{ri} + V_{rj} \tag{2.21}$$

According to this definition, trilateration is a special case of multilateration, which measures only those signal paths for which the receiving sensor is also the transmitting one.

One such system based on a network of short range pulse radar sensors using trilateration technique for automotive radar is described in [76]. Trilateration has been used along with a variety of tracking algorithms in automotive radar [77]. The two-dimensional target position is realized by signal processing techniques applied to the range measurements.

Fölster and Rohling [78] describe the use of range only radar sensors to estimate target position in a new bottom-up estimation technique that does not estimate a target position for a set of trilateration measurements but finds the matching measurement for an assumed position.

In an algorithm to trilaterate and track multiple targets [79] tracks were represented in different coordinate systems to maximise the likelihood that associations will be formed.

Another trilateration technique was described in [80] which was used for localization of targets in multi-target situations. Their contribution presented an approach which was based on trilateration. They detected point scatterers in a two-dimensional plane using the reflection and transmission information of only two antennas. It was based on systematic description of the generation of ghost targets which depended on antenna distance and scatterer placing. It was concluded that a trade-off between reconstruction precision and the occurrence of ghost targets had to be made using two-antenna setup.

In an automotive multi-target scenario as the number of targets increases, trilateration technique gives rise to ghost target situations.

2.8 Matched filter and the radar ambiguity function

In a radar system information about the target is obtained by comparing the received echo signal with the transmitted signal. Radio frequency interference or noise limits the ability of a radar to detect the presence of an echo signal. Similarly, noise also limits the reliability with which a feature in the radar echo signal may be detected. The echo signal should be larger than the noise for reliable detection. The impact of this noise is often minimised by using a matched filter [15]. A matched filter maximises the signal-to-noise ratio of echo signals which are buried in additive noise. A matched filter may be applied by correlating a known signal, or template, with an unknown signal to detect the presence of the template in the unknown signal. This is equivalent to the convolution of the unknown signal with time-delayed conjugate of the known signal.

This concept is used to identify the optimal detection of the ambiguity function. The ambiguity function is the response of the matched filter to the signal for which it is matched as well as the Doppler frequency shifted (mismatched) signal.

If one target parameter, range or velocity, is known or is the same for all targets then the other can be defined more precisely. It is not always possible to have prior knowledge of the target characteristics and hence the combined effect of a shift in range and frequency cannot always be estimated. This results in a mismatch output from the filter. For example, if the filter was originally matched to a nominal center frequency and a nominal delay, there will be no mismatch if the input signal is returned from a point target at that nominal delay and Doppler shift [34]. However, if the input signal is returned from some other point target that does not correspond to the nominal delay and Doppler shift that the filter matches then the output is a mismatch output. The result is an additional delay, τ, and an additional frequency shift, f_D. Thus, the radar ambiguity function can be defined as the output of the matched filter when the input to the filter is a Doppler shifted version of the original signal, to which the filter was matched [81].

Although ambiguity function is seldom used as a basis for practical system design, but to indicate the limitations and utility of particular radar waveforms; it is a design and evaluation tool [82].

The output of the matched filter is the cross correlation between the received signal and the transmitted signal. When the received signal is large, compared to the noise, and assuming a moving target generating a Doppler frequency f_D, the output of the matched filter can be written as Eq. (2.22), [83]

$$\chi(\tau, f_D) = \int_{-\infty}^{+\infty} s(t)s^*(t-\tau)exp(j2\pi f_D t)dt \tag{2.22}$$

Where, $s(t)$ is the transmitted signal and $s^*(t)$ is its complex conjugate, τ is the time delay and f_D is the Doppler frequency.

The modulus of Eq. (2.22) shown in Eq. (2.23) is often referred to as an uncertainity function, given by:

$$|\chi(\tau, f_D)| = \left| \int_{-\infty}^{+\infty} s(t)s^*(t-\tau)exp(j2\pi f_D t)dt \right| \tag{2.23}$$

And, yet another form, Eq. (2.24), the modulus squared of Eq. (2.22) is also referred as an ambiguity function expressed as:

$$|\chi(\tau, f_D)|^2 = \left| \int_{-\infty}^{+\infty} s(t)s^*(t-\tau)exp(j2\pi f_D t)dt \right|^2 \tag{2.24}$$

Thus, $|\chi(0,0)|$ represents the output when the input signal is returned from the point target to which the filter was matched. Any other values of τ and f_D correspond to the additional delay or Doppler shift respectively indicating a return from the target at some other range and/or velocity. Hence, it is obvious that the ambiguity function will peak at $\tau = 0$ and $f_D = 0$ and will ideally be zero elsewhere [34].

Different waveforms have different ambiguity functions. There is no single ideal ambiguity function which fits all requirements. The radar ambiguity function is normally used by a radar designer to study different waveforms. It is also used to determine the range and Doppler resolutions for a particular radar waveform. An ideal ambiguity function is represented by a spike of infinitesimally small width that peaks at the origin and is zero elsewhere. An ideal ambiguity function provides perfect resolution between two targets regardless of how close they may be to each other. But an ideal ambiguity function cannot exist because it must have a finite peak and volume under the curve. Ambiguity functions for various waveforms are discussed in the following sections.

2.8.1 Ambiguity function for a single pulse

The complex envelope, $s(t)$, of a single pulse is defined in Eq. (2.25), as:

$$s(t) = \frac{1}{T_{pulse}} Rect\left(\frac{t}{T_{pulse}}\right) \tag{2.25}$$

Where, T_{pulse} is the width of the pulse and $Rect$ is a rectangular function.

From Eq. (2.22) we have:

$$\chi(\tau, f_D) = \int_{-\infty}^{+\infty} s(t)s^*(t-\tau)exp(j2\pi f_D t)dt \tag{2.26}$$

Substituting Eq. (2.25) in Eq. (2.26) and performing integration yields Eq. (2.27)

$$|\chi(\tau, f_D)|^2 = \left|\left(1 - \frac{|\tau|}{T_{pulse}}\right)\frac{sin\left(\pi f_D T_{pulse}\left(1-\frac{|\tau|}{T_{pulse}}\right)\right)}{\left(\pi f_D T_{pulse}\left(1-\frac{|\tau|}{T_{pulse}}\right)\right)}\right|^2 \qquad |\tau| \leq T_{pulse} \tag{2.27}$$

The ambiguity function cut along the time delay axis τ is obtained by setting f_D= 0, as described in Eq. (2.28), and shown in Figure 2.21. Since the zero Doppler cut along the time-delay axis extends between $-T_{pulse}$ and T_{pulse}, close targets will be unambiguous if they are atleast T_{pulse} seconds apart.

$$|\chi(\tau, 0)|^2 = \left(1 - \frac{|\tau|}{T_{pulse}}\right)^2 \qquad |\tau| \leq T_{pulse} \tag{2.28}$$

The time autocorrelation of the signal $s(t)$ corresponds to $\chi(\tau, 0)$. The cut along the Doppler axis in this case is shown in Eq. (2.29).

$$|\chi(0, f_D)|^2 = \left|\frac{sin(\pi f_D T_{pulse})}{(\pi f_D T_{pulse})}\right|^2 \tag{2.29}$$

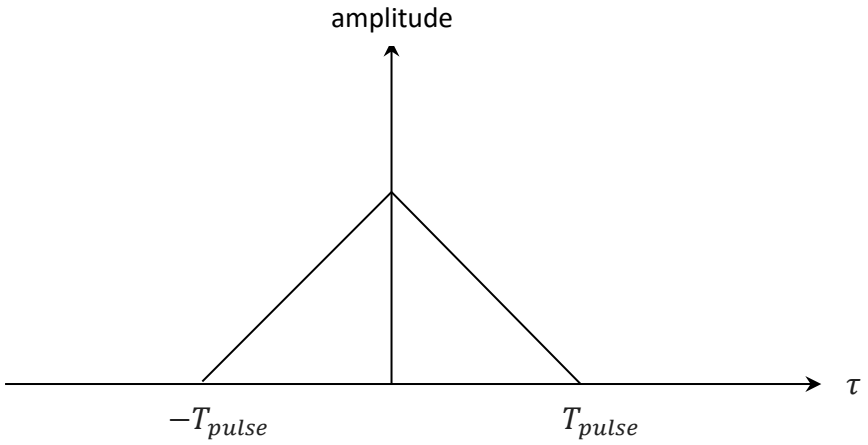

Figure 2.21: Zero Doppler ambiguity function cut along the time-delay axis.

The shape of zero Doppler comes from the sinc function, $\frac{\sin x}{x}$ and extends from $-\infty$ to $+\infty$. The first null occurs at $f_D = \pm {}^{1}/_{T_{pulse}}$. Hence, unambiguous detection of two targets, shifted by ${}^{1}/_{T_{pulse}}$ is possible. Thus, the pulse width T_{pulse} defines the range and Doppler resolution of a single pulse. A very short pulse has to be used for better range resolution. However, very short pulses have a very large bandwidth and must have a large amplitude to convey a significant power level. This is difficult to achieve.

2.8.2 Ambiguity function for an LFM waveform

If μ is the rate of frequency change, the complex envelope of the LFM waveform is defined by Eq. (2.30) as:

$$s(t) = \frac{1}{T_{pulse}} Rect\left(\frac{t}{T_{pulse}}\right) \exp(j\pi\mu t^2) \tag{2.30}$$

By diffentiating the phase, we get the instantaneous frequency,

$$\omega(t) = 2\pi\mu t \tag{2.31}$$

or

$$f_D(t) = \mu t \tag{2.32}$$

which is linear. Therefore, the total frequency deviation for a chirp of period T_{chirp} is , μT_{chirp}.

Using Eq. (2.30) in Eq. (2.22) and integrating yields the ambiguity function for the LFM waveform.

The chirp ambiguity function for an up-chirp is of the form given in Eq. (2.33) [83]

$$|\chi(\tau, f_D)|^2 = \begin{cases} \left| \left(1 - \frac{|\tau|}{T_{chirp}}\right) \frac{\sin\left(\pi T_{chirp}(\mu\tau + f_D)\left(1 - \frac{|\tau|}{T_{chirp}}\right)\right)}{\pi T_{chirp}(\mu\tau + f_D)\left(1 - \frac{|\tau|}{T_{chirp}}\right)} \right|^2 & if\ |\tau| \le T_{chirp} \\ 0 & otherwise \end{cases} \quad (2.33)$$

The ambiguity function contours for the up chirp represented by Eq. (2.33) are shown in Figure 2.22.

The ambiguity function contours for the down chirp of Eq. (2.34) are shown in Figure 2.23.

$$|\chi(\tau, f_D)|^2 = \begin{cases} \left| \left(1 - \frac{|\tau|}{T_{chirp}}\right) \frac{sin\left(\pi T_{chirp}(\mu\tau - f_D)\left(1 - \frac{|\tau|}{T_{chirp}}\right)\right)}{\pi T_{chirp}(\mu\tau - f_D)\left(1 - \frac{|\tau|}{T_{chirp}}\right)} \right|^2 & if\ |\tau| \le T_{chirp} \\ 0 & otherwise \end{cases} \quad (2.34)$$

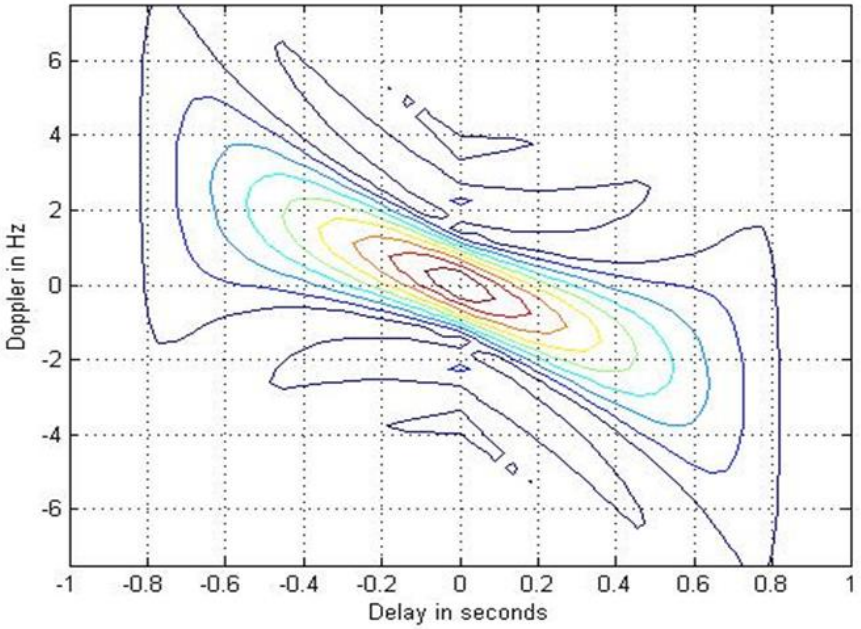

Figure 2.22: A contour plot of the ambiguity function for an upchirp (T=1 sec, BW=2.5 Hz).

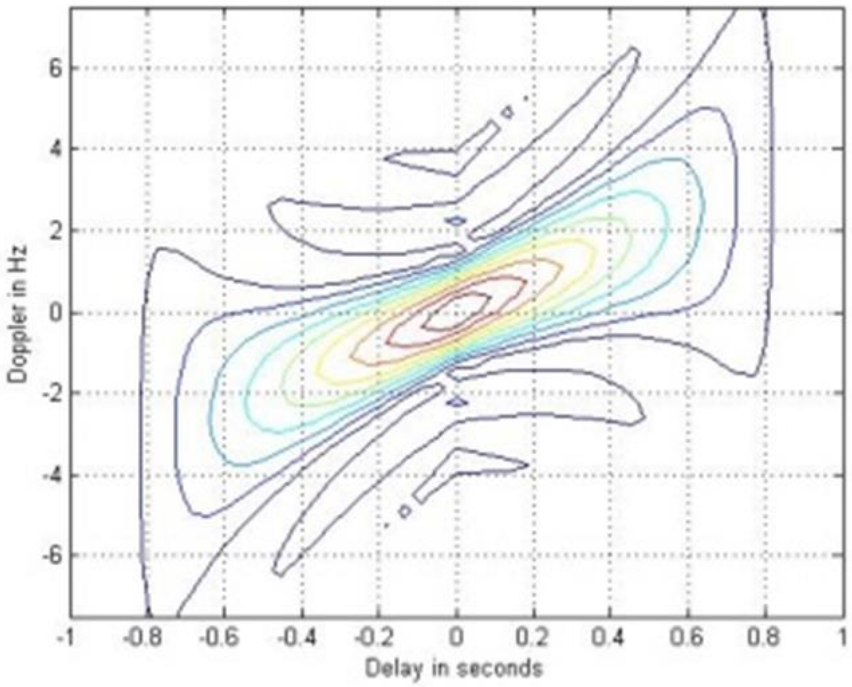

Figure 2.23: A contour plot of the ambiguity function for a downchirp (T=1 sec, BW=2.5 Hz).

It is not directly evident from Eq. (2.33) and Eq. (2.34) how the ambiguity function changes with the change in target position or velocity. This aspect of ambiguity function dependence has not been considered in text books, neither has it been a part of research reported here. Various ambiguity functions for different target positions at changing velocities are considered and reported in Chapter 3 and 4.

The projection of the upchirp ambiguity function onto the time delay axis τ is given by Eq. (2.35).

$$|\chi(\tau,0)| = \begin{cases} \left|\left(1-\frac{|\tau|}{T_{chirp}}\right)\frac{\sin\left(\pi T_{chirp}\mu\tau\left(1-\frac{|\tau|}{T_{chirp}}\right)\right)}{\pi T_{chirp}\mu\tau\left(1-\frac{|\tau|}{T_{chirp}}\right)}\right| & if\ |\tau| \le T_{chirp} \\ 0 & otherwise \end{cases} \quad (2.35)$$

The projection of the LFM ambiguity function onto the Doppler frequency axis is similar to that of the single pulse. This is because only frequency modulation is added and the pulse shape has not been changed. However, the projection of the ambiguity function onto the time-delay axis differs significantly being much narrower than to the projection of the unmodulated pulse, with the first null at:

$$\tau_{n1} \approx {}^{1}/_{B} \quad (2.36)$$

Where, B is the bandwidth of the chirp signal. This equation indicates that the effective pulse width of the matched filter output is determined by the radar waveform bandwidth.

A misinterpretation of the range to a target will also lead to a misinterpretation of its velocity, since at a given range, the peak in the ambiguity function has an associated velocity that depends on the range.

2.8.3 Ambiguity function for a coherent pulse train

A pulse train consists of a number of pulses repeated at a fixed time interval, as depicted in Figure 2.24. The pulse width is denoted by T_{pulse}, the pulse repitition interval (PRI) by T and the number of pulses in the train by N. Hence the train length is $(N-1)T$ seconds. The complex envelope of the pulse is given by Eq. (2.37).

$$s_1(t) = \frac{1}{T_{pulse}} Rect\left(\frac{t}{T_{pulse}}\right) \tag{2.37}$$

For a coherent train of N pulses the complex envelope is defined as in Eq.(2.38):

$$s(t) = \frac{1}{N}\sum_{i=0}^{N-1} s_1(t - iT) \tag{2.38}$$

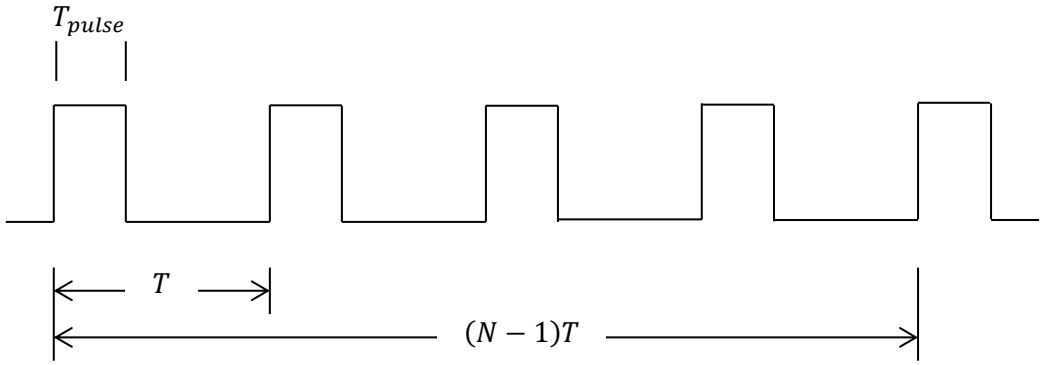

Figure 2.24: A coherent pulse train with N = 5.

Substituting Eq. (2.38) into the Eq. (2.22) gives Eq. (2.39).

$$\chi(\tau, f_D) = \frac{1}{N}\sum_{i=0}^{N-1} e^{j2\pi f_D iT} \sum_{j=0}^{N-1} \int_{-\infty}^{+\infty} s_1(t - iT)s^*(t - jT - \tau)exp(j2\pi f_D t)dt \tag{2.39}$$

Solving the integral yields Eq. (2.40) [83].

$$\chi(\tau, f_D) = \frac{1}{N} \sum_{q=-(N-1)}^{N-1} |\chi_1(\tau - qT, f_D)| \left| \frac{\sin[\pi f_D (N - |q|)T]}{\sin(\pi f_D T)} \right|; \qquad |\tau| \leq NT \tag{2.40}$$

Where, $q = i - j$. Within the region $|\tau| \leq T_{pulse} \Longrightarrow q = 0$. Therefore, Eq. (2.40) can be written as Eq. (2.41), a superposition of the ambiguity function for each pulse.

$$|\chi(\tau, f_D)| = |\chi_1(\tau, f_D)| \left| \frac{\sin[\pi f_D NT]}{N \sin(\pi f_D T)} \right|; \qquad |\tau| \leq T_{pulse} \tag{2.41}$$

2.8.4 Ambiguity function for pulse train with LFM

The transmitted signal is illustrated in Figure 2.25. The ambiguity function is given as in the previous section except that each pulse is linear frequency modulated. Each modulated pulse or chirp has a width of T_{chirp} and PRI of T. The number of pulses in the train is N and the length of the pulse train is $(N-1)T$ seconds.

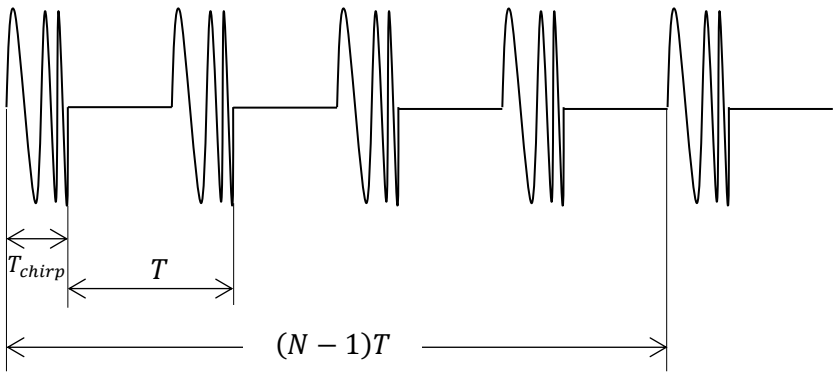

Figure 2.25: LFM pulse train with N = 5.

The individual LFM pulse is given represented by Eq. (2.42) and the transmitted LFM pulse train with N pulses by Eq.(2.43)

$$s_1(t) = \frac{1}{T_{pulse}} Rect\left(\frac{t}{T_{pulse}}\right) \exp(j\pi\mu t^2) \tag{2.42}$$

$$s(t) = \frac{1}{N}\sum_{i=0}^{N-1} s_1(t - iT) \tag{2.43}$$

These equations lead to the ambiguity function of Eq. (2.44)

$$\chi(\tau, f_D) = \sum_{q=-(N-1)}^{N-1} |\chi_1(\tau - qT, f_D + \mu\tau)| \left|\frac{\sin[\pi f_D(N - |q|)T]}{N\sin(\pi f_D T)}\right|; \ |\tau| \leq NT \tag{2.44}$$

Where, χ_1 is the ambiguity function for a single pulse. Again the shape of the ambiguity function is the same as the unmodulated pulse train, along the delay axis because only a phase modulation has been added and this only affects the shape of the ambiguity function along the frequency axis.

2.8.5 Multistatic ambiguity function

Several attempts have been made in recent years to describe multistatic radar using ambiguity function. Tsao et al. [84] developed the ambiguity function for bistatic radar systems. Performance analysis of bistatic radar was carried out by [85]. The ambiguity function for bistatic radar system was extended by [86] to the case of multistatic radar systems. The multistatic ambiguity function was then used for waveform selection and coherent signal processing strategies [87]. The results showed how the ambiguity function of a signal depends on the modulation format. In [88] the significance of waveform selection in multistatic radar systems was presented. In the design, development and construction of a coherent multistatic radar [89] a detailed description of a multistatic ambiguity function was given. However, it did not describe target detection, tracking and identification using multistatic radar.

Capraro et al. formulated a multistatic ambiguity function given the range to a target from a single transmitter and the radial velocity [90]. This formulation described the

ambiguity function of the radar system in a similar way to that described for the monostatic ambiguity function. The shape of the ambiguity function depends on the choice of the modulation waveform. Subsequently [91] defined multiple performance measures based on a multistatic ambiguity function and investigated how different performance requirements lead to different rules for combining signals from multiple receivers. The results were achieved by optimizing the weighting coefficients associated with each receiver. The two approaches were combined [92]. Later in the same year a sensor repositioning approach to shape the multistatic ambiguity function and improve radar system performance using a single transmitter multiple receiver radar system was described [93]. The problem formulation for the case of multiple transmitters was similar to the case of single transmitter but required additional signal processing at each receiver to form a matched filter. The corresponding analysis was given by [94].

Waveform diversity refers to the use of various waveforms in both transmitter and receiver design for improving the overall performance such as detection and/or identification of targets in interference and noise. Waveform diversity can be exploited spatially using a multiple set of sensors. In multistatic radar systems, waveform diversity enhances the distributed radar system performance. Waveform diversity technology allows one or more sensors to change their operating parameters such as frequency and pulse repitition automatically [95]. A system of sensors will then adapt to meet the needs of a changing environment. In the near future sensor and communication devices will have the capability to receive information from multiple sources and decide which signal modulation and antenna parameters need to change in order to function most effectively. However, this will not be relevant in automotive radar as there is little scope for the parameters to be varied under current regulations.

The multistatic radar ambiguity function has been computed for various sensor topologies in [96]. In the first case of multiple transmitters and one receiver, the multiple radar echos will be combined in one sensor representing different facets of the target. With coherent processing the various radar echos are aligned and fed to a matched filter. If $\chi_1, \chi_2, \ldots\ldots, \chi_n$ are the ambiguity functions with respect to each transmitter-receiver path, the overall ambiguity function, $\chi_{netted,}$ for n transmitters of such a system is given by Eq.(2.45).

$$\chi_{netted} = |\chi_1 + \chi_2 + \cdots + \chi_n|^2 \tag{2.45}$$

The complexity of the system increases with the increase in the number of the transmitters.

In the second case of multiple receivers and a common transmitter the echoes received are physically separated and coherent processing is not relevant. A matched filter is applied to each echo and the output is the summation of the various bistatic responses. Mathematically this ambiguity function is represented in Eq. (2.46) as:

$$\chi_{netted} = |\chi_1|^2 + |\chi_2|^2 + \cdots + |\chi_n|^2 \tag{2.46}$$

The general netted case where the transmitter-receiver nodes are spatially disributed a combination of the above two methods was used. Thus, for a system with n receivers where each receiver in the network will accept all the echoes originating from m transmitters, the ambiguity function was defined by Eq.(2.47).

$$\chi_{netted} = |\chi_1 + \chi_2 + \cdots + \chi_m|^2 + |\chi_1 + \chi_2 + \cdots + \chi_m|^2 + \cdots \underline{n\ times} \ldots + |\chi_1 + \chi_2 + \cdots + \chi_m|^2 \tag{2.47}$$

The properties of the multistatic ambiguity function strongly depend on the multistatic topology, target properties and the waveform of the transmitted radar signal. The multistatic ambiguity function for coherent and incoherent systems were derived in

[97]. The spatial coherency of target fluctuations were demostrated to affect the ambiguity response and it was shown that the latter was dependent on the multistatic geometry.

Derham et al. introduced a new set of plots to describe the ambiguity, the PAP (position ambiguity plot) and the VAP (velocity ambiguity plot). The PAP is a snapshot of the position ambiguity response over the entire two-dimensional plane for a fixed hyposthesized velocity, while the VAP is the snapshot of the response for all possible velocity vectors on polar axes for a fixed hypothesized target position [98]. The use of these plots is made on the argument that the traditional ambiguity diagram for analysing multistatic systems is limited since the range and speed axes can only be defined for a single and arbitrary vector direction, whereas the key feature of a multistatic system is the ability to resolve targets based on position and velocity. To measure propagation delay in a multistatic system the transmitters and receivers must be time synchronised. Derham et al. integrated the standard constraint on range and velocity that comes from the radar return, producing Position and Velocity Ambiguity Plots but did not describe how these plots might be used to interpret radar returns.

2.9 Summary

Radar has been used in a variety of applications with designs specialized to each application to be effective. The operating frequency, transmitted waveform, bandwidth etc. are chosen for each application.

Different types of radar waveforms especially those that are suitable for automotive applications have been discussed. The objective with these waveforms is to reduce the ambiguity between range and velocity. However, in automotive radar the range-velocity

ambiguity is particularly severe because the range and velocity of targets produce similar frequency shifts and large numbers of targets are commonly encountered. Consequently, waveform design cannot completely disambiguate range and velocity with this large number of targets. Moreover, as the number of targets increases, the likelihood of ghost targets also increases. The traditional and more advanced approaches which have been reviewed and are in use for target detection and range and velocity estimation use a predefined threshold in the power spectrum. These methods are not well suited to automotive application as they can result in important targets being missed. A critical target having a response below the threshold due to small radar cross-section will not be detected and can prove hazardous in vehicle radar.

The ambiguity functions for a variety of waveforms were reviewed to identify how the waveform influences resolution and suitability for various applications. Methods for computing ambiguity function for multistatic radar with different topologies was also reviewed. The review revealed that the ambiguity function had not previously been used to interpret radar returns. Since the ambiguity function is the output of the matched filter, using this will optimize the detection of the radar echo. In this thesis a novel strategy is proposed which uses ambiguity function in a novel way to interpret FMCW radar returns. This avoids an early rejection of responses lying below the threshold. Thus all responses from the target are preserved and confidence estimates are used to detect targets and calculate their range and velocity.

Chapter 3

3 Novel Strategy for Target Detection

3.1 Overview of target detection

As discussed in Chapter 2 the returned radar signal can contain information about the range to, velocity of and radar cross-section of the target. This reflected signal is processed in different ways to extract target information. In the research reported here, a novel way to process FMCW radar returns is presented. There is a considerable scope for the design of radar waveforms, as discussed in Section 2.4 of Chapter 2. Here we consider a common pattern with two different up and down chirps, as used in RadarNet project [99]. We consider multiple sensors which help to detect more targets as they cover a wider area for observation and helps to reduce ambiguity by combining the information from multiple sensors.

We describe the simulation of a radar system with four FMCW radar transducers operating at 76 GHz with a maximum chirp modulation of 1 GHz. The overall system for target detection consists of two major parts:

1. Data generation system
2. Interpretation system

The data generation system creates a record of frequency shifts given the position and velocity of targets using the FMCW equation given by Eq. (2.11). This frequency shift corresponds to the signal that would be returned by a radar system, without noise or clutter.

The interpretation system is a key aspect of the simulation wherein information from the data generation system is processed to find the target position and its velocity with respect to the sensors. It implements the novel strategy of using an ambiguity function (AF) for target detection and building confidence plots to find the most likely target ranges. Multilateration techniques described in Chapter 2 are used to compute the orientation of the targets.

3.1.1 Novel use of ambiguity functions for target detection

There are many possible solutions for the range and velocity from a frequency shift using the FMCW equation Eq. (2.11). This is graphically illustrated in Figure 2.10. The graphical solution of beat frequency equation was discussed in Section 2.5.1. For large number of targets this solution produces ghost targets and increases range-velocity ambiguity. Also, a small error in one of the frequency shift calculation will result in the R-V lines not intersecting at a point and a solution not being found. Simple pragmatic solutions to this are possible. The bigger problem to be resolved is that of ambiguity.

A new strategy is adopted to overcome the ambiguity that arises with many targets in a practical FMCW waveform and a limited number of sensors. The ambiguity was explained and illustrated in Chapter 2, Figure 2.12. Here information from the FMCW equation is combined with the ambiguity function and other information can also be used to reduce the level of ambiguity. The additional information is the continuity of target position and trajectory.

3.1.2 Ambiguity function of LFM chirps at varying positions

As discussed in the preceding chapter, an ambiguity function is a two dimensional function of delay and Doppler shift that shows the likelihood that a target is present at a

given position. The delay and Doppler can be easily changed into range and velocity respectively using the beat frequency equation. The form of the ambiguity function changes with the change in target position and velocity.

The Figure 3.1 shows how the ambiguity function for a chirp waveform changes with the chirp bandwidth. This is the introduction to the concept with nominal parameters as an example.

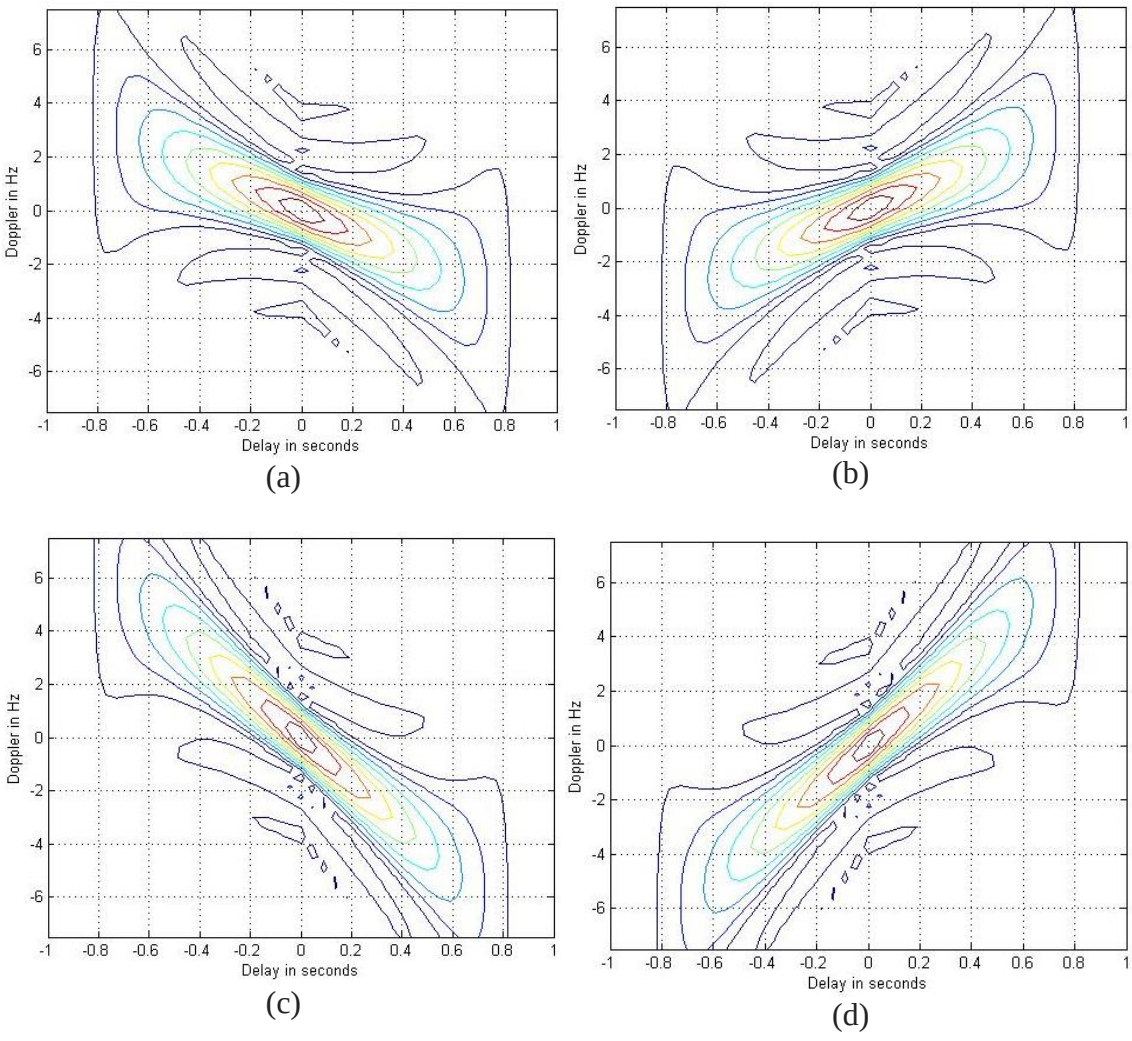

Figure 3.1: Ambiguity function for an up and down chirp with a period of 1 second (a) an up-chirp of bandwidth 2.5 Hz, (b) a down-chirp of bandwidth 2.5 Hz, (c) an up-chirp of bandwidth 5 Hz and (d) a down-chirp of bandwidth 5 Hz.

Figure 3.1 shows the ambiguity function of a single chirp. When the transmitted waveform consists of four chirps, each with parameters as shown in Figure 3.1, the ambiguity function of this waveform, is as shown in Figure 3.2, as a function of delay and Doppler frequency shift.

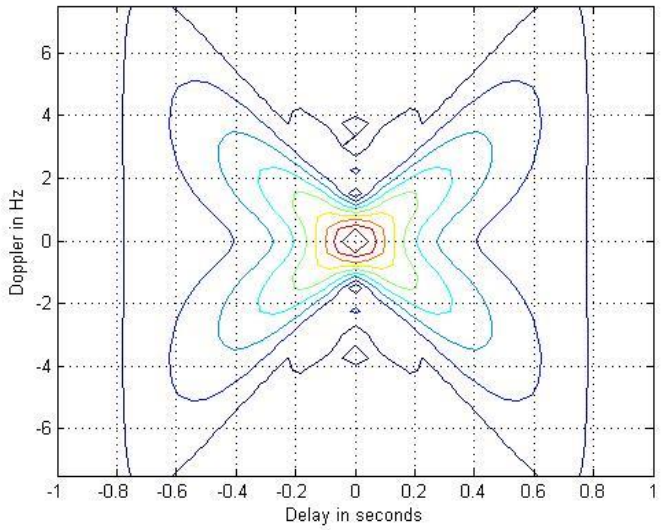

Figure 3.2: Combined ambiguity function for four chirps with varying slopes and bandwidth.

The ambiguity function for a 76 GHz sensor and four LFM chirps with two different up and down chirp slopes, one with a bandwidth of 1 GHz and one of 0.5 GHz at three target positions is shown in Figure 3.4. The Figure 3.3 shows the physical layout to define the co-ordinate system used in this thesis. Generally, in radar context the target position is expressed in terms of range and cross-range. However, in this thesis target position is expressed in terms of latitude and longitude where range, $\mathrm{R} = \sqrt{\mathrm{Latitude}^2 + \mathrm{Longitude}^2}$ and cross-range, $\theta = \tan^{-1}\left(\frac{\mathrm{Longitude}}{\mathrm{Latitude}}\right)$. The target velocity is set to a constant 30 m/s towards the radar sensor. This assumption is made to simplify presentation of the ambiguity function initially.

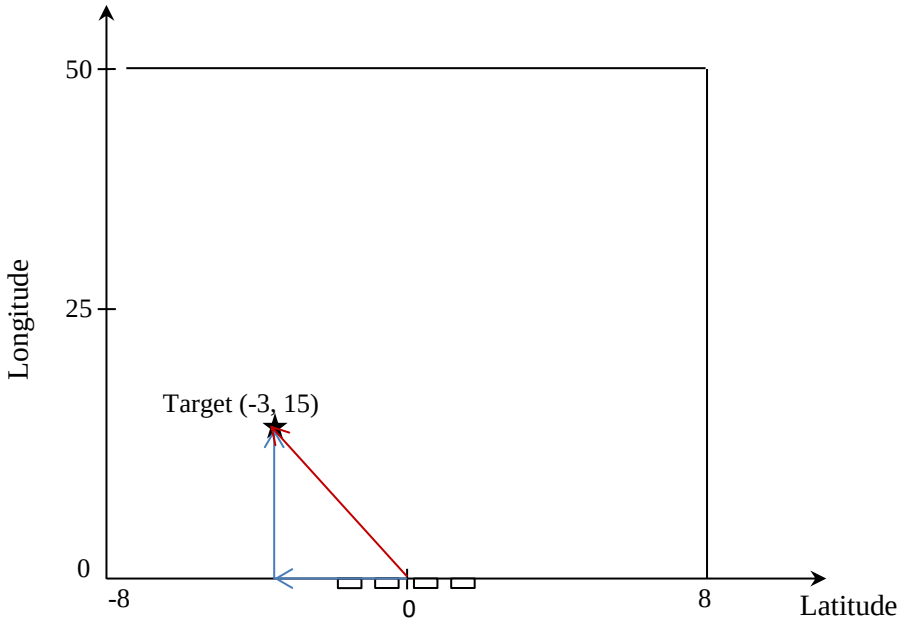

Figure 3.3: Physical layout of the search space

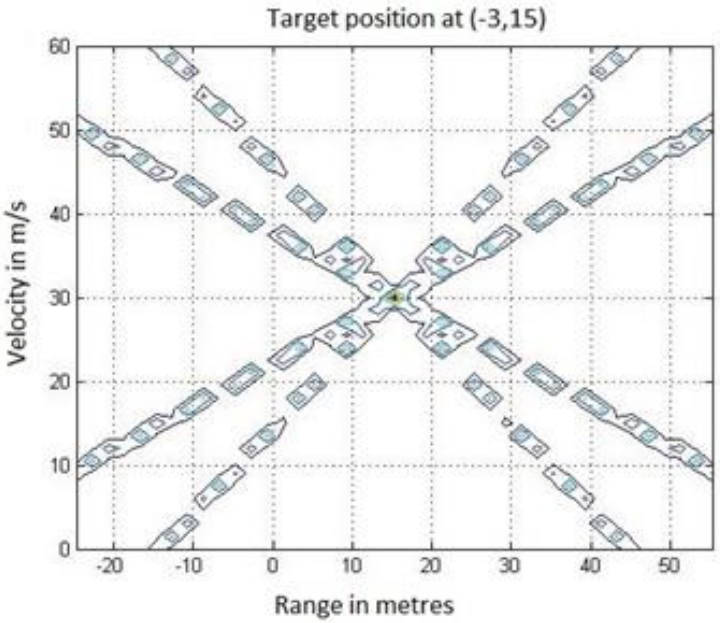

Figure 3.4 (a)

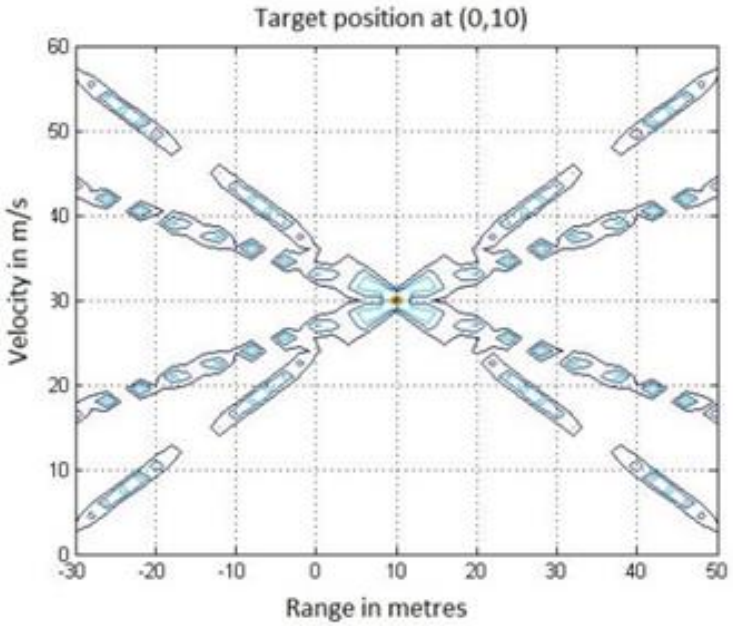

Figure 3.4 (b)

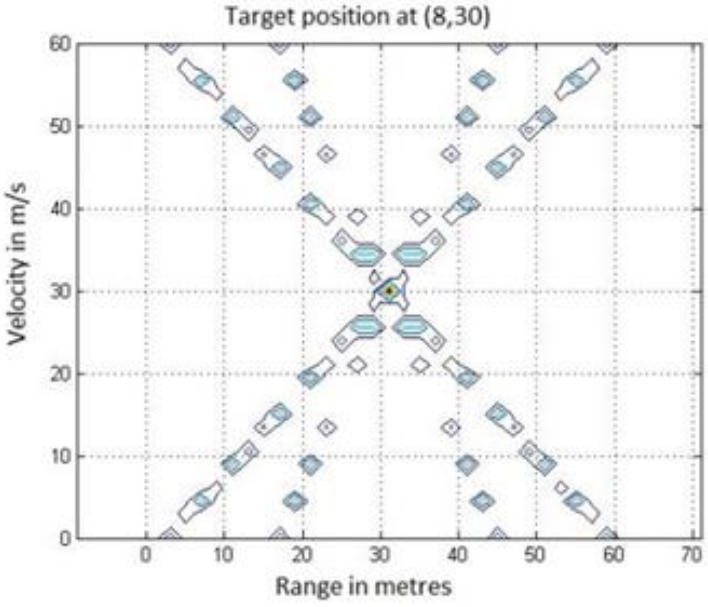

Figure 3.4 (c)

Figure 3.4: Ambiguity function for four chirps (a) target at (-3, 15), (b) target at (0, 10) and (c) target at (8, 30)

It is evident from Figure 3.4 that the ambiguity function changes with target position. The ambiguity function has a central peak and decreasing side lobes. That this should be the case is apparent from the sinc function in Eq. (2.33) and Eq. (2.34). The central peak

represents the most likely range and radial velocity for the target. The probability of finding a target with a different range or velocity decreases rapidly as we move away from this central peak.

Figure 3.5 shows the variation of the ambiguity function with the change in (target) position in x and y direction within an observation area.

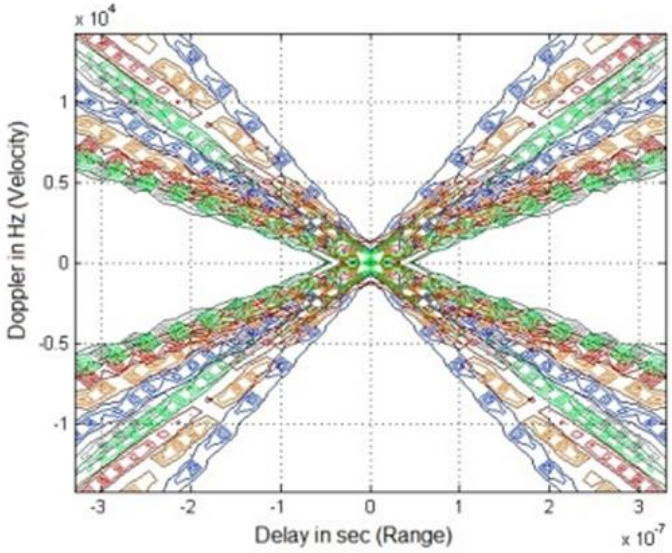

(a)

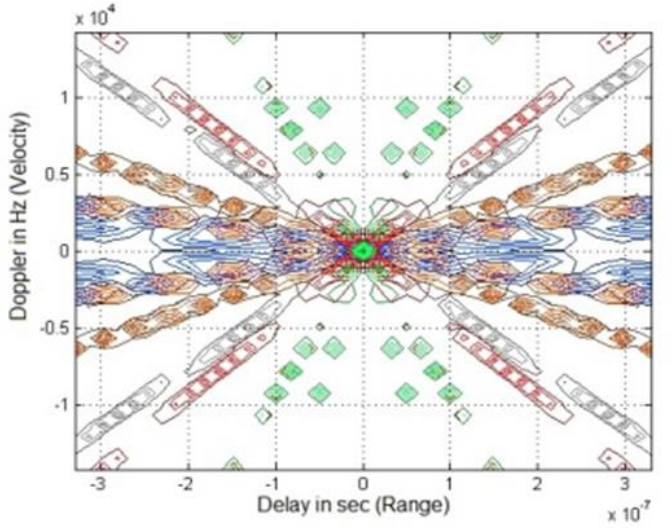

(b)

Figure 3.5: Variation in ambiguity function with position. (a) lateral change in position (blue-8, orange -6, red -4, green-2, black 0 m) at a longitude of 10 m and (b) longitudinal change in position (blue 2, orange 5, black 10, red 25, green 50 m) on central line of set of sensors.

3.1.3 Range-Velocity graphs for the LFM radar returns

The radar return signal carries information about the target range and velocity in accordance with Eq. (2.11). Multiple combinations of R and V_r may satisfy the beat frequency equation giving rise to range-velocity ambiguity. In Chapter 2 the range-velocity lines for LFM waveforms were demonstrated and it was shown how targets may be detected using multiple chirps. It was shown that to detect two targets unambiguously we require two up-down chirps with different gradients to generate four R-V lines. It is not practically possible to use a sufficient number of up-down chirps to disambiguate the range and velocity for a large number of targets. This is because each chirp has its own transmission and processing time. The number of chirps needed would be prohibitive and the cycle time for the complex waveform would be excessively long for real time processing. For automotive applications of the order of 60 to 70 chirps would be needed. With a chirp period of 2 ms to 10 ms this would give a cycle time of 120 ms to 700 ms for each sensor. With four sensors this becomes 480 ms to 2.8 s. A vehicle travelling with 60 km/h will travel 8 m to ~50 m. Therefore, depending on the application there will be a limit to the number of chirps that can be used. With the increasing number of targets but a fixed number of chirps, ambiguity arises as the R-V lines intersect at positions where the targets are not present. This was shown in Chapter 2, Figure 2.12.

Even though the R-V lines result in ambiguities, they contain the target range and velocity information. Here a novel way to extract this information from the R-V lines using the ambiguity function is described.

3.2 Target detection using ambiguity function and range-velocity graph

We present a novel approach which considers ambiguity function and the information from the radar return simultaneously to detect targets and estimate their range and velocities unambiguously.

We begin by considering a fixed target velocity and focus on estimating the range to the target. This is a first step which can be more easily verified while the computation is less complex.

3.2.1 Range measurement using ambiguity function and range-velocity graph

Here we describe the use of the ambiguity function and the range-velocity lines to determine target range. The frequency shift received from the target defines R-V line which will intersect the ambiguity function at a position. The nature of intersection will be either of the following:

1. The range-velocity line passes through the centre of the ambiguity function plot, or
2. The range-velocity line does not pass through the centre of the ambiguity function plot.

The illustration of this concept is shown in Figure 3.6 with a single chirp and fixed velocity. If the range-velocity lines are generated from a target at the same position as that at which the ambiguity function plot is generated, then the range-velocity line will pass through the centre of the plot, as shown in Figure 3.6 (c). In contrast to this, if the range-velocity lines generated do not correspond to the target position at which the

ambiguity function plot was generated, then the range-velocity line will not pass through the centre of that plot, as shown in Figure 3.6 (a) and (b).

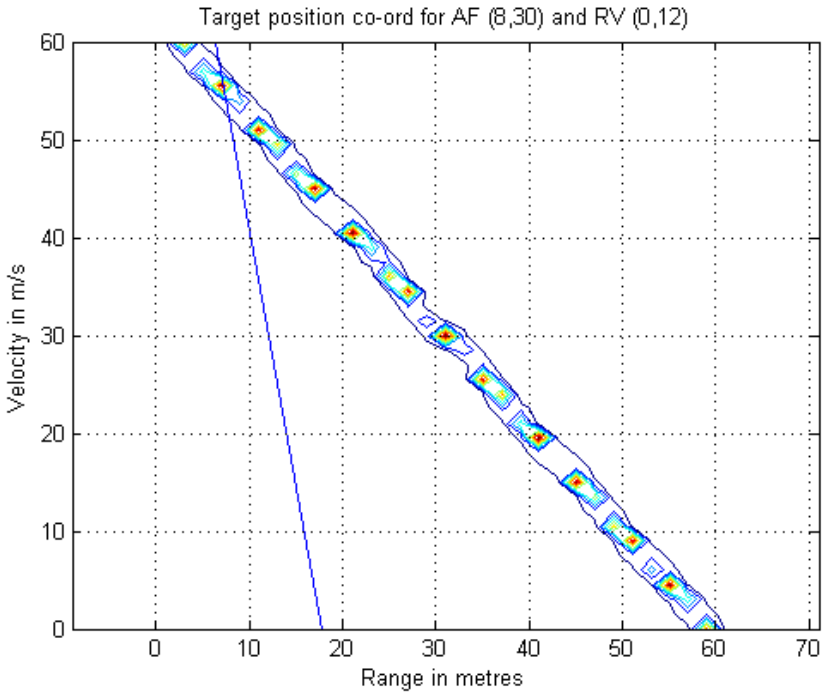

Figure 3.6 (a)

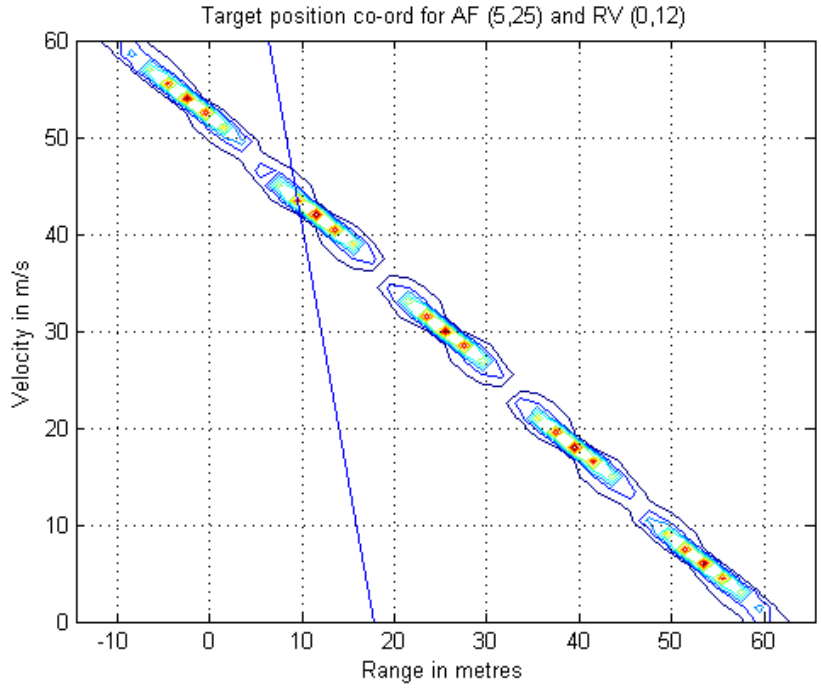

Figure 3.6 (b)

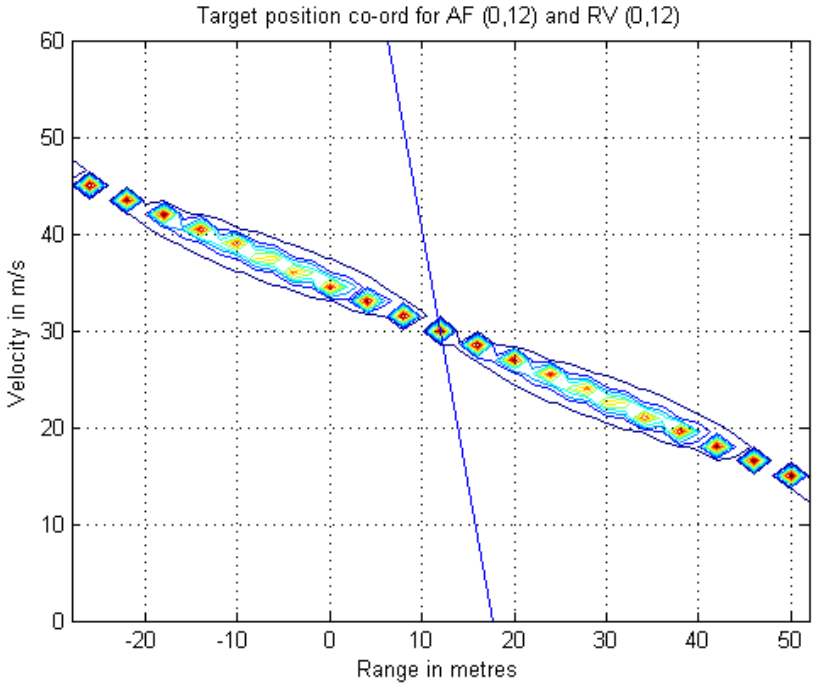

(c)

Figure 3.6: Intersection of ambiguity function (AF) plots at different positions with R-V line at (0, 12) (a) AF plot at (8, 30), (b) AF plot at (5, 25) and (c) AF plot at (0, 12).

For the four chirp waveform used in the simulation of this project, the intersection of the ambiguity function plots with the R-V lines is shown in Figure 3.7.

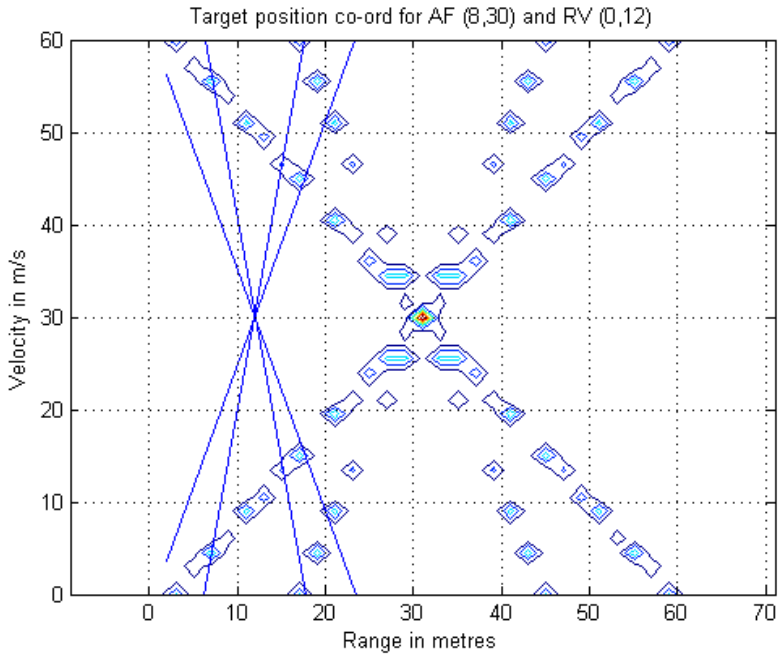

Figure 3.7 (a)

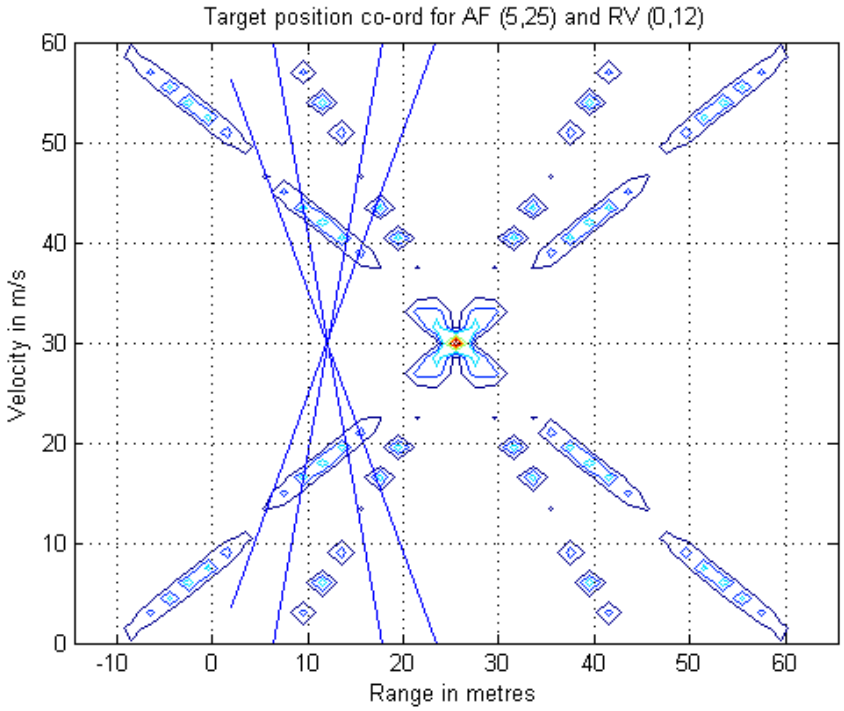

Figure 3.7 (b)

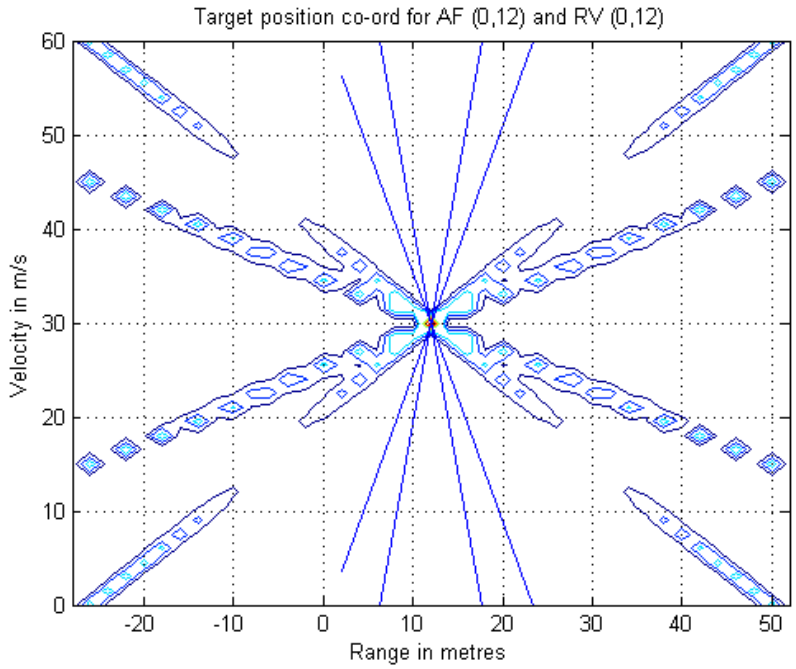

(c)

Figure 3.7: Intersection of ambiguity function plot with R-V lines for four chirps at (0, 12) (a) R-V line does not pass through the centre of AF plot at (8, 30), (b) R-V line does not pass through the centre of AF plot at (5, 25) and (c) R-V line passes through the centre of AF plot at (0, 12).

The ambiguity function has a peak at the centre and decreasing side lobes as defined by the sinc function. The ambiguity function peaks at the centre with a high probability of finding the target there and decreases away from the centre. The ambiguity function value at the intersection of the R-V line with the AF plot samples the likeliness of finding the target at that position. The greater the values at the intersection of the AF plot by the R-V line, the closer the R-V line is to the centre of the ambiguity function plot. This in turn suggests that for higher intersection values between R-V and AF plots, their ranges coincide. Hence, target range can be estimated.

The implementation of this process involves taking samples along the R-V lines on the AF plot. The intersection values which we call ‘confidence values’ are recorded for all

the samples. High confidence values at a range suggest a greater likelihood that the range considered is the target range. Confidence is plotted using the information accumulated from sampling the AF plot along R-V lines and the range determined from the location of the highest peak. Multilateration is used to find the target position (as opposed to range). This work is a theoretical study of a concept with no consideration of practical constraints such as noise. Figures 3.8, 3.9 and 3.10 show the confidence plots obtained by sampling the AF plot with each R-V line.

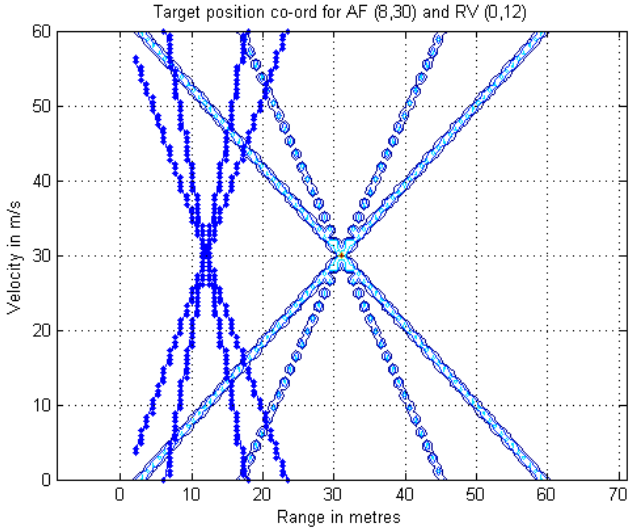

Figure 3.8 (a)

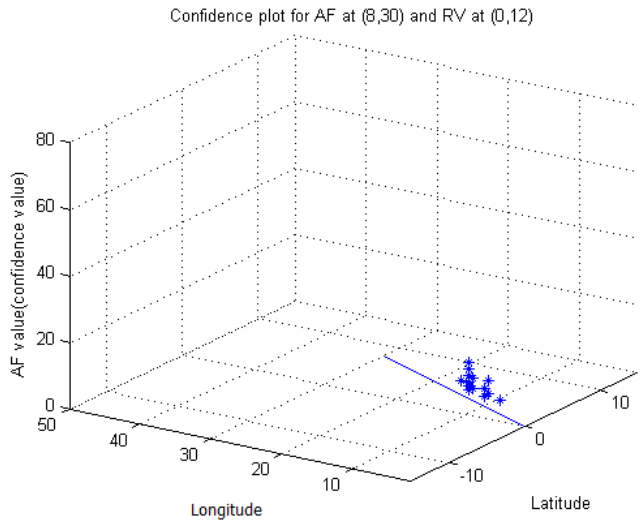

(b)

Figure 3.8: (a) Samples of AF values taken along R-V lines at (0, 12) and AF at (8, 30) and (b) shows a plot of the sampled confidence values from (a).

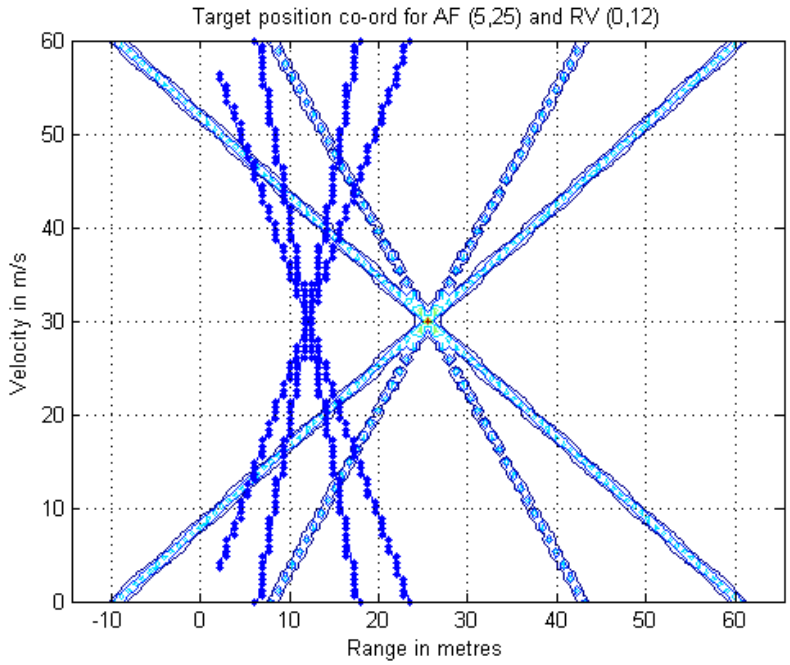

Figure 3.9 (a)

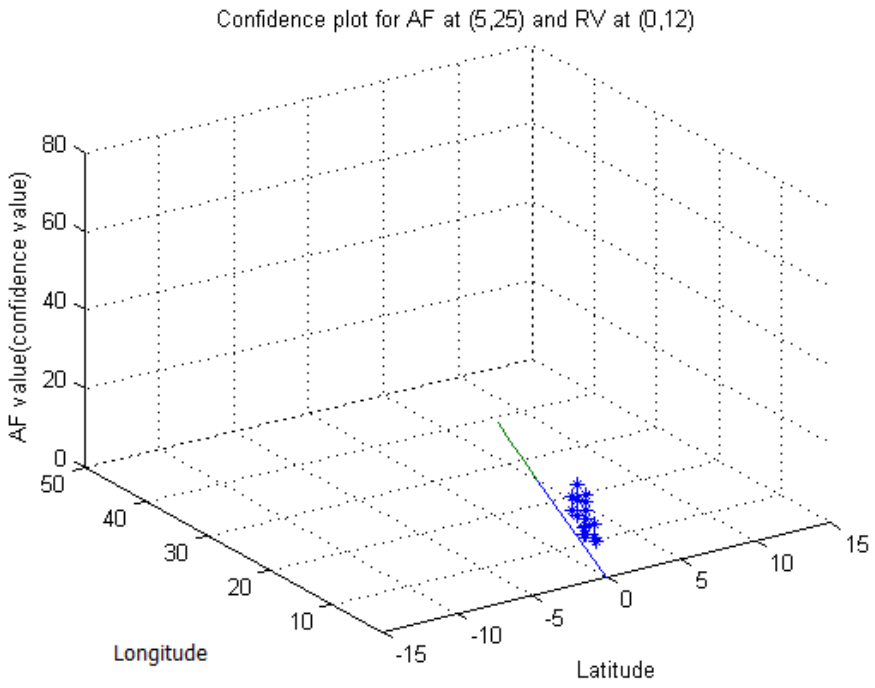

(b)

Figure 3.9: (a) Samples of AF values taken along R-V lines at (0, 12) and AF at (5, 25) and (b) shows a plot of the sampled confidence values from (a).

Figure 3.10 (c) and (d) show the two dimensional plots of latitude versus confidence values and longitude versus confidence values. These two plots help to visualize the high confidence values for the plot of Figure 3.10 (a).

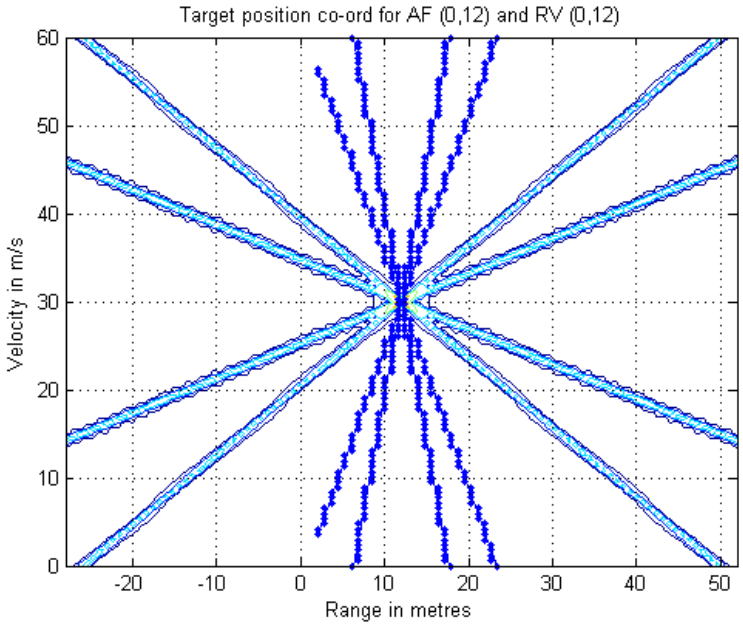

Figure 3.10 (a)

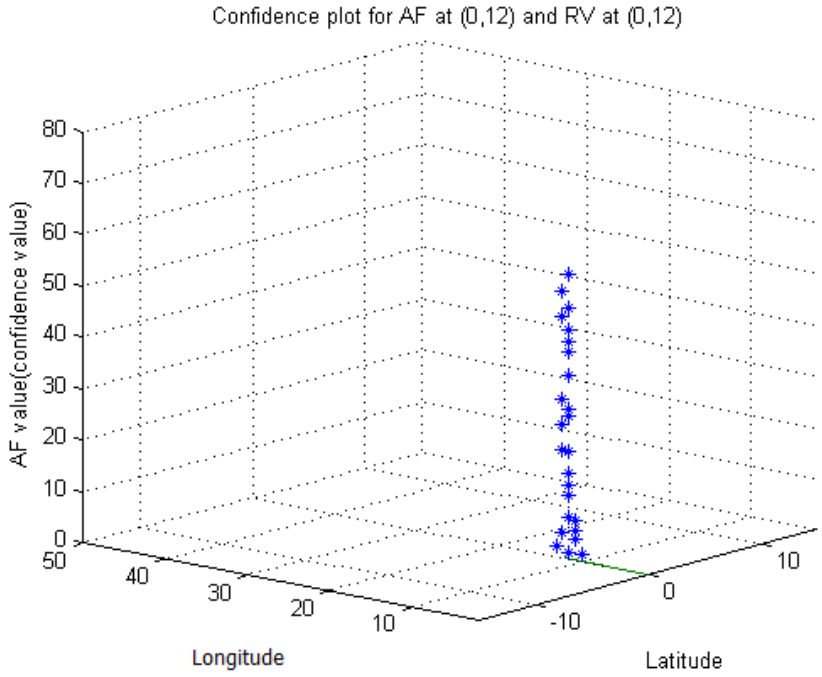

Figure 3.10 (b)

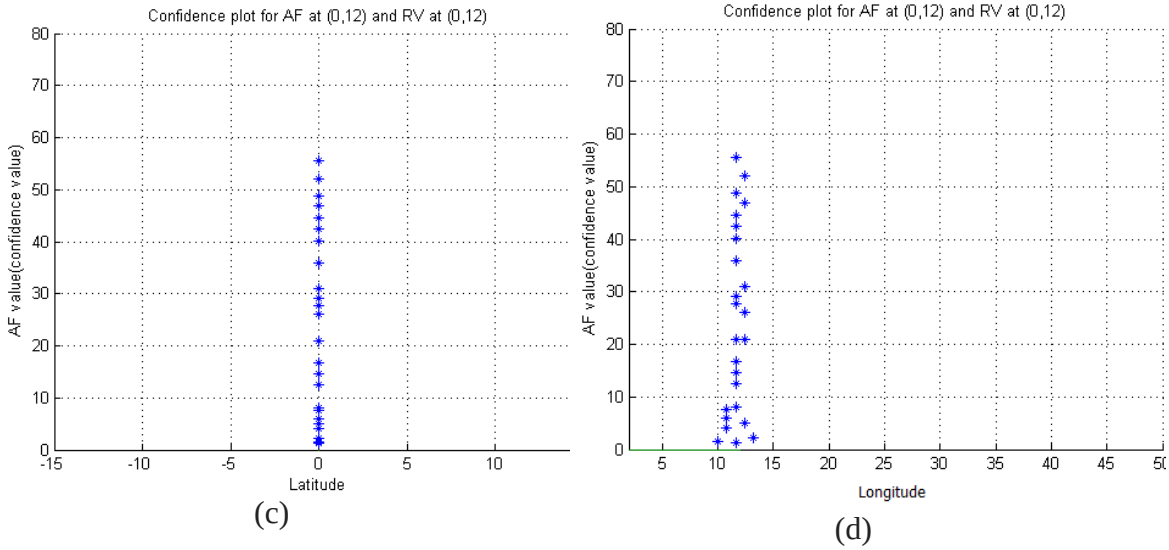

Figure 3.10: (a) Samples of AF values taken along the R-V lines at (0, 12) for AF plot at (0, 12), (b) Confidence plot built from (a), (c) 2D plot of latitude and confidence values and (d) 2D plot of longitude and confidence values.

To locate the target position the range-velocity lines are generated from the received frequency shifts (using the beat frequency equation for FMCW radar) and the AF plots at various locations are sampled along these lines. The Figure 3.11 shows the physical search space of the system under consideration and a part of the selected AFs that are used. Each sensor will have its own search space.

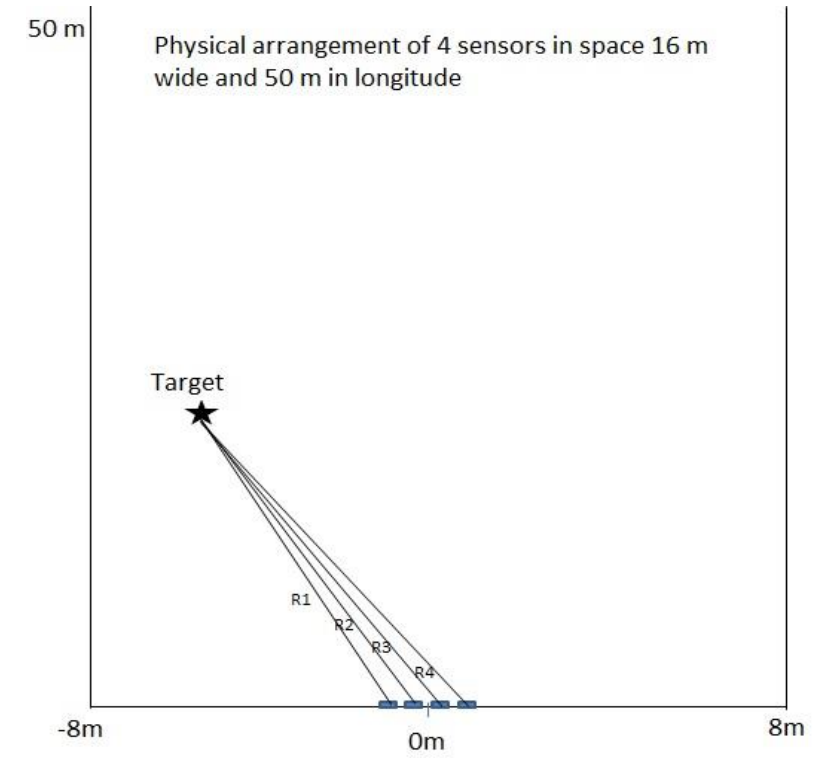

(a)

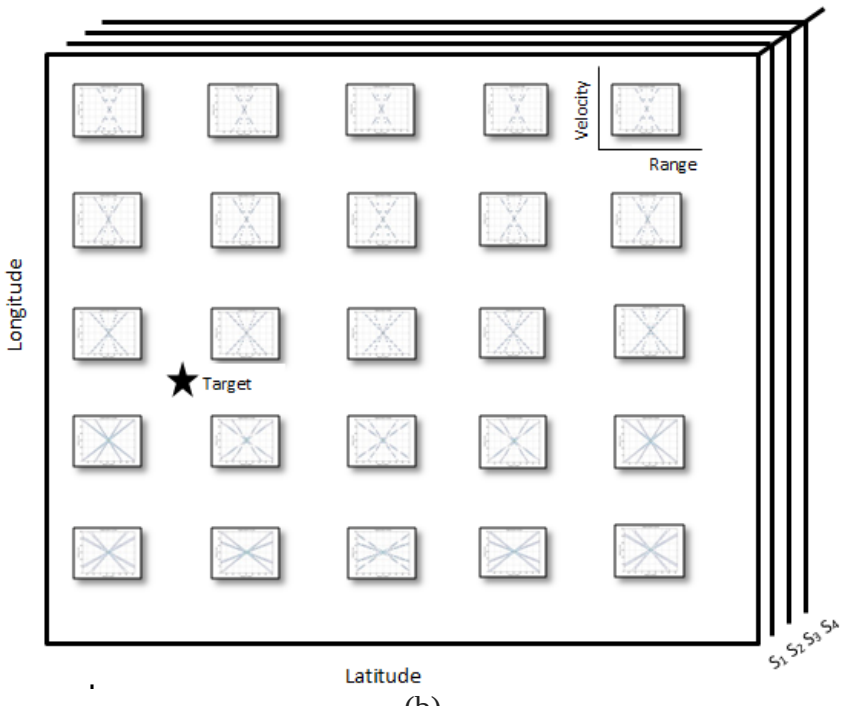

(b)

Figure 3.11: (a) The physical search space and (b) the distribution of ambiguity functions at various positions within the search space.

When an R-V line is generated from the frequency shift received from the target, the position of the target is not known. Therefore some way to select an AF that matches the R-V line is needed. To achieve this, the R-V line for the received frequency difference is intersected with a number of ambiguity functions spread evenly over the observation area. The confidence values from these intersections are high when the R-V line intersects with the required ambiguity function plot and not for other intersections. These confidence values accumulate rapidly when the range of the target corresponds to the range at which ambiguity function is plotted. Otherwise, the intersections do not accumulate rapidly. The cumulative confidence value is thus an indication that allows the correct range to be selected. The accumulated intersection values are referred to as 'confidence values' because they denote the level of confidence that there is a target at a particular range. A threshold is set to eliminate the low confidence values from further consideration. Hence finding the confidence value peaks and their corresponding range will give the estimated target range. Multilateration is used to locate the position of confidence peaks at each range.

In the above discussion the velocity is fixed to simplify the number of computations needed and to enable initial experiments to be performed to test the concept. The calculation of the target radial velocity is described in the following section.

3.2.2 Radial velocity calculation in a multistatic radar sensor topology

There are two ways to obtain the radial velocity, V_r for a target. Successive measurement of range enables the rate of change of range with time to be computed. Alternatively the Doppler change in frequency can be used to estimate velocity.

In a network of four sensors, the radial velocity of the target with respect to each sensor is different. With knowledge of the radar sensor topology, the net velocity of the target can be computed.

The target can be either to the left or to the right of the central line of the set of sensors. Moreover, the target might be moving in any of four directions, defined by reference to the four coordinate directions. Thus, the following eight cases arise:

1. When the target is to the **left** of the central line of the sensors and moving across (a) the first, (b) the second, (c) the third or (d) the fourth quadrant.
2. When the target is to the **right** of the central line of the sensors and moving across (a) the first, (b) the second, (c) the third or (d) the fourth quadrant.

These cases are shown in Figure 3.12 and Figure 3.13.

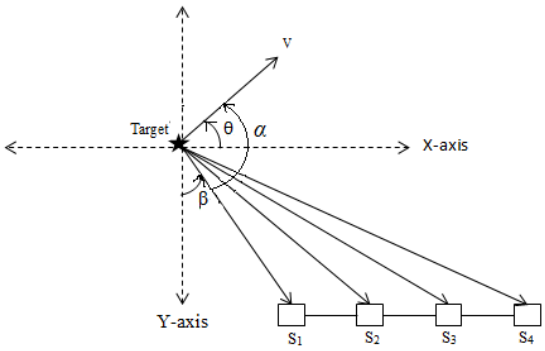

Figure 3.12 (a)

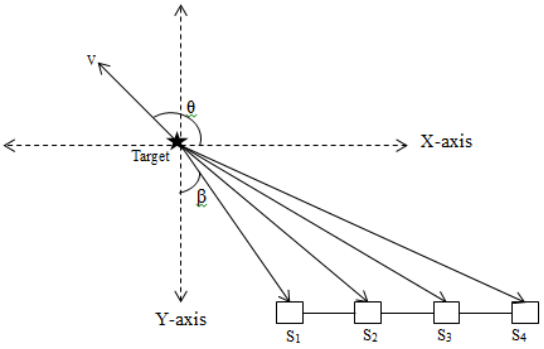

Figure 3.12 (b)

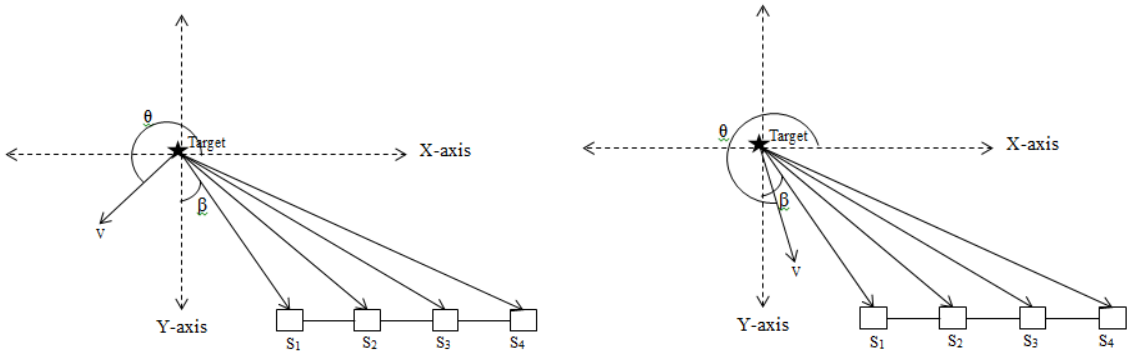

(c) (d)

Figure 3.12: Target is on left side of the central line of the sensors and moving across (a) quadrant 1, (b) quadrant 2, (c) quadrant 3 and (d) quadrant 4.

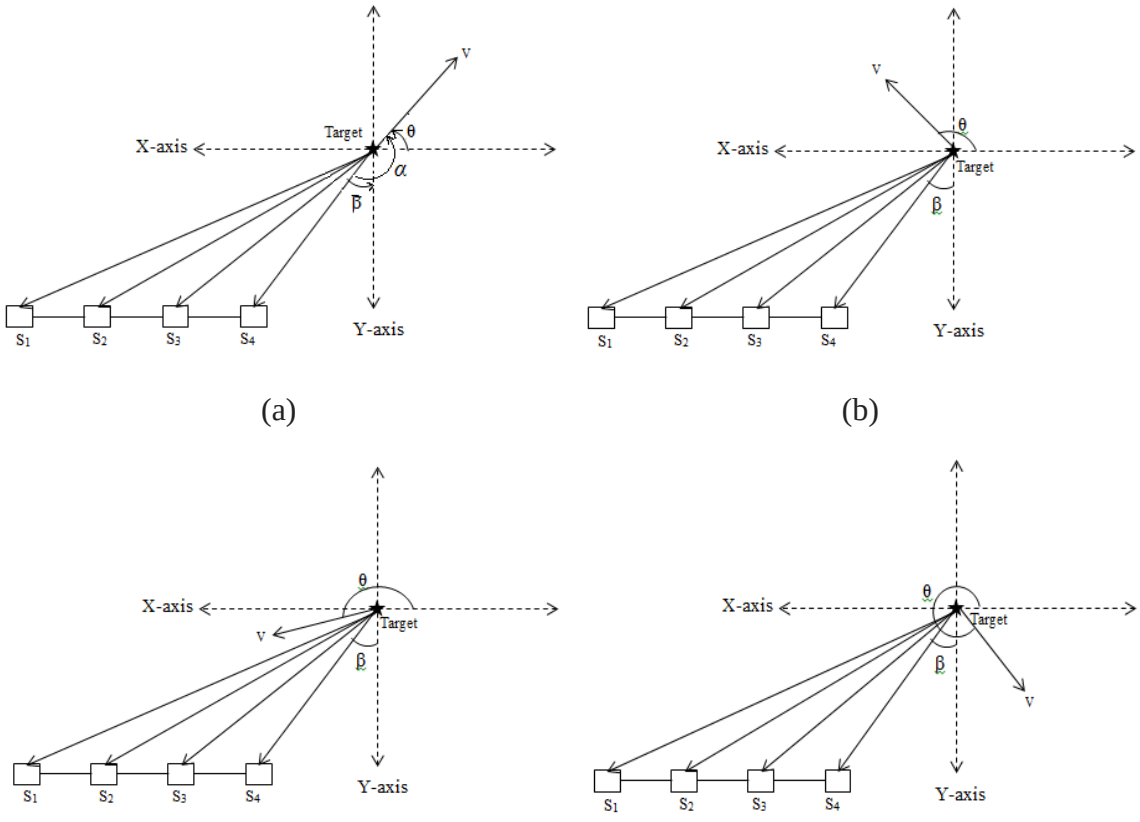

(a) (b)

(c) (d)

Figure 3.13: Target is on right side of the central line of the sensors and moving across (a) quadrant 1, (b) quadrant 2, (c) quadrant 3 and (d) quadrant 4.

Let θ be the angle between the positive x-axis and the targets true velocity and β the angle between the negative y-axis and the targets radial velocity with respect to the sensor, as shown in Figures 3.12 and 3.13. The angles are measured positive counter clockwise. Then the angle between the targets radial velocity and true velocity, α, is given by:

When the target is on the LHS of the central line for the sensors, as shown in Figure 3.12,

$$\alpha = 90 + \theta - \beta \tag{3.1}$$

When the target is on the RHS of the central line for the sensors, as shown in Figure 3.13,

$$\alpha = 90 + \theta + \beta \tag{3.2}$$

From the vector geometry, the radial velocity of the target with respect to the sensor is given by:

$$V_r = V cos\alpha \tag{3.3}$$

This is shown in Figure 3.14 for one of case and one sensor.

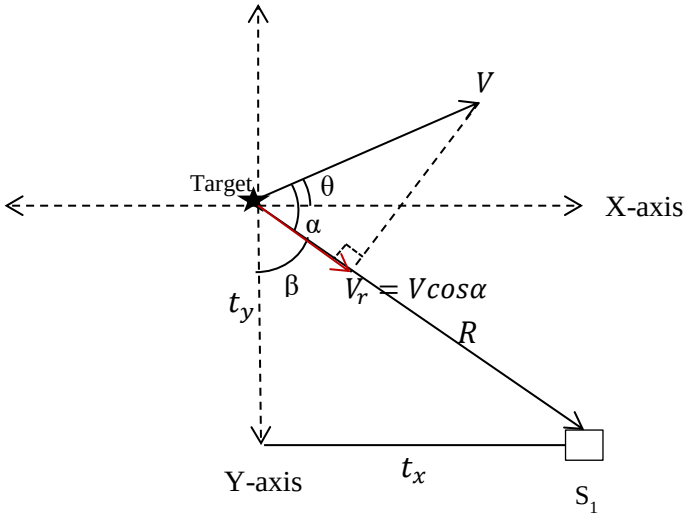

Figure 3.14: Radial velocity as a vector component of the targets true velocity.

To plot the ambiguity function at a target position $(t_x,\ t_y)$ and velocity (V, θ), the angle β can be calculated, using the law of cosines, as:

$$\beta = cos^{-1}\left(\frac{R^2 + {t_y}^2 - {t_x}^2}{2Rt_y}\right) \tag{3.4}$$

Since it is a right angled triangle, the angle β can also be calculated as:

$$\beta = cos^{-1}\left(\frac{t_y}{R}\right) \tag{3.5}$$

Angle α is obtained by substituting for β in Eq. (3.1) or Eq. (3.2) and hence the radial velocity is calculated from Eq. (3.3). The angle β changes with each sensor because the range R from the target to each sensor is different. When the range is computed different cases arise when the target is along the central line of the sensors, on the LHS or the RHS of the central line through the sensors. When the target is along the central line of the sensors, the range R_i varies for different sensors, $i = 1, 2, 3, 4$ are follows:

$$R_i = \sqrt{{R_0}^2 + \left\{\left(i - \frac{5}{2}\right)d\right\}^2} \tag{3.6}$$

Where, R_0 is the perpendicular distance from the target to x-axis (y co-ordinate distance) and d is the distance between the sensors which is fixed and known as shown in Figure 3.15.

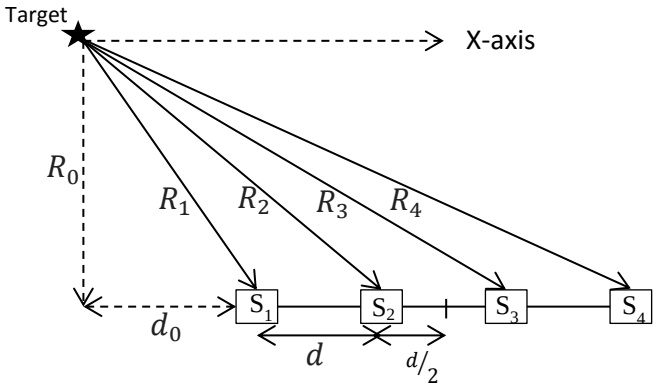

Figure 3.15: When the target is on the LHS of the central line for the sensors.

When the target is on the LHS of the sensors as shown in Figure 3.15,

$$R_i = \sqrt{{R_0}^2 + [d_0 + (i-1)d]^2} \tag{3.7}$$

When the target is on the RHS of the sensors,

$$R_i = \sqrt{{R_0}^2 + [d_0 - (i-1)d]^2} \tag{3.8}$$

Where, d_0 is the x-coordinate distance from the target to the first sensor as shown in Figure 3.15.

In multistatic radar the radial velocity of the target to each sensor and the sensor geometry can be used to find the true velocity of the target. This is illustrated graphically in Figure 3.16. Lines are constructed from the velocity vector, perpendicular to the lines from the target to each sensor to define the component of the velocity towards the sensor. The intersection point is obtained using the coordinates of the target

position (t_x, t_y) and the radial velocity to each sensor, i, (V_{rxi}, V_{ryi}). If $m_{v_{ri}}$ represents the gradient of the radial velocity lines then,

$$m_{v_{ri}} = \frac{V_{ryi}}{V_{rxi}} \tag{3.9}$$

The gradient of the perpendicular lines, m_{perp_i} is negative inverse of $m_{v_{ri}}$, given by Eq. (3.10).

$$m_{perp_i} = -\frac{1}{m_{vr_i}} \tag{3.10}$$

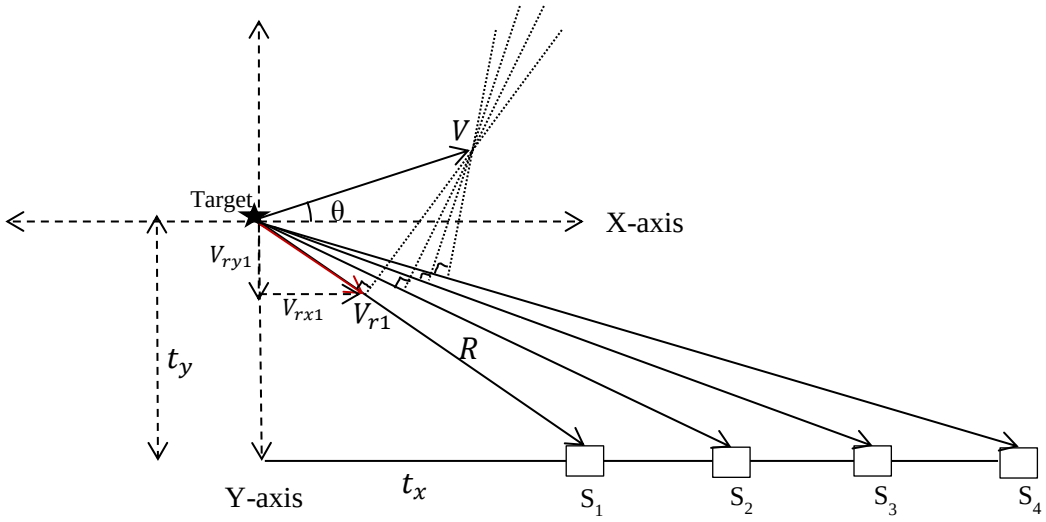

Figure 3.16: Targets velocity obtained by the intersection of perpendiculars from radial velocity to each sensor.

Using the equation of a line in intercept form, $y = mx + c$, the intercept c_i for each sensor i, is given by Eq. (3.11).

$$c_i = v_{ryi} - m_{perp_i} \times V_{rxi} \tag{3.11}$$

Therefore, the coordinates of intersection are given by Eq. (3.12) and Eq. (3.13).

$$x_{inter_i} = \frac{c_{i+1} - c_i}{m_{perp_i} - m_{perp_{i+1}}} \tag{3.12}$$

$$y_{inter_i} = m_{perp_i} * x_{inter_i} + c_i \tag{3.13}$$

These intersection coordinates are the true velocity coordinates. Therefore the velocity of the target is calculated as speed, S_T and direction, θ_T :

$$S_T = \sqrt{{x_{inter}}^2 + {y_{inter}}^2} \tag{3.14}$$

$$\theta_T = tan^{-1}\left(\frac{y_{inter}}{x_{inter}}\right) \tag{3.15}$$

3.2.2.1 Velocity measurement using ambiguity function and R-V line

In the initial stages velocity was assumed to be constant and known in order to simplify the interpretation. However, target detection is not complete until both range and velocity are estimated unambiguously. To include the measurement of the velocity in the proposed strategy, the velocity must be allowed to change within the permissible limits whilst computing the ambiguity function. The ambiguity function will change with velocity. As a result, within the observation area, a greater number of precomputed ambiguity functions have to be considered for the same target positions but varying velocities. This will increase the number of precomputed ambiguity functions required in proportion to the number of steps in speed and direction.

The initial steps of data processing are the same. The data generation is unchanged; the interpretation system takes these frequency shifts as the input for further processing. The first difference is that a very large number of ambiguity function plots must be computed to accommodate velocity variation. The R-V lines are generated for each frequency shift received by the sensors, intersected with the precomputed ambiguity functions and the intersection values recorded.

When the R-V line passes through or very close to the centre of the ambiguity function plot the probability that target is located at the position and velocity where ambiguity function was generated is high. The intersection values between the R-V line and ambiguity function in these cases are high. R-V line for each target is intersected with precomputed ambiguity functions for changing target positions and velocities. All the intersections are recorded and accumulated at the relevant range and velocity (not just range) for each ambiguity function plot. As before when the intersections occur near the centre, the accumulation of the ambiguity function rises rapidly, as shown in Figure 3.10, in contrast to the situation illustrated in Figures 3.8 and 3.9 where the R-V line does not pass close to the centre of the ambiguity function plot. Again the cumulative values are referred to as 'confidence values'. High confidence values indicate a high confidence that the target is at the range and velocity of the confidence plot peak. A threshold is set to eliminate low confidence values from further analysis. Multilateration is used to find the target position after range estimation. The target velocity is also calculated using the radial velocities with respect to each sensor which was explained in Section 3.2.2.

3.3 Algorithm for simulation of range and velocity estimation

Algorithm for 'Data generation system' and 'Data interpretation system' is presented here.

3.3.1 Data generation algorithm

The data generation system described in this section generates frequency shifts for moving targets. Using LFM waveform, the input to this system is:

1. Target position.
2. Sensor position.
3. Chirp time period.
4. Carrier frequency.
5. Modulation frequency and hence bandwidth.
6. Velocity of light.

The output of this algorithm is a frequency shift.

Figure 3.17 describes the definition of the constants and variables required for the simulation. Figure 3.18 describes the steps to calculate the range to the target. Figure 3.19 describes the steps to calculate the radial velocity to the target. And hence Figure 3.20 uses the range and velocity calculated to estimate the frequency shift.

```
% Define Constants
c:        Velocity of light, 3*10^8 m/sec
f_0:      Carrier centre frequency, 76 GHz
f_h:      Modulation frequency, 1 GHz
T_chirp:  Chirp period, 2.5*10^-3 sec.
b:        Bandwidth of chirp, 1 GHz
d:        Distance between the sensors, 0.5m

%Define Variables
(t_x, t_y): Target positon coordinates
V_T:      Target velocity in m/sec
θ:        Target direction(Angle w.r.t x-axis in degrees)
(s_x1, s_y1): Sensor 1 position
(s_x2, s_y2): Sensor 2 position
(s_x3, s_y3): Sensor 3 position
(s_x4, s_y4): Sensor 4 position

% Calculate parameters
        p = 2*f_h / (T_chirp*c)        q = 2*f_0 / c
% Input data
Input the number of targets, n
Input the target coordinates, (t_x, t_y)
Input the target speed and direction, (V_T, θ)
```

Figure 3.17: Definition of constants and variables required for data generation system.

%Calculate range to the target

Algorithm: Target_Range

Input: Target position, sensor position

Output: Range to the target from each sensor, Angle between y-axis and radial velocity

FOR each target, n DO

  FOR each sensor, $i = 1$ to 4, DO

$s_x(i) = (i - 2.5) * d$

$d_0 =$ absolute$(t_x - s_x(1))$

IF $(t_x = 0 \; and \; 0 \le t_y \le 50)$

$R(i) = \sqrt{{R_0}^2 + s_x(i)^2}$

$\beta(i) = cos^{-1}\left\{ {R_0}^2 + R(i)^2 - [(i - 2.5) * d]^2 \Big/ 2 * R_{0*}R(i) \right\}$

ELSEIF $(-8 \le t_x \le -0.75 \; and \; 0 \le t_y \le 50)$

$R(i) = \sqrt{{R_0}^2 + [d_0 + (i - 1) * d]^2}$

$\beta(i) = cos^{-1}\left\{ {R_0}^2 + R(i)^2 - [d_0 + (i - 1) * d]^2 \Big/ 2 * R_{0*}R(i) \right\}$

ELSEIF $(0.75 \le t_x \le 8 \; and \; 0 \le t_y \le 50)$

$R(i) = \sqrt{{R_0}^2 + [d_0 - (i - 1) * d]^2}$

$\beta(i) = cos^{-1}\left\{ {R_0}^2 + R(i)^2 - [d_0 - (i - 1) * d]^2 \Big/ 2 * R_{0*}R(i) \right\}$

ELSEIF$(-0.75 \le t_x \le 0.75 \; and \; 0 \le t_y \le 50)$

$R(i) = \sqrt{{R_0}^2 + [s_x(i) - t_x]^2}$

$\beta(i) = cos^{-1}\left\{ {R_0}^2 + R(i)^2 - [s_x(i) - t_x]^2 \Big/ 2 * R_{0*}R(i) \right\}$

ELSE 'Target out of range'

ENDIF

  ENDFOR

ENDFOR

Figure 3.18: Algorithm to calculate target range.

%Calculate the radial velocity using angles θ and β

Algorithm: Radial_Velocity

Input: Target position, sensor position, target speed and direction

Output: Radial velocity towards each sensor

FOR each target, n DO

  FOR each sensor, $i = 1$ to 4, DO

    IF sensor, i is first sensor

IF $t_x < s_x(1)$ $\alpha(i) = 90 + \theta - \beta(i)$

ELSE $\alpha(i) = 90 + \theta + \beta(i)$

ENDIF

ELSEIF sensor, i is second sensor

IF $t_x < s_x(2)$ $\alpha(i) = 90 + \theta - \beta(i)$

```
                ELSE  α(i) = 90 + θ + β(i)
        ENDIF
    ELSEIF sensor, i is third sensor
            IF  t_x < s_x(3)  α(i) = 90 + θ − β(i)
            ELSE  α(i) = 90 + θ + β(i)
            ENDIF
     ELSEIF sensor, i is fourth sensor
             IF  t_x < s_x(4)  α(i) = 90 + θ − β(i)
             ELSE  α(i) = 90 + θ + β(i)
             ENDIF
     ENDIF
     V_r(i) = V_T * cosα(i)
  ENDFOR
ENDFOR
```

Figure 3.19: Algorithm to calculate the radial velocity of the target towards the sensor.

```
% Frequency shift calculation for four up and down LFM chirps
Algorithm: Frequency_Shift
Input: Target range, radial velocity, carrier frequency, modulation
frequency, speed of light and chirp period
Output: frequency shift for each chirp
FOR each target, n DO
  FOR each sensor, i = 1 to 4, DO
     Δf_1 = p * R(i) + q * V_r(i)
     Δf_2 = −p * R(i) + q * V_r(i)
     Δf_3 = 0.5p * R(i) + q * V_r(i)
     Δf_4 = −0.5p * R(i) + q * V_r(i)
  ENDFOR
ENDFOR
```

Figure 3.20: Algorithm to estimate the frequency shift for each chirp.

3.3.2 Data interpretation algorithm

To simplify processing, the data interpretation system is divided into the following functions:

1. Ambiguity function computation.
2. R-V line and AF plot intersection.
3. Accumulation of confidence values.
4. Target position and velocity estimation.

The algorithm for each of these steps is described in the following sections.

3.3.2.1 Algorithm for ambiguity function computation

This is concerned with the pre-computation of the ambiguity function using Eq. (2.33) and Eq. (2.34). The inputs to this algorithm are:

1. Target position.
2. Target velocity.
3. Target direction of motion.
4. Sensor position.
5. Chirp time period.
6. Carrier frequency.
7. Modulation frequency and hence bandwidth.
8. Velocity of light.

Figure 3.21 defines all the constants and variables used to generate ambiguity function.

Figure 3.22 describes the steps used to generate ambiguity function.

```
% Define Constants and variables
c:          Velocity of light, 3*10^8 m/sec
f_0:        Carrier centre frequency, 76 GHz
f_h:        Modulation frequency, 1 GHz
T_chirp:    Chirp period, 2.5*10^-3 sec
b:          Bandwidth of chirp, 1 GHz
d:          Distance between the sensors, 0.5m
(t_x, t_y): Target positon coordinates
V_T:        Target velocity in m/sec
θ:          Target direction(Angle w.r.t positive x-axis in degrees)
(s_x1, s_y1): Sensor 1 position
(s_x2, s_y2): Sensor 2 position
(s_x3, s_y3): Sensor 3 position
(s_x4, s_y4): Sensor 4 position

        p = 2*f_h / (T_chirp*c)          q = 2*f_0 / c
R_0 = t_y       Perpendicular distance from target to sensor baseline in
metres
d_0 = abs(t_x - s_x1)
            Horizontal distance from target to the first sensor in
metres
R(i)        Target range w.r.t each sensor
```

$\alpha(i)$	Angle between target velocity and radial velocity
$\tau(i)$	Time delay to each sensor
$V_r(i)$	Radial velocity to each sensor
$f_d(i)$	Doppler frequency corresponding each sensor
χ	Ambiguity function
$\mu = b/T_{chirp}$	Chirp slope
m	xAxis counter
n	yAxis counter

% Input data

Input the range of target coordinates, (t_x, t_y)

Input the permissible target speed and direction, (V_T, θ)

Figure 3.21: Definition of constants and variables required to generate an ambiguity function.

% Computation of ambiguity function

Algorithm: Ambiguity_Function

Input: Target position, sensor position, target speed and direction

Output: Ambiguity function at a target position and velocity

FOR target x-coordinate, t_x from -8 to 8 DO

$d_0 = abs(t_x - s_{x1})$

FOR target y-coordinate, t_y from 0 to 50 DO

FOR target velocity, V_T from 0 to 30 DO

FOR target direction, θ from 0 to 360 DO

Initialize χ_{old}=0

FOR sensor, i from 1 to 4 DO

$s_x(i) = (i - 2.5) * d$

IF $(t_x = 0 \; and \; 2 \leq t_y \leq 50)$ DO

$$R(i) = \sqrt{{R_0}^2 + s_x(i)^2}$$

$$\beta(i) = cos^{-1}\left\{ {R_0}^2 + R(i)^2 - [(i - 2.5) * d]^2 \Big/ 2 * R_{0*} R(i) \right\}$$

ELSEIF $(-8 \leq t_x \leq -0.75 \; and \; 0 \leq t_y \leq 50)$ DO

$$R(i) = \sqrt{{R_0}^2 + [d_0 + (i - 1) * d]^2}$$

$$\beta(i) = cos^{-1}\left\{ {R_0}^2 + R(i)^2 - [d_0 + (i - 1) * d]^2 \Big/ 2 * R_{0*} R(i) \right\}$$

ELSEIF $(0.75 \leq t_x \leq 8 \; and \; 0 \leq t_y \leq 50)$ DO

$$R(i) = \sqrt{{R_0}^2 + [d_0 - (i - 1) * d]^2}$$

$$\beta(i) = cos^{-1}\left\{ {R_0}^2 + R(i)^2 - [d_0 - (i - 1) * d]^2 \Big/ 2 * R_{0*} R(i) \right\}$$

ELSEIF$(-0.75 \leq t_x \leq 0.75 \; and \; 0 \leq t_y \leq 50)$ DO

$$R(i) = \sqrt{{R_0}^2 + [s_x(i) - t_x]^2}$$

$$\beta(i) = cos^{-1}\left\{ {R_0}^2 + R(i)^2 - [s_x(i) - t_x]^2 \Big/ 2 * R_{0*}R(i) \right\}$$

ELSE PRINT "Target is out of range"

ENDIF

%Calculate the angle alpha

IF sensor, i is first sensor
  IF $t_x < s_x(1)$ $\alpha(i) = 90 + \theta - \beta(i)$
  ELSE $\alpha(i) = 90 + \theta + \beta(i)$
  END IF
ELSEIF sensor, i is second sensor
  IF $t_x < s_x(2)$ $\alpha(i) = 90 + \theta - \beta(i)$
  ELSE $\alpha(i) = 90 + \theta + \beta(i)$
  END IF
ELSEIF sensor, i is third sensor
  IF $t_x < s_x(3)$ $\alpha(i) = 90 + \theta - \beta(i)$
  ELSE $\alpha(i) = 90 + \theta + \beta(i)$
  END IF
ELSEIF sensor, i is fourth sensor
  IF $t_x < s_x(4)$ $\alpha(i) = 90 + \theta - \beta(i)$
  ELSE $\alpha(i) = 90 + \theta + \beta(i)$
  END IF
ENDIF

$\tau_1(i) = (R(1) + R(i))/c$

$V_r(i) = V_T * cos\alpha(i)$

$f_{d1}(i) = (2 * Vr(i) * f_0)/c$

Initialize counter $m = 0$

FOR $\tau = -\tau_1(i)$ to $\tau_1(i)$ in small steps DO
  Increment counter $m = m + 1$
  Initialize counter $n = 0$
  FOR $f_d = -f_{d1}(i)$ to $+f_{d1}(i)$ in small steps DO

    Increment counter $n = n + 1$

$$|\chi_1(\tau, f_d)| = \left| \left(1 - \frac{|\tau|}{T_{chirp}}\right) \frac{\sin\left(\pi T_{chirp}(f_d + \mu\tau)\left(1 - \frac{|\tau|}{T_{chirp}}\right)\right)}{\pi T_{chirp}(f_d + \mu\tau)\left(1 - \frac{|\tau|}{T_{chirp}}\right)} \right|$$

$$|\chi_2(\tau, f_d)| = \left| \left(1 - \frac{|\tau|}{T_{chirp}}\right) \frac{\sin\left(\pi T_{chirp}(f_d - \mu\tau)\left(1 - \frac{|\tau|}{T_{chirp}}\right)\right)}{\pi T_{chirp}(f_d - \mu\tau)\left(1 - \frac{|\tau|}{T_{chirp}}\right)} \right|$$

$$|\chi_3(\tau, f_d)| = \left| \left(1 - \frac{|\tau|}{T_{chirp}}\right) \frac{\sin\left(\pi T_{chirp}(f_d + 0.5\mu\tau)\left(1 - \frac{|\tau|}{T_{chirp}}\right)\right)}{\pi T_{chirp}(f_d + 0.5\mu\tau)\left(1 - \frac{|\tau|}{T_{chirp}}\right)} \right|$$

$$|\chi_4(\tau, f_d)| = \left| \left(1 - \frac{|\tau|}{T_{chirp}}\right) \frac{\sin\left(\pi T_{chirp}(f_d - 0.5\mu\tau)\left(1 - \frac{|\tau|}{T_{chirp}}\right)\right)}{\pi T_{chirp}(f_d - 0.5\mu\tau)\left(1 - \frac{|\tau|}{T_{chirp}}\right)} \right|$$

$$\chi(n, m) = |\chi_1|^2 + |\chi_2|^2 + |\chi_3|^2 + |\chi_4|^2$$

```
            END FOR
          END FOR
          χ = χ + χ_old
          χ_old = χ
        END FOR
        SAVE/WRITE ambiguity function values, χ to a file
      END FOR
    END FOR
  END FOR
END FOR
```

Figure 3.22: Algorithm to compute ambiguity function for a 4 sensor 4 chirp LFM waveform.

3.3.2.2 Algorithm for R-V line and AF plot intersection

This function computes the parameters of the R-V lines given the frequency shift data from the data generation system. The R-V lines are then used to sample each pre-computed ambiguity function and the values recorded.

The inputs to this algorithm are:

1. Sensor position.
2. Chirp time period.
3. Carrier frequency.
4. Modulation frequency and hence bandwidth.
5. Velocity of light.
6. Frequency shifts obtained in data generation system.

The outputs of this algorithm are:

1. R-V lines calculated from the frequency shifts.
2. Intersections values of these sampled R-V lines with the ambiguity function plots.

The Figure 3.23 defines all the constants and variables used to generate the intersection values between the ambiguity function plot and R-V line. Figure 3.24 shows the algorithm to read the available data for use in further processing. Figure 3.25 shows the algorithm used to obtain the R-V line and AF intersection values.

```
% Define Constants
c:        Velocity of light, 3*10^8 m/sec
f_0:      Carrier centre frequency, 76 GHz
f_h:      Modulation frequency, 1 GHz
T_chirp:  Chirp period, 2.5*10^-3 sec
b:        Bandwidth of chirp, 1 GHz
d:        Distance between the sensors, 0.5m

%Define Variables
(t_x, t_y): Target positon coordinates
V_T:      Target velocity in m/sec
θ:        Target direction(Angle w.r.t x-axis in degrees)
(s_x1, s_y1): Sensor 1 position
(s_x2, s_y2): Sensor 2 position
(s_x3, s_y3): Sensor 3 position
(s_x4, s_y4): Sensor 4 position
R_T1:     Set lower limit of range
R_T2:     Set upper limit of range

% Calculate constants
        p = 2*f_h / (T_chirp*c)          q = 2*f_0 / c
```

Figure 3.23: Definition of the constants and variables used to sample the ambiguity function using the range velocity line.

```
% Read frequency shifts, Δf's from file
OPEN file
READ file
CLOSE file

% Read ambiguity function values for a target position and velocity
OPEN file
READ the number of blocks
FOR each block DO
    READ Target position, (t_x, t_y)
    READ Velocity, V_T
    READ Direction, θ
    READ ambiguity function values, χ
ENDFOR
CLOSE file
```

Figure 3.24: Reading data from the files of pre-computed frequency shifts and ambiguity function.

% Sample ambiguity function along R-V line
Algorithm: Sample_Ambiguity_Function
Input: Frequency shift, carrier frequency, modulation frequency, speed of light, range limits, ambiguity function values for a target position and velocity
Output: Samples of ambiguity function along R-V line
FOR each target DO
    FOR chirp 1 to 4 DO
        FOR sensor 1 to 4 DO
            IF the chirp is first one
                $V_{r1} = (\Delta f_1 - pR_{T1})/q$
                $V_{r2} = (\Delta f_1 - pR_{T2})/q$
            ELSEIF the chirp is second one
                $V_{r1} = (\Delta f_2 + pR_{T1})/q$
                $V_{r2} = (\Delta f_2 + pR_{T2})/q$
            ELSEIF the chirp is third one
                $V_{r1} = (\Delta f_3 - 0.5pR_{T1})/q$
                $V_{r2} = (\Delta f_3 - 0.5pR_{T2})/q$
            ELSEIF the chirp is fourth one
                $V_{r1} = (\Delta f_4 + 0.5pR_{T1})/q$
                $V_{r2} = (\Delta f_4 + 0.5pR_{T2})/q$
            ENDIF
        R-V line starts at (R_{T1}, V_{r1})
        R-V line ends at (R_{T2}, V_{r2})
        ENDFOR
    ENDFOR
    FOR each sensor 1 to 4 DO
        FOR each block DO
            INPUT target position, (t_x, t_y)
            INPUT target velocity, V_T
            INPUT target velocity direction, θ
            INPUT ambiguity function, χ
            FIND target range, R
            FIND angle between y-axis and radial velocity, β
            FIND angle between true velocity and radial velocity, α
            FIND radial velocity, $V_r = V_T cos\ \alpha$
            FOR chirp 1 to 4 DO
                PLOT each R-V line on AF plot using Bresenhams algo
                GET R-V line samples from Bresenhams algorithm, *Line*
                FIND matches between *Line* and χ to get *intersection*
            ENDFOR chirp

            SAVE target position, (t_x, t_y)
            SAVE target velocity, V_T
            SAVE target velocity direction, θ
            SAVE *intersection* to a file
        ENDFOR
    ENDFOR
ENDFOR

Figure 3.25: Sampling the ambiguity function with the R-V line.

3.3.2.3 Algorithm for accumulating confidence values

This part of the simulation accumulates the intersection ambiguity values at a range and velocity.

Figure 3.26 shows the algorithm used for accumulation of confidence values.

```
% Accumulate confidence values
Algorithm: Accumulate_Confidence_Values
Input: AF samples along R-V line
Output: Peaks of cumulative AFs, range, radial velocity
FOR each sensor 1 to 4 DO
    READ RV-AF intersection file
    READ the number of blocks
    FOR each block
        READ position
        READ velocity
        READ direction
        READ RV-AF intersection matrix
        Accumulate AF values for same range-velocity pairs
        Obtain a unique matrix of cumulative intersections
    ENDFOR
    Set a threshold for AF value
    Find peaks of cumulative AFs (confidence values)
    Find corresponding Range and Radial velocity of confidence values
ENDFOR
Save this Range and Radial velocity pair for each sensor
```

Figure 3.26: Algorithm for accumulating confidence values.

3.3.2.4 Algorithm for target position and velocity estimation

Having obtained the range and radial velocity for each sensor in the preceding step, here the target position and velocity are estimated. The information obtained from each sensor is combined to obtain the target position and velocity using multilateration, a technique described in Section 2.7.1 of Chapter 2. Target velocity is computed using Figure 3.16 and Eq. (3.14) and Eq. (3.15).

Figure 3.27 shows the algorithm to determine on which side of the sensor central line the target lays and to find target position. Figure 3.28 describes the algorithm to compute the true velocity of the target.

```
% Estimate target position
Algorithm: Target_Position
Input: Target range to each sensor
Output: Target position
%Check if target is on RHS of the sensors central line
IF (R(2) > R(3))
   ∠A = cos^-1 ( R(3)^2 + d^2 − R(4)^2 / 2 * R(3) * d )
   IF (∠A is obtuse) ∠A = 180^0 − ∠A
   ∠B = 90^0 − ∠A
   t_x_increment = R(3) * sin ∠B
   IF (∠A is obtuse) t_x = d/2 − t_x_increment
   ELSE t_x = d/2 + t_x_increment
   t_y_increment = R(3) * sin ∠A
ENDIF
%Check if target is on LHS of the sensors central line
IF (R(2) < R(3))
   ∠A = cos^-1 ( R(2)^2 + d^2 − R(1)^2 / 2 * R(2) * d )
   IF (∠A is obtuse) ∠A = 180^0 − ∠A
   ∠B = 90^0 − ∠A
   t_x_increment = R(2) * sin ∠B
   IF (∠A is obtuse) t_x = −(d/2 − t_x_increment)
   ELSE  t_x = −(d/2 + t_x_increment)
   t_y_increment = R(2) * sin ∠A
ENDIF

%Check if target is on the sensors central line
IF (R(2) = R(3))
    t_x = 0
    t_y = √(R(2)^2 − (d/2)^2)
ENDIF
```

Figure 3.27: Algorithm to estimate target position.

```
% Estimate target velocity
Algorithm: Target_Position
Input: Radial velocity to each sensor, target position, sensor
position
Output: Target velocity
FOR sensor 1 to 4 DO
     s_x(i) = (i − 2.5) * d
     Change the origin so that target is at(0,0).
     Hence the sensors are now at:
         s_x_shift(i) = s_x(i) − t_x
         s_y_shift(i) = s_y(i) − t_y

 %Radial velocity coordinates after change of origin
```

$$V_{rx\_shift}(i) = \left(V_r(i) * s_{x\_shift}(i)\right) \Big/ \sqrt{\left(s_{x\_shift}(i)\right)^2 + \left(s_{y\_shift}(i)\right)^2}$$

$$V_{ry\_shift}(i) = \left(V_r(i) * s_{y\_shift}(i)\right) \Big/ \sqrt{\left(s_{x\_shift}(i)\right)^2 + \left(s_{y\_shift}(i)\right)^2}$$

Gradients of radial velocity lines, $Grad\_V_r(i) = V_{ry\_shift}(i) \Big/ V_{rx\_shift}(i)$

Gradients of lines perpendicular to radial velocity lines, $GradPerp\_V_r(i) = -\left(1 \Big/ Grad\_V_r(i)\right)$

Intercept of perpendicular lines, using $(y = mx + c)$

$c(i) = V_{ry\_shift}(i) - GradPerp\_V_r * V_{rx\_shift}(i)$

ENDFOR

$$x_{intersection}(i) = (c(i+1) - c(i)) \Big/ (GradPerp\_V_r(i) - GradPerp\_V_r(i+1))$$

$$y_{intersection}(i) = GradPerp\_V_r(i) * x_{intersection}(i) + c(i)$$

Find target speed, $S_T = \sqrt{(x_{intersection})^2} + (y_{intersection})^2$

Find target direction, $\theta_T = \tan^{-1}\left(y_{intersection} \Big/ x_{intersection}\right)$

Plot t_x, t_y

Plot S_T, θ_T

Figure 3.28:Algorithm to estimate target velocity.

Chapter 4 presents some of the results achieved using this method.

Chapter 4

4 Experimental system

4.1 Introduction

In order to evaluate the novel strategy proposed in Chapter 3 we present the simulation results obtained for each part of our proposed method. Section 4.2 gives an overview of the system under consideration, the observation area and defines the system parameters for simulation which form the basis of experimental method. The later sections present the results of the simulation. The simulation results for estimating the range to a single target, to each of multiple targets are presented, assuming that the velocity of each target is known and constant. Results are also presented for single and multiple targets with an unknown and variable velocity.

4.2 Overview of the system setup

The simulation considers a system with four short range, wide angle radar sensors mounted behind the front bumper of an experimental car, as illustrated in Figure 4.1. This configuration is based on that of the RadarNet European Commission project [99]. Within this project several applications have already been implemented and tested using a variety of interpretation strategies but not that reported here.

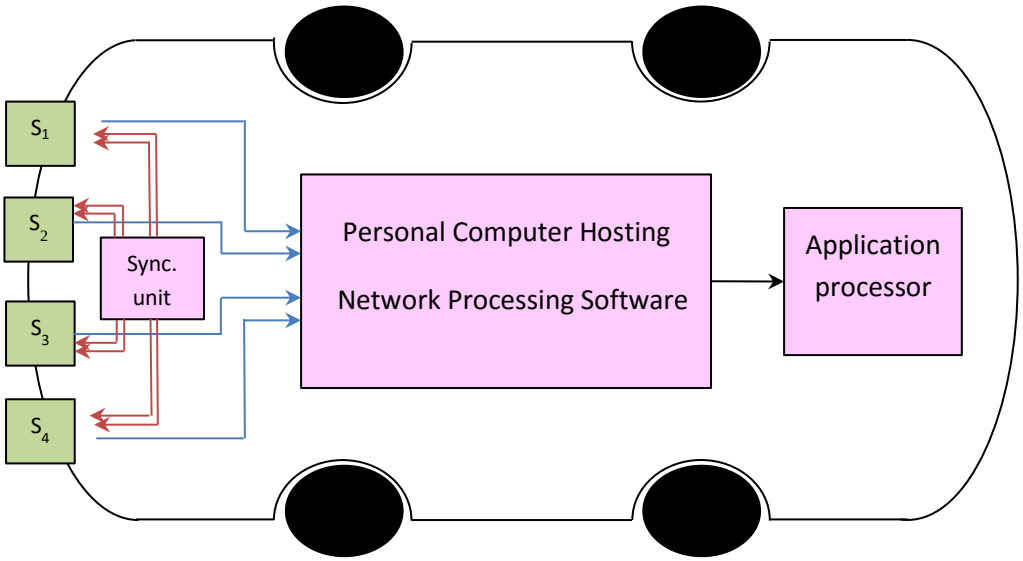

Figure 4.1: Overview of radar network hardware

4.2.1 Sensor positioning and observation area

The network of radar sensors envisaged in this project would have four short range, wide angle sensors facing forwards. For convenience these sensors would be positioned equidistant from each other, at the same height behind the front bumper of the vehicle. Here we assume that the distance between each pair of sensors is 0.5 m. The observation area for target detection is shown diagrammatically in Figure 4.2 for a multi-lane road. Each lane is assumed to be a nominal 4.5 metres wide. In addition to the lanes on either side of the "experimental vehicle", an additional band, roughly 1 m wide is also considered as a safety margin. Figure 4.2 shows the physical arrangement of the sensors in a space 16 m wide and 50 m in length. This observation area is sufficient to consider the operation of short range radar on an urban road. These parameters can easily be varied to consider motorways or countryside roads.

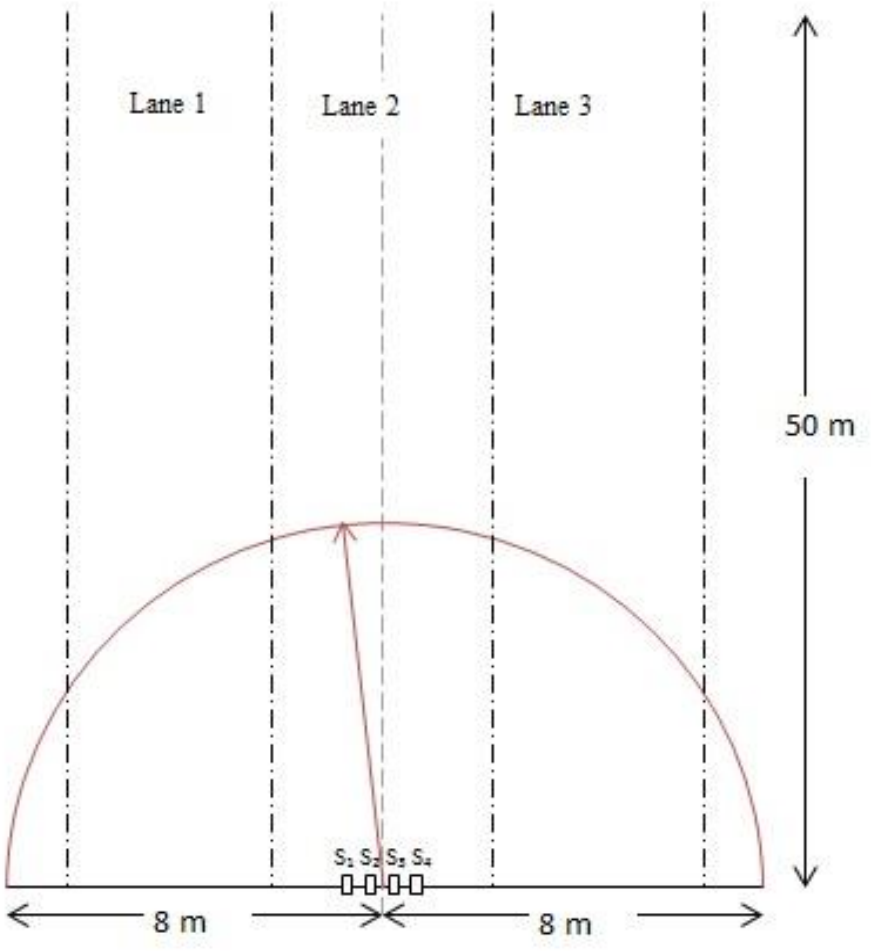

Figure 4.2: Arrangement of four sensors in a space that represents an urban road.

4.2.2 Experimental parameters

A four chirp waveform operating at 76 GHz was considered as the transmission waveform. The four chirps, each with a period of 2.5 ms, consist of an up and down chirp with a bandwidth of 1 GHz and an up and down chirp with a bandwidth of 0.5 GHz. This waveform is designed to resolve multiple targets with a short cycle time of 10 ms. The operating frequency can be varied in accordance with the regulations of various countries. The Table 4.1 shows the specification parameters.

Table 4.1: Project experimental parameters

Radar Parameters		
1.	Radar type	FMCW radar
2.	Radar waveform	4 chirp FMCW
3.	Carrier frequency	76 GHz
4.	Modulating frequency	0.5-1 GHz
5.	Chirp time period	2.5 ms
6.	Distance detection range	Up to 50 m
7.	Velocity detection range	0-30 m/s

A vehicle on an urban road is considered to have a maximum speed of 100 km/h = 27.78 m/s or, rounded to the closest decade, 30 m/s. The velocity of the target therefore could be 0 to 30 m/s. However, this velocity can be higher when considering vehicles on a motorway.

4.3 Simulation results for target range

Target range is estimated using information from the ambiguity function plot and the R-V line. In this section results are presented for the simulation for ambiguity function plots at a variety of target positions, sampled along R-V lines with confidence values accumulated at the same range for each AF plots.

4.3.1 Ambiguity function plots

The ambiguity function plot of a single up or down chirp is very well established. This function is commonly plotted for low frequencies of few Hertz and a time period of few seconds. The shape of the ambiguity function changes with these parameters as shown in Figure 4.3. The ambiguity function plotted in Figure 4.3 (a) is for a single chirp at

low operating frequency which can be seen in many text books such as [21], [34] and [22].

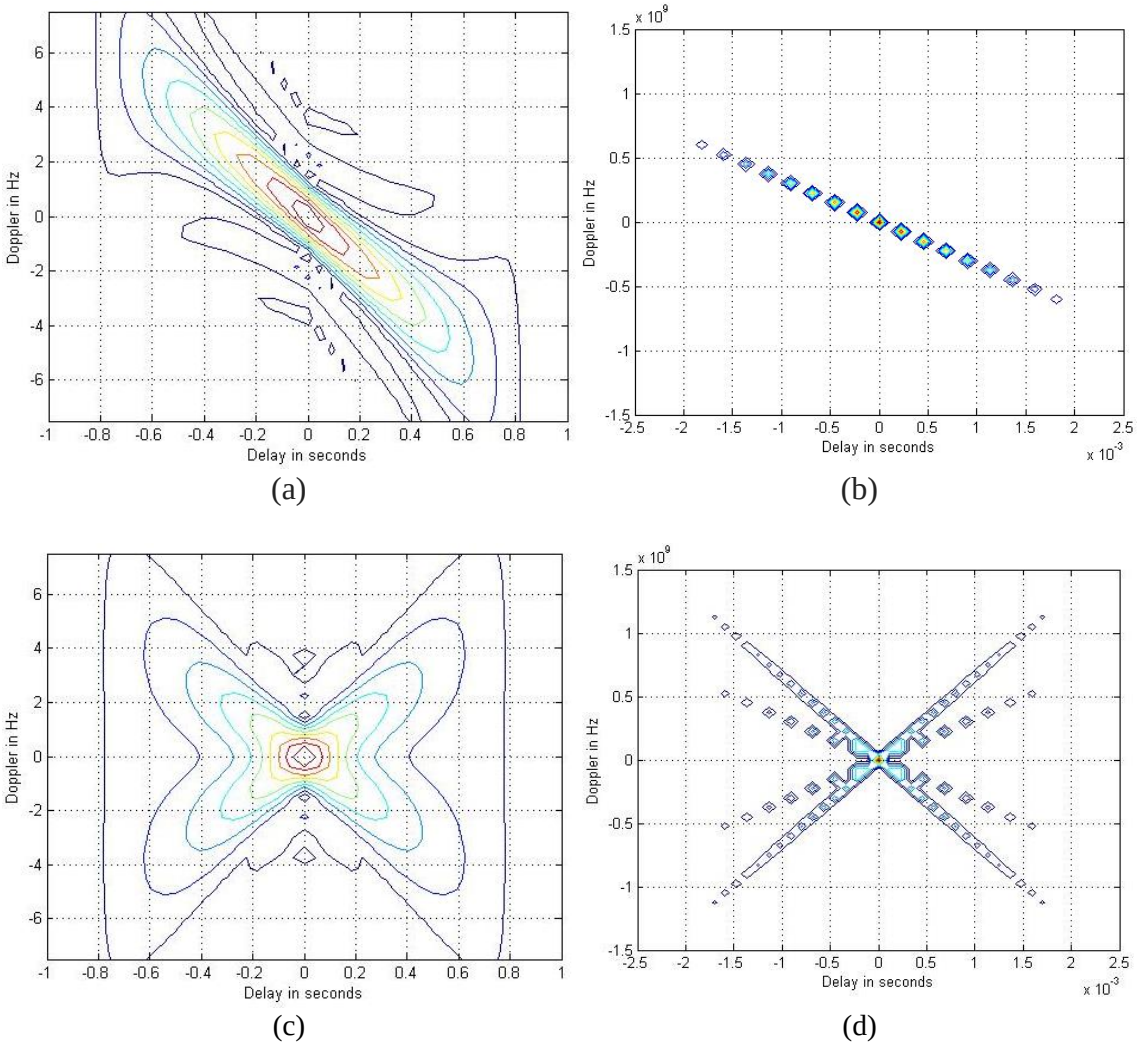

Figure 4.3: Ambiguity function plots for a single up chirp with (a) a bandwidth of 5 Hz and a time period of 1s, (b) a bandwidth of 1 GHz and a time period of 2.5 ms. Ambiguity function plot for a four chirp waveform with (c) a bandwidth of 2.5-5 Hz and a time period of 1 s and (d) a bandwidth of 0.5-1 GHz and a time period of 2.5 ms

.

The low frequency plot of Figure 4.3 (a) has a series of peaks close to the zero delay Doppler axis. In the high frequency plot of Figure 4.3 (b) there are a series of peaks along the ridge of the ambiguity function. The ambiguity function for a chirp was first cited in Chapter 2 as Eq. (2.33) and is repeated here in Eq. (4.1).

$$|\chi(\tau, f_D)|^2 = \begin{cases} \left| \left(1 - \frac{|\tau|}{T_{chirp}}\right) \frac{\sin\left(\pi T_{chirp}(\mu\tau + f_D)\left(1 - \frac{|\tau|}{T_{chirp}}\right)\right)}{\pi T_{chirp}(\mu\tau + f_D)\left(1 - \frac{|\tau|}{T_{chirp}}\right)} \right|^2 & if\ |\tau| \le T_{chirp} \\ 0 & otherwise \end{cases} \quad (4.1)$$

It is not easy to see how the ambiguity function varies with position in Eq. (4.1), therefore we consider a series of empirical plots starting with Figure 4.4. Figure 4.4 shows the ambiguity function at a series of positions. Only the position at which the ambiguity function is computed is changed in the plots of Figure 4.4.

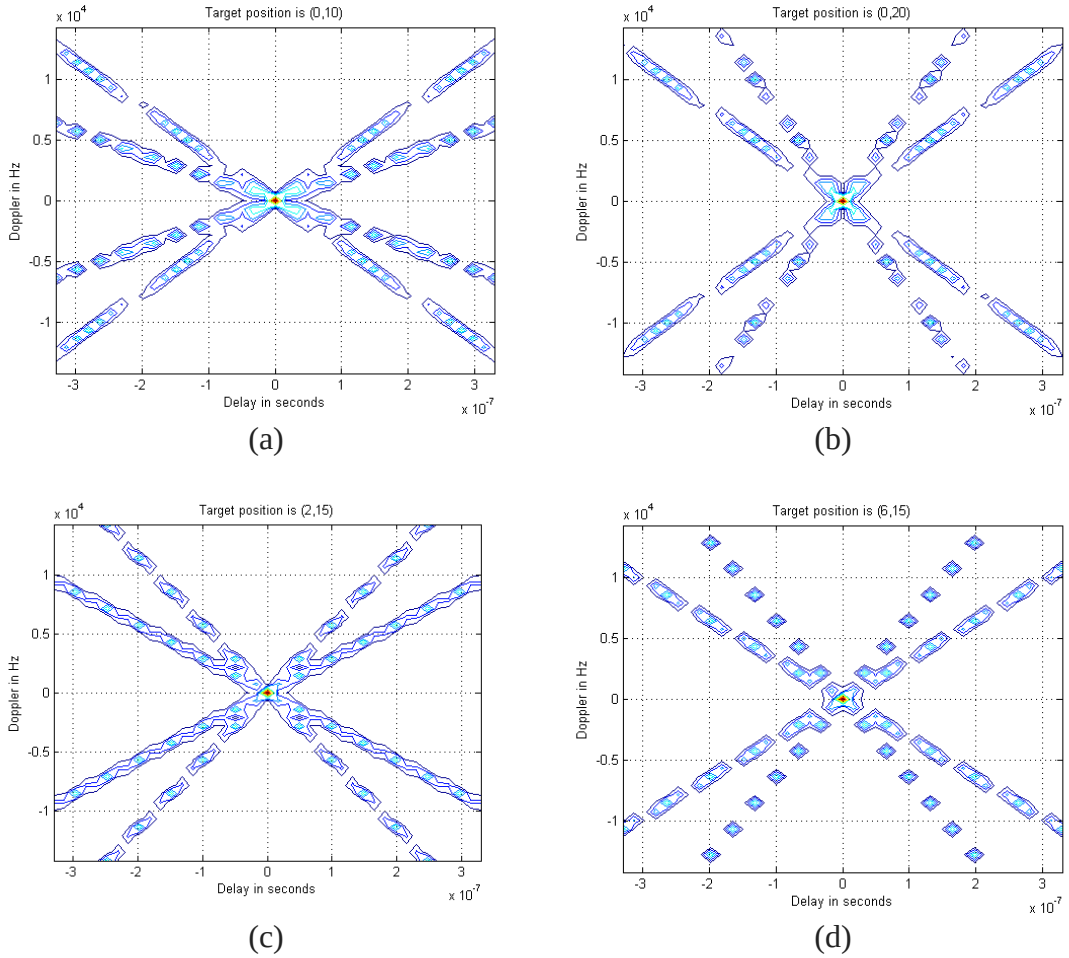

Figure 4.4: Ambiguity function for a four chirp waveform for targets at (a) (0, 10), (b) (0, 20), (c) (2, 15) and (d) (6, 15).

Figure 4.4 (a) and (b) show how the ambiguity function plot changes with longitude and Figure 4.4 (c) and (d) show how it changes with latitude.

4.3.2 Ambiguity function and range-velocity lines intersection

Knowledge of how the ambiguity function changes with position is used to estimate target range. However, knowing just the ambiguity function at various positions is not sufficient for target range estimation. The frequency shift of the signal reflected from a target can correspond to a target at a variety of ranges travelling at various velocities towards the sensor. These range and velocity values are related by an equation for FMCW radar as discussed in Chapter 2 and re-cited in Eq. (4.2).

$$f_b = \frac{2V_r f_0}{c} \pm \frac{2Rf_h}{T_{chirp}c} \tag{4.2}$$

Eq. (4.2) defines the relationship between the range and velocity, the R-V line. An R-V line is intersected with a number of AF plots within the physical search space. Figure 4.5 shows the ambiguity function at different target positions within the observation area adopted for this project. These AF plots are intersected by R-V lines for a target at the same position as one AF plot. Where the R-V lines cut the ambiguity function is highlighted by the red circle in Figure 4.5 (a). From this crossing, the intersection values are sampled for further processing. The ambiguity functions in Figure 4.5 have a higher resolution with 101 steps compared to Figure 4.4 which has only 41. If the resolution is not sufficiently fine sampling with the R-V lines will generate null values.

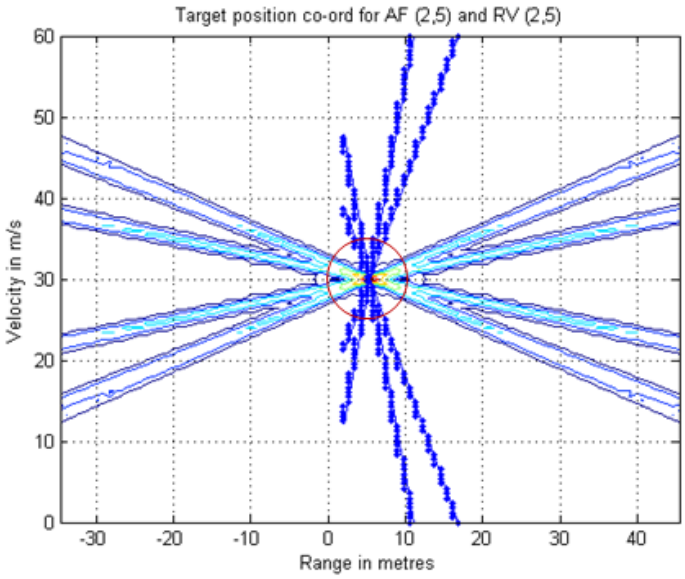

Figure 4.5 (a)

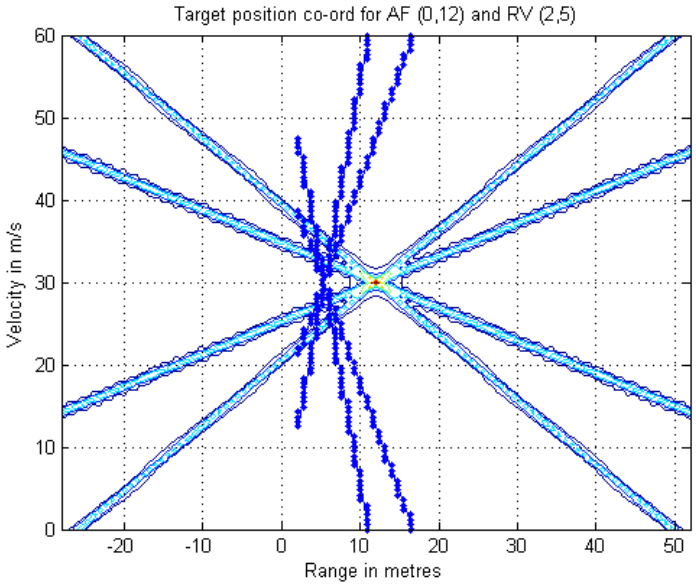

Figure 4.5 (b)

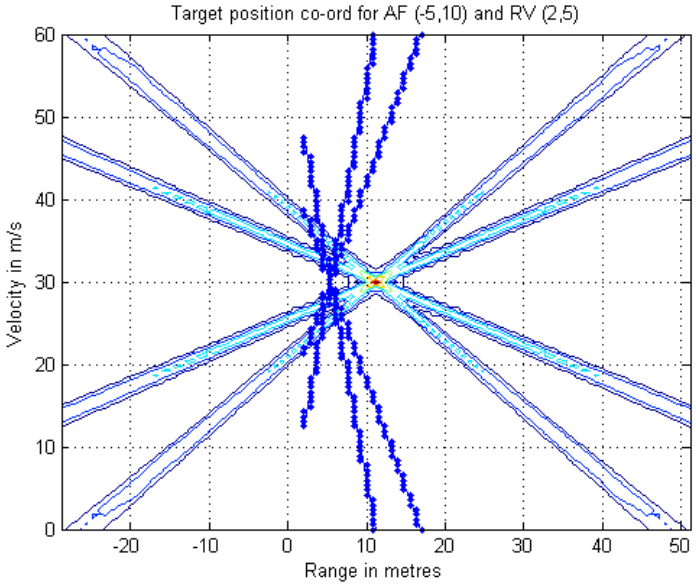

(c)

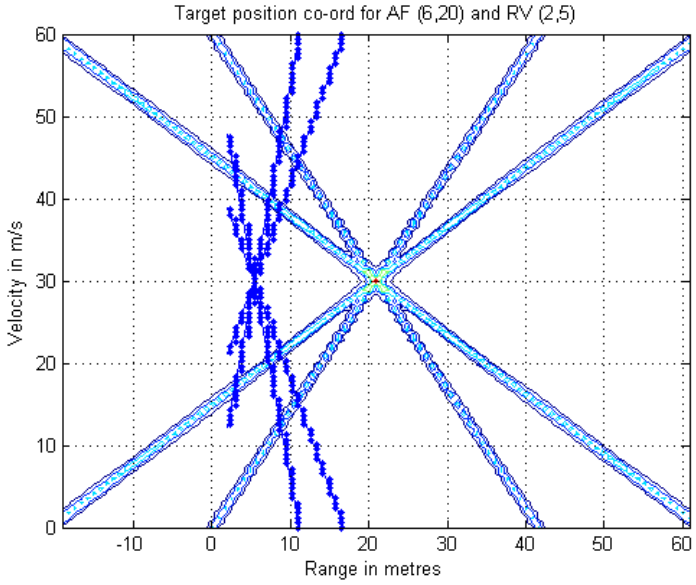

(d)

Figure 4.5: Intersection of ambiguity function plot with 101 steps and range-velocity lines (a) AF plot and the R-V line are at the same target positions (2, 5), (b) AF plot is at (0, 12) and the R-V line at (2,5), (c) AF plot is at (-5, 10) and the R-V line at (2,5) and (d) AF plot is at (6, 20) and the R-V line at (2,5).

The plots of Figure 4.5 show the intersection of a number of ambiguity function plots at different target positions with the R-V lines at the same target position. Figure 4.5 (a) shows that when the R-V lines and the ambiguity function are generated for the same

target position, the R-V lines pass through the centre of the ambiguity function. If the positions are not the same then the R-V lines do not pass through the centre of the ambiguity function as shown in Figure 4.5 (b), (c), (d). The R-V lines are then intersected with ambiguity function plots for a variety of target positions. The ambiguity function plots corresponding to the target position are selected as those which return the maximum value in the R-V line sampling. We refer to these sampled values as 'confidence values' and they are used to indicate the likelihood of finding the target at that position as shown in Figure 4.6. The confidence plots built from the intersection of AF plots and R-V lines of Figure 4.5 show that there is higher value of confidence when the R-V line passes close to the centre of the AF plot.

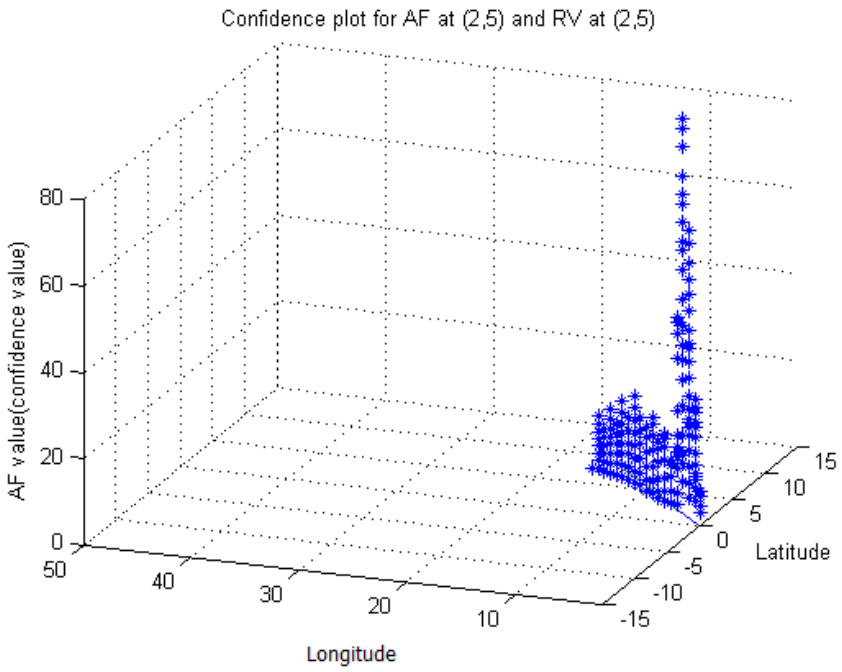

Figure 4.6 (a)

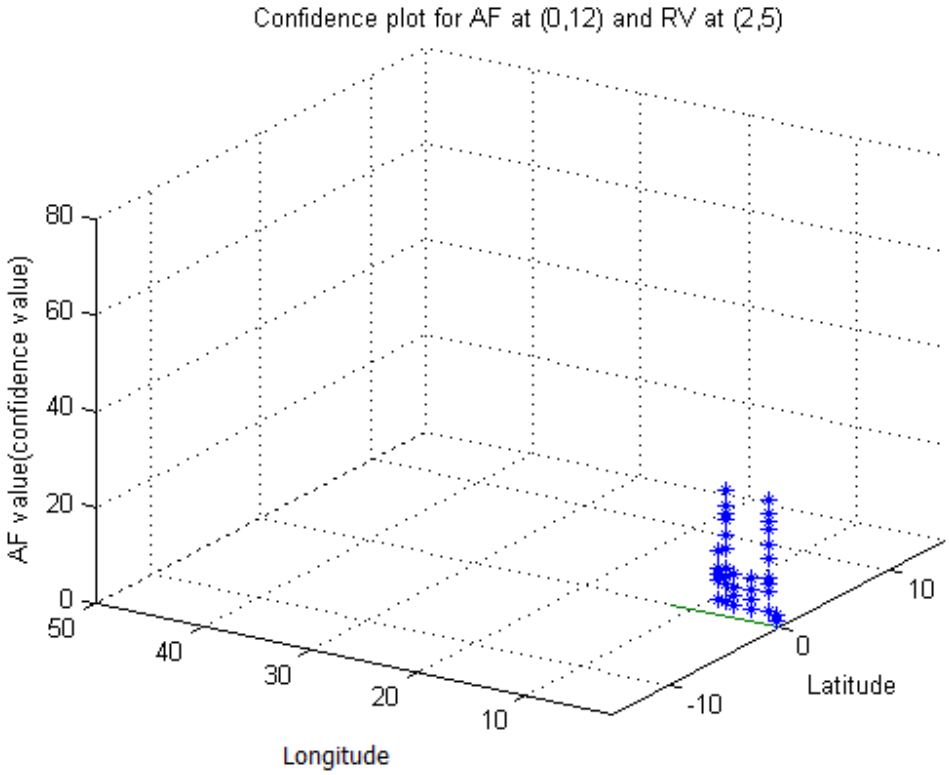

Figure 4.6 (b)

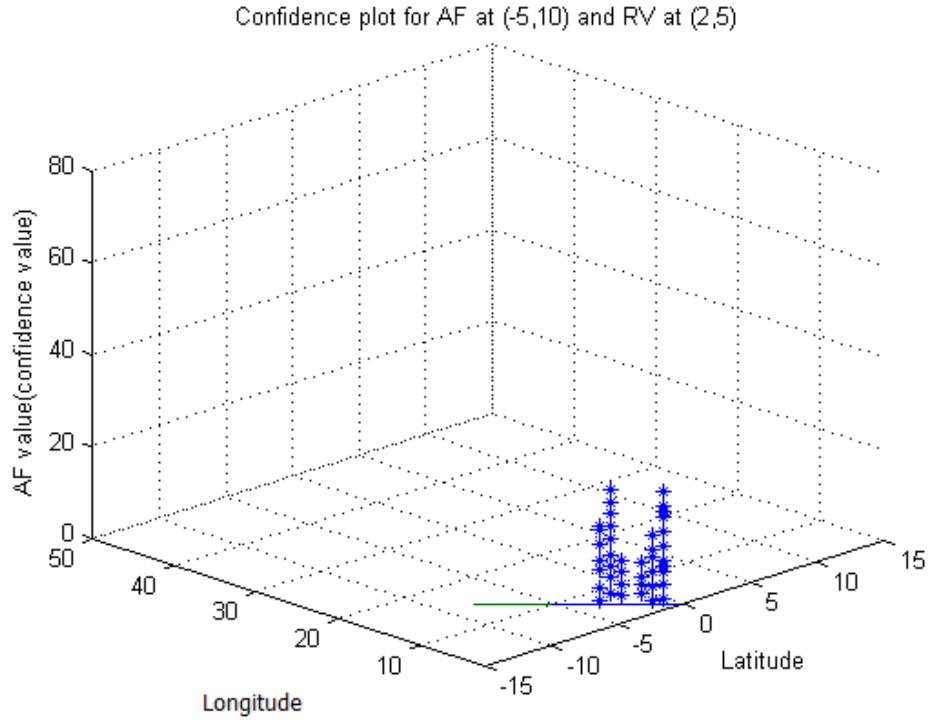

Figure 4.6 (c)

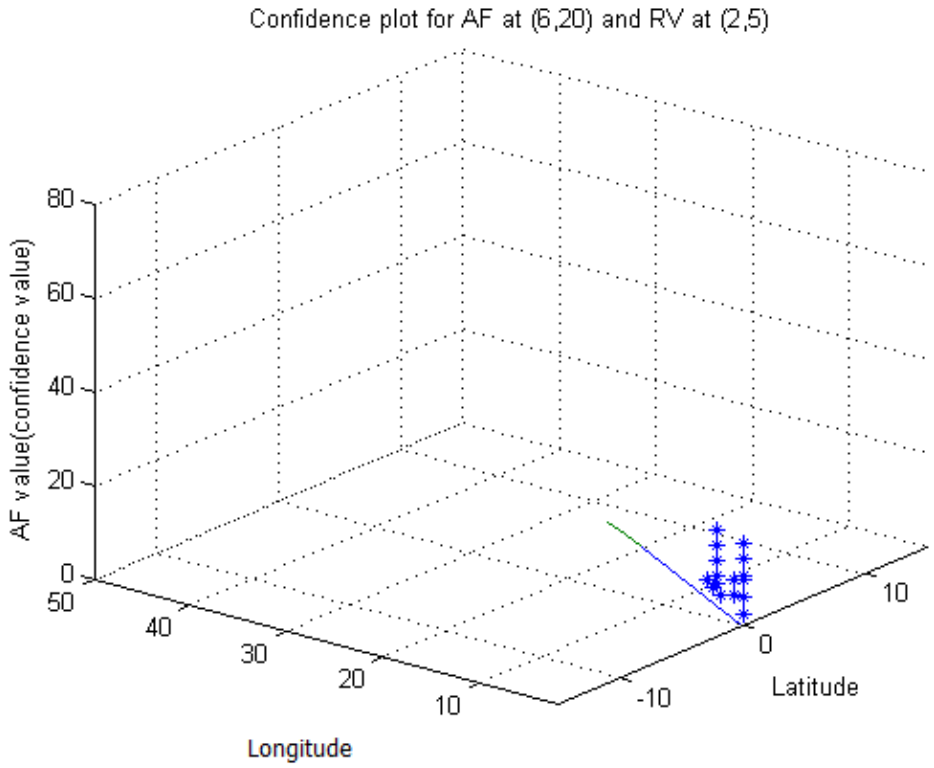

(d)

Figure 4.6: Confidence plot obtained from the intersection values of AF plot and R-V lines at position (2, 5) with (a) AF plot at (2, 5), (b) AF plot at (0, 12), (c) AF plot at (-5, 10) and (d) AF plot at (6, 20).

Figures 4.7 – 4.10 show the same results for another set of target positions and demonstrate the concept of confidence building when R-V line passes through the centre of the AF plot.

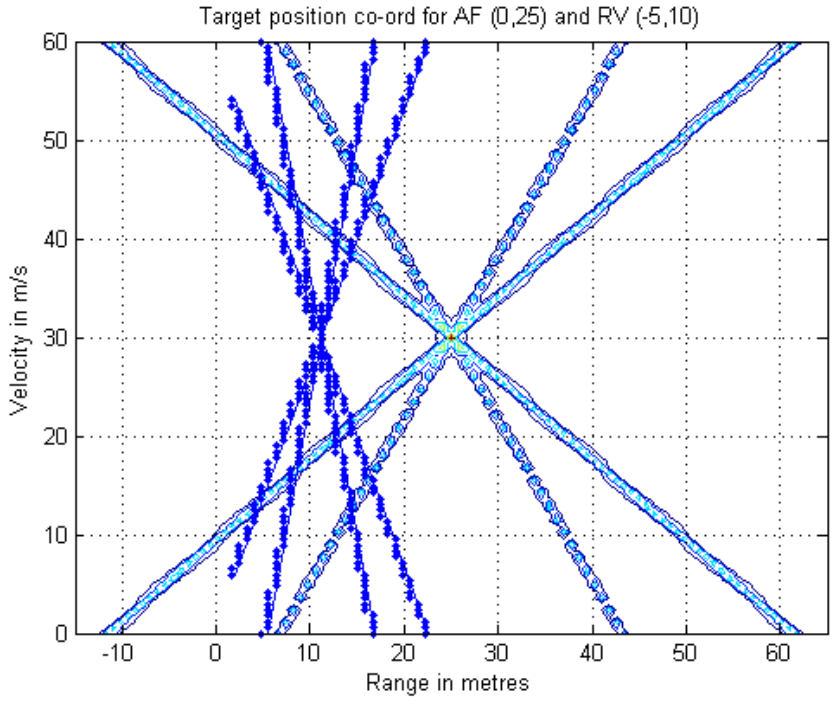

(a)

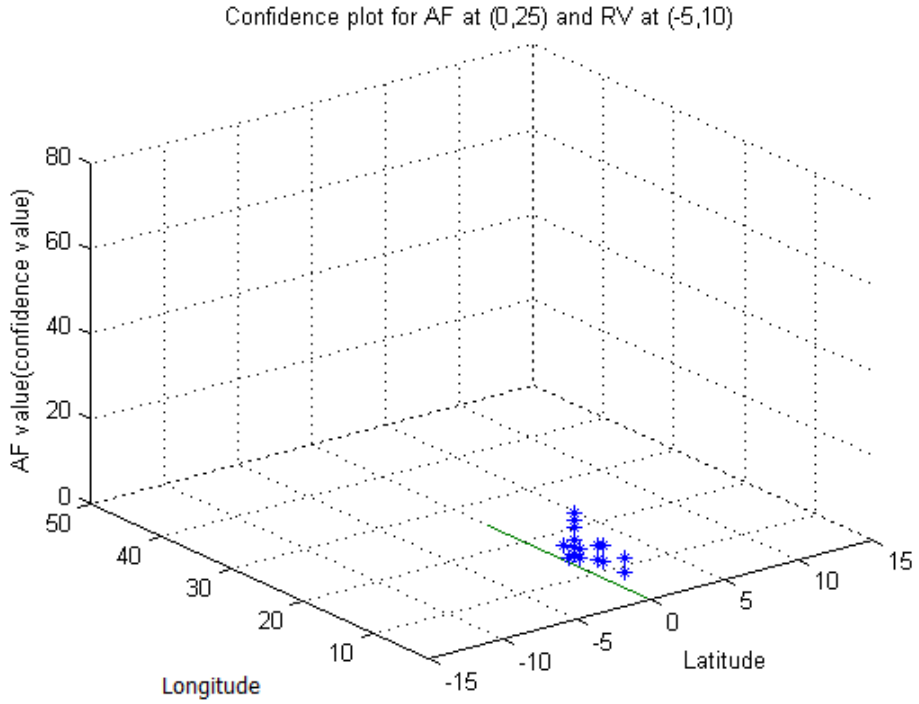

(b)

Figure 4.7: (a) Intersection of AF plot at (0, 25) and R-V line at (-5, 10) and (b) Confidence plot.

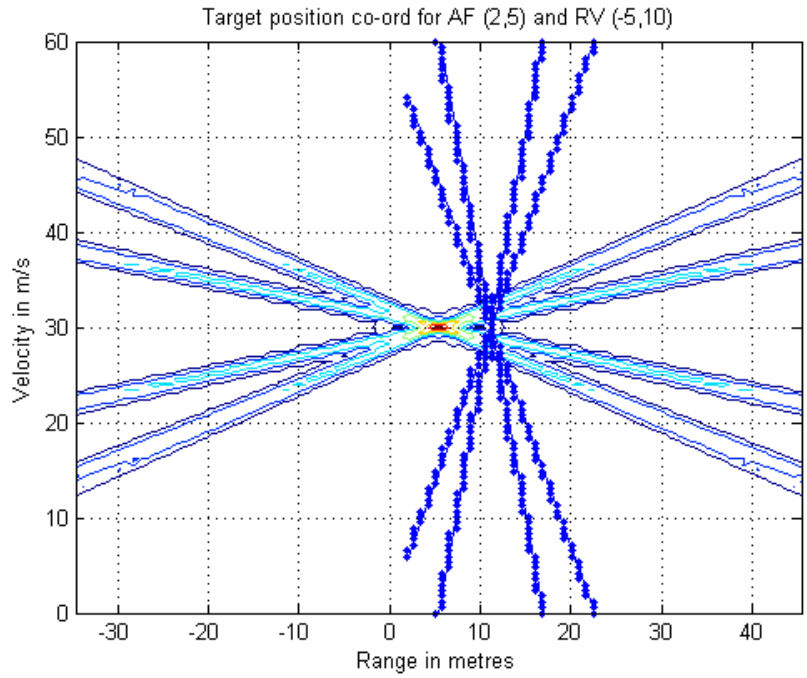

(a)

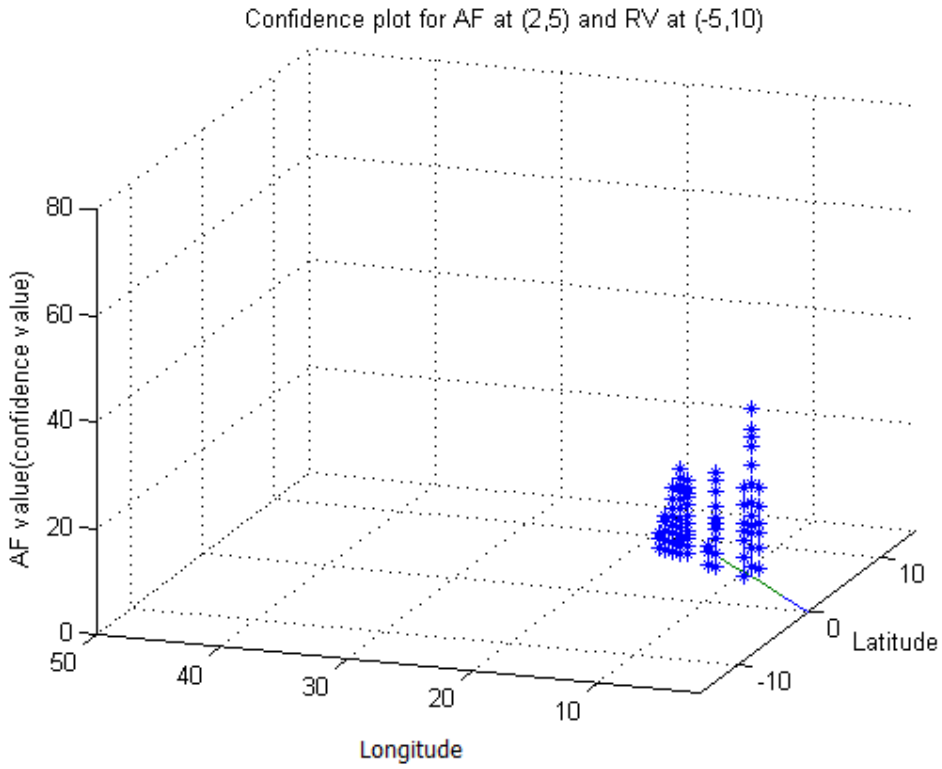

(b)

Figure 4.8: (a) Intersection of AF plot at (2, 5) and R-V line at (-5, 10) and (b) Confidence plot.

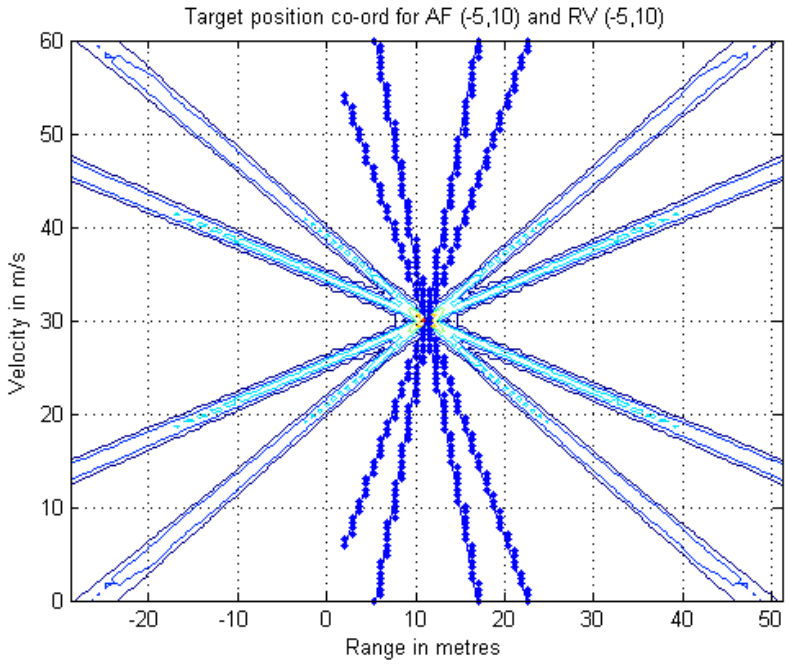

(a)

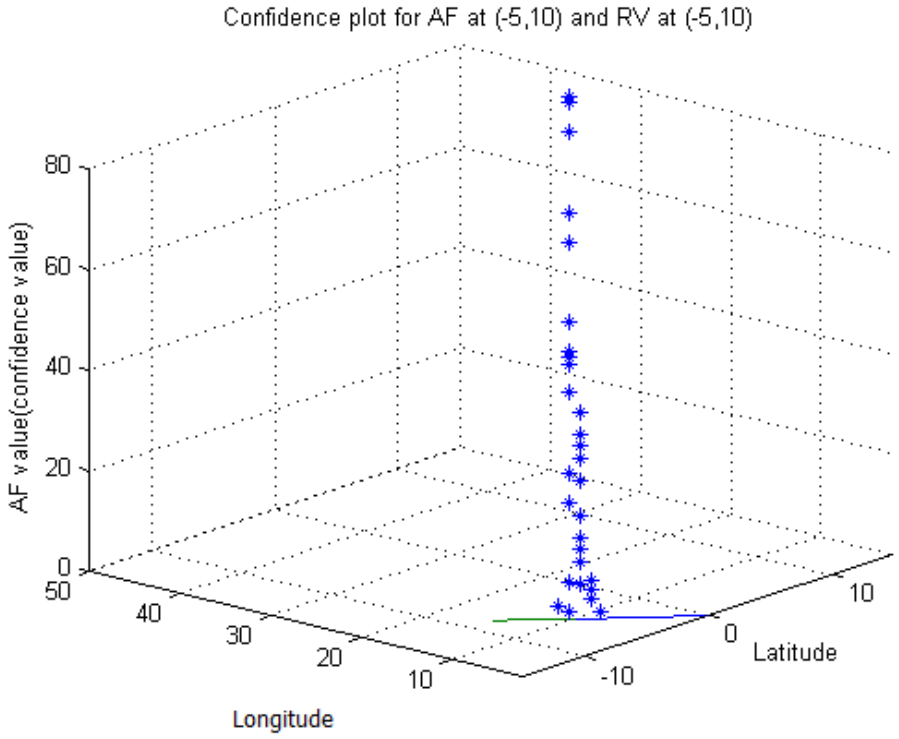

(b)

Figure 4.9: (a) Intersection of AF plot at (-5, 10) and R-V line at (-5, 10) and (b) Confidence plot.

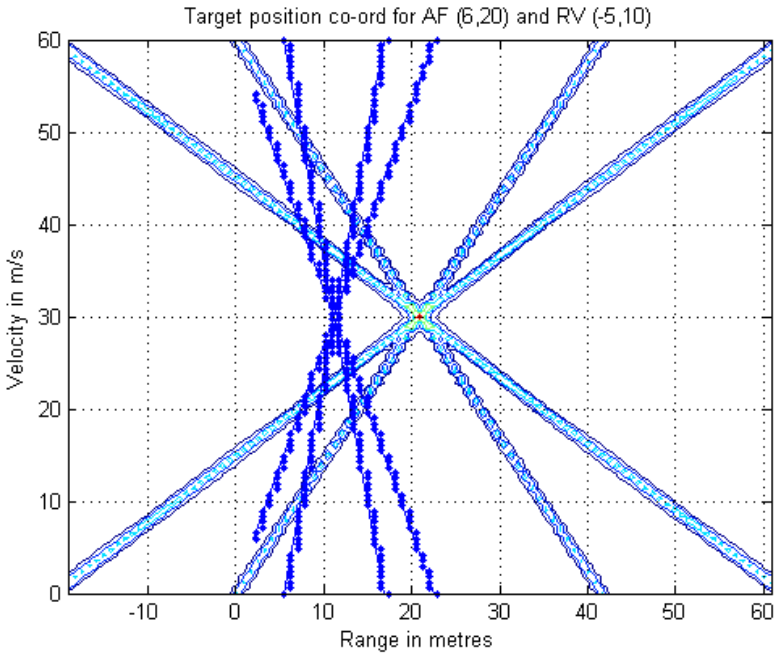

(a)

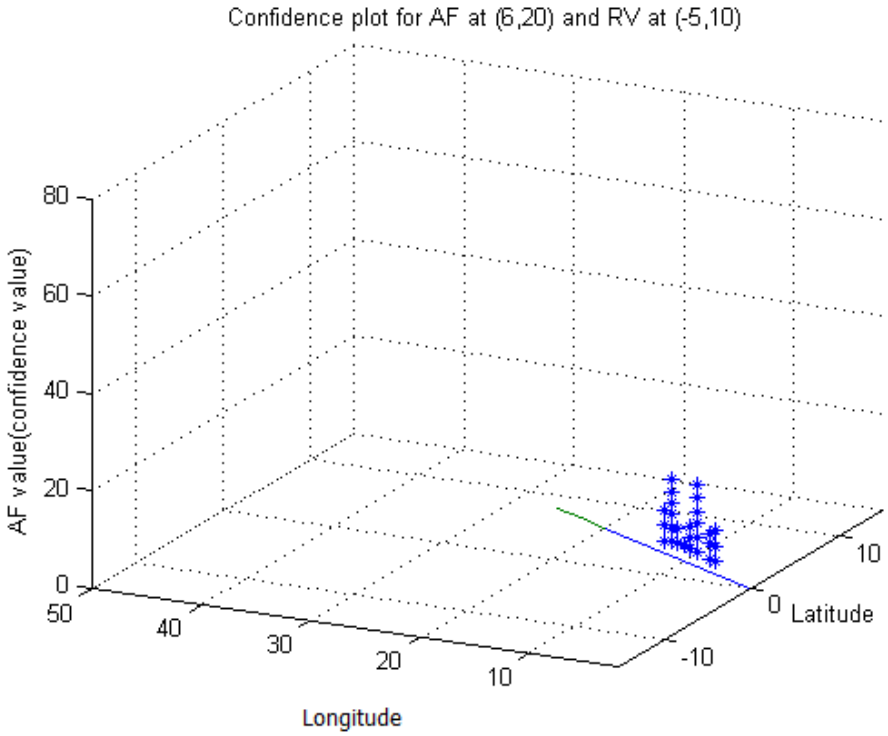

(b)

Figure 4.10: (a) Intersection of AF plot at (6, 20) and R-V line at (-5, 10) and (b) Confidence plot.

Figures 4.6 – 4.10 show how the confidence values accumulate when the R-V line generated at a target position coincides with the target position at which the ambiguity function was plotted. In each plot the velocity was assumed to be known and fixed at 30 m/s to simplify initial simulation.

4.3.3 Building confidence plots for a single target

When the R-V line generated for a target return was used to sample a set of AF plots, high confidence values, corresponding to the location of the target were obtained. This is because the R-V line passed close to the centre of ambiguity function plots for the matching ranges as compared to the R-V lines which passed away from the centre. This is also confirmed by the simulation results in the later part of this section.

The number of ambiguity function plots that must be considered for intersection with an R-V line at each target position is not predefined. Based on the extent by which ambiguity function changes with position, a step of 2 m in latitude and 5 m in longitude was considered. Figures 4.11 and 4.12 show the change in ambiguity function in steps of two metres for latitude and steps of five metres for longitude.

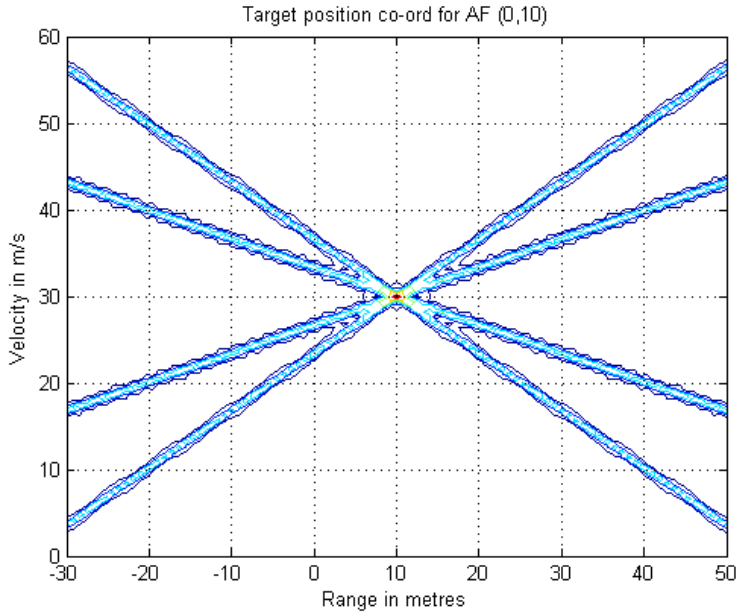

Figure 4.11 (a)

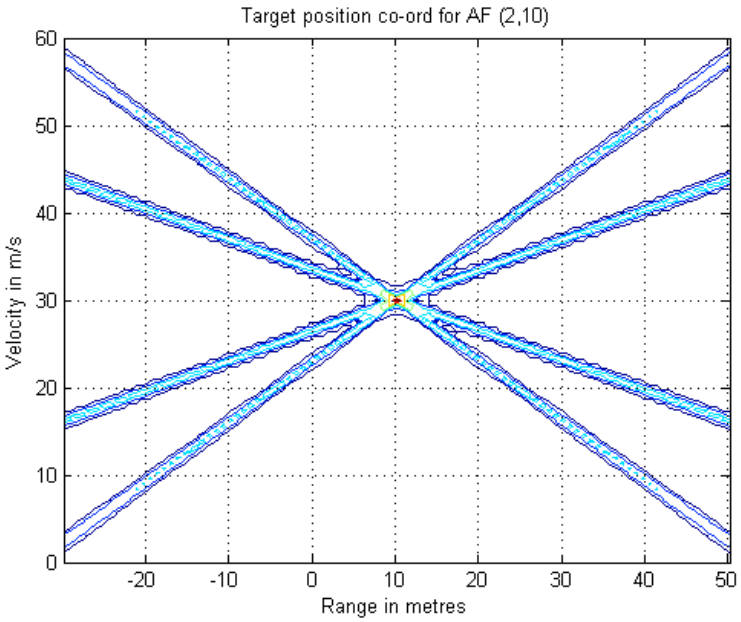

Figure 4.11 (b)

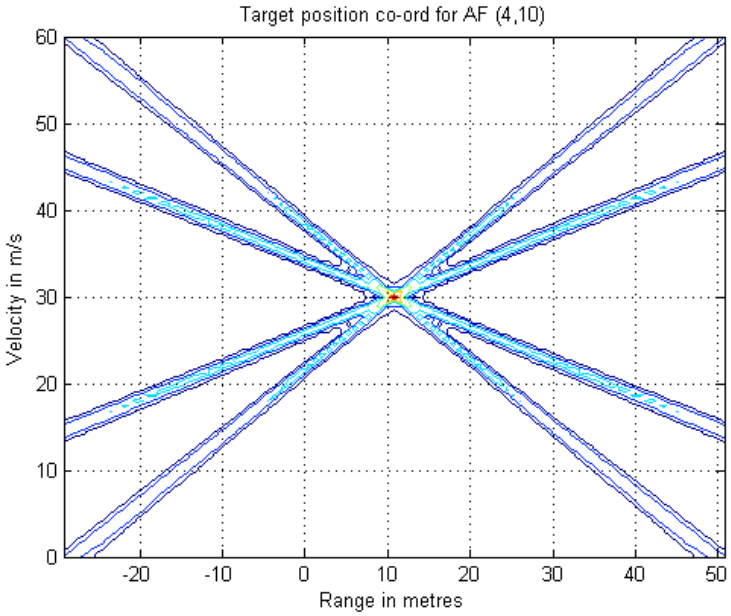

(c)

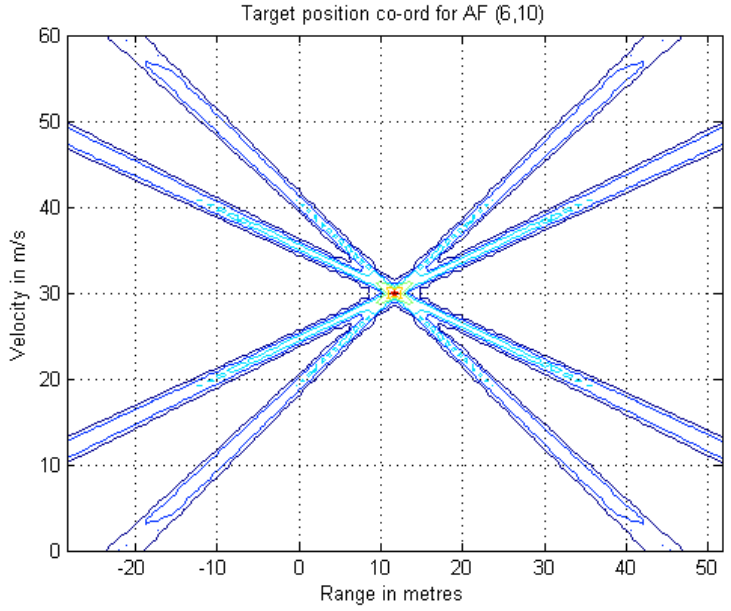

(d)

Figure 4.11: Change in ambiguity function with a 2 m step change in latitude. AF plot at longitude of 10 m and latitude of (a) 0 m, (b) 2 m, (c) 4 m and (d) at 6 m.

Figure 4.11 (a), (b), (c) and (d) show that there is not a significant change between the two consecutive ambiguity functions and the steps considered are justified. Similarly,

the change in the ambiguity function with 5 m steps in longitude is shown in Figure 4.12.

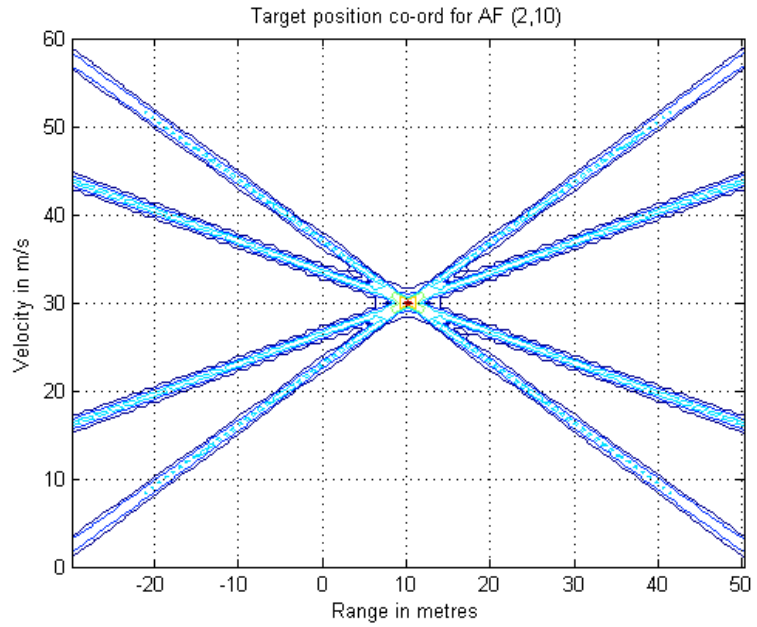

Figure 4.12 (a)

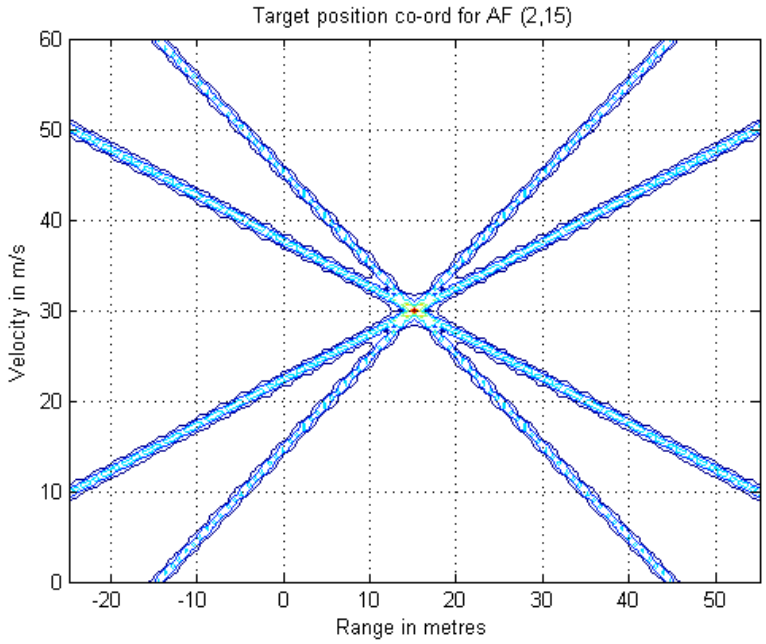

Figure 4.12 (b)

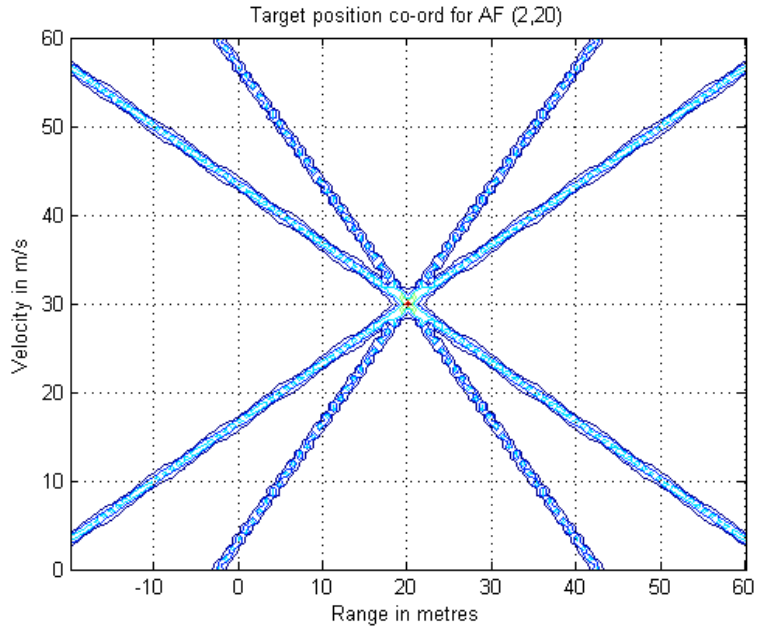

(c)

Figure 4.12: Change in ambiguity function with a 5 m step change in longitude. AF plots at a latitude of 2 m and a longitude of (a) 10 m, (b) 15 m and (c) 20 m.

Figure 4.11 shows that there is no significant change in the two consecutive ambiguity functions taken at the same longitude but two metre apart latitude. Figure 4.12 shows no significant change in the two consecutive ambiguity functions taken at the same latitude but five metre apart longitude.

Sampling of various ambiguity function plots along the R-V lines is recorded and accumulated at the same range. Cumulative values at a range are the confidence values of the targets presence at that range. A threshold is applied to eliminate low confidence values. Peaks in confidence values are detected and their associated positions give the estimated target position.

Figures 4.13 – 4.15 show the cumulative confidence plot and the plot of detected peaks for a single target at different positions. The positions are selected to cover a wide range of target positions within the observation area.

Figure 4.13 (a), (b) and (c) show the accumulation of confidence values when the R-V line is generated at the target position coordinates (-5,10) and used to sample a number of ambiguity function plots spread across the observation area at fixed intervals. Peaks are detected in the cumulative confidence values. Closely spaced multiple peaks can occur as shown in Figure 4.13 (b) and (c). An average of the target position associated with top 15% closely spaced peaks is found. Figure 4.13 (d) shows the peak of the confidence values that are considered to represent the target position. The target position co-ordinates obtained from this simulation are (-5.04, 10.08) as compared to the actual position of the target being (-5, 10). This results in a target position error of < 1% for each co-ordinate.

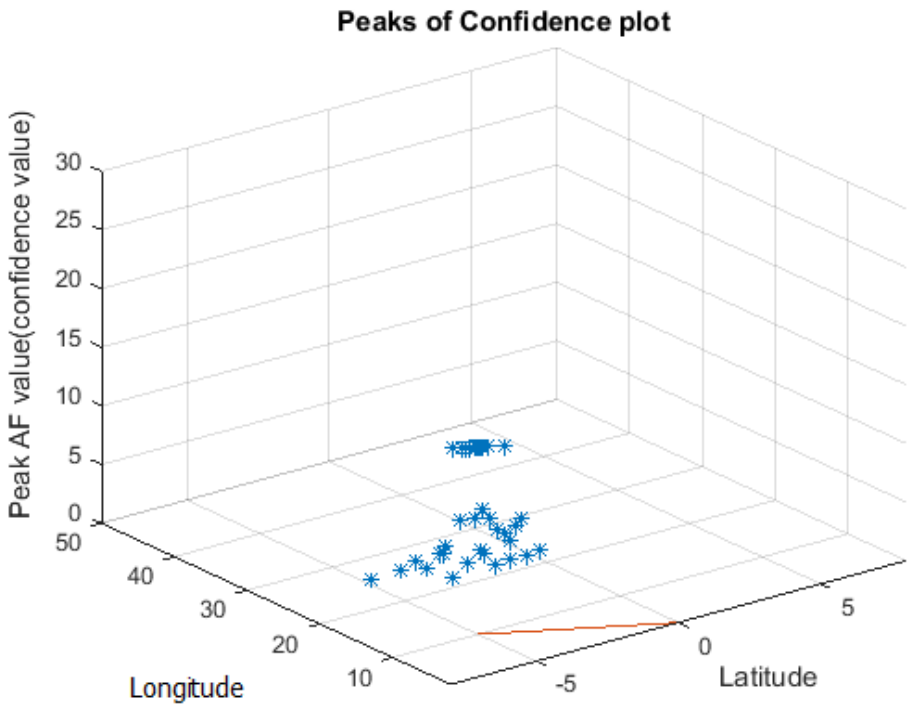

Figure 4.13 (a)

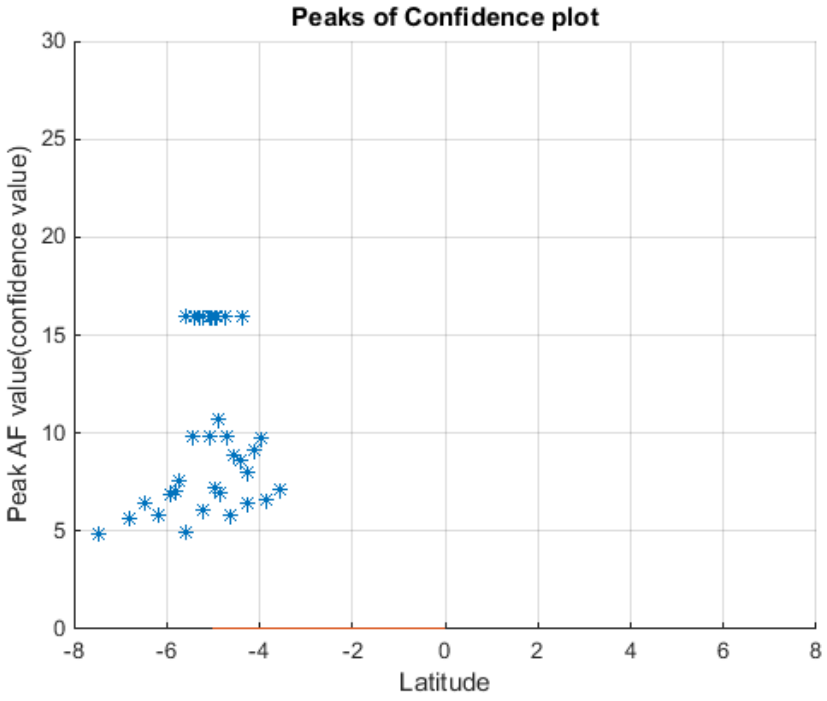

Figure 4.13 (b)

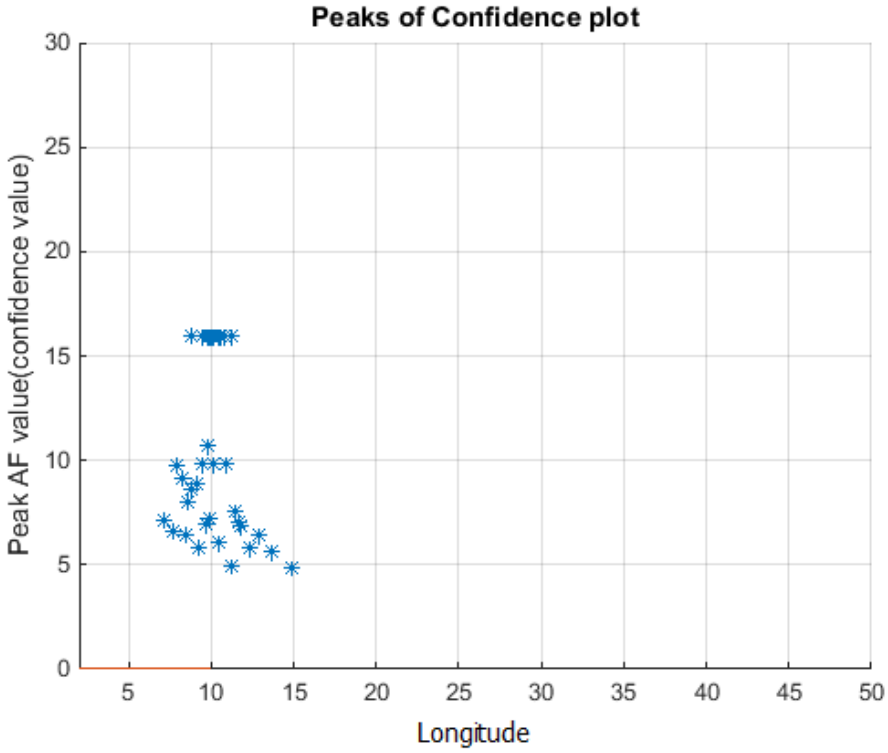

Figure 4.13 (c)

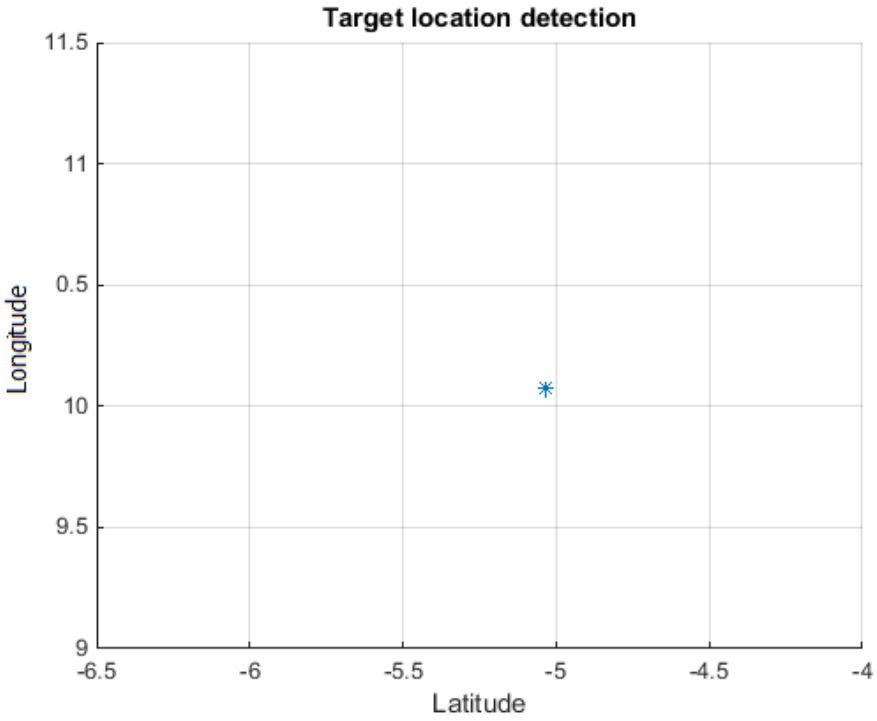

(d)

Figure 4.13: (a) The cumulative confidence values for a target at (-5, 10), (b) A 2D view of latitude and cumulative confidence values, (c) A 2D view of longitude and cumulative confidence values and (d) Location of the peak in confidence value.

Figure 4.14 (a), (b) and (c) show the accumulation of confidence when the R-V line is generated at the target position (2, 5) and used to sample ambiguity function plots. To identify the target position the peak in the plot of confidence values was detected as shown in Figure 4.14 (d). The target position obtained from this simulation was (2.24, 5.6) as compared to the actual target at (2, 5). This results in a target position error of 12% for each co-ordinate.

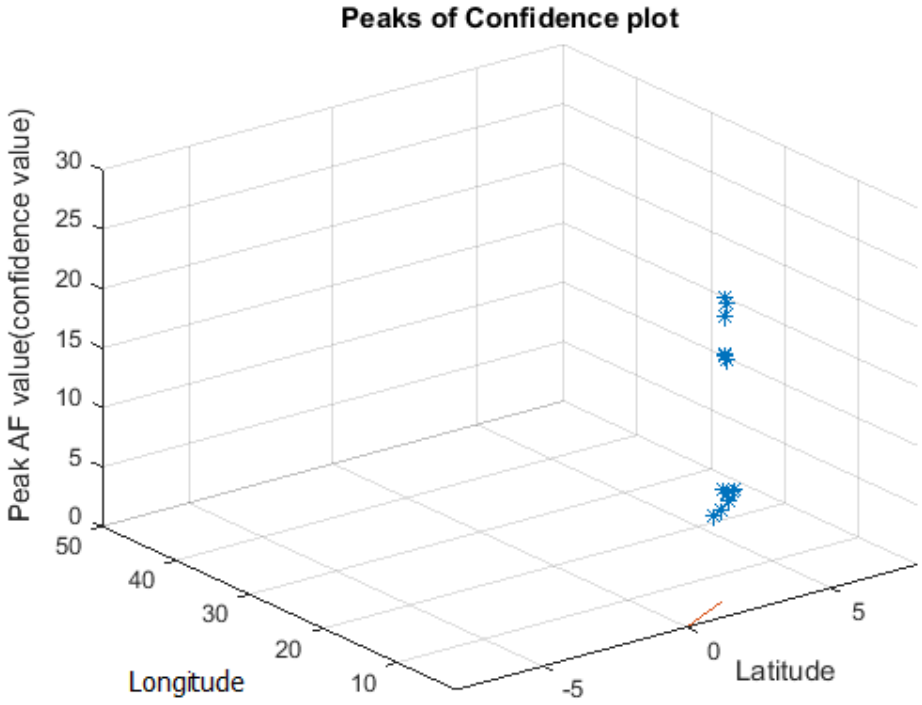

Figure 4.14 (a)

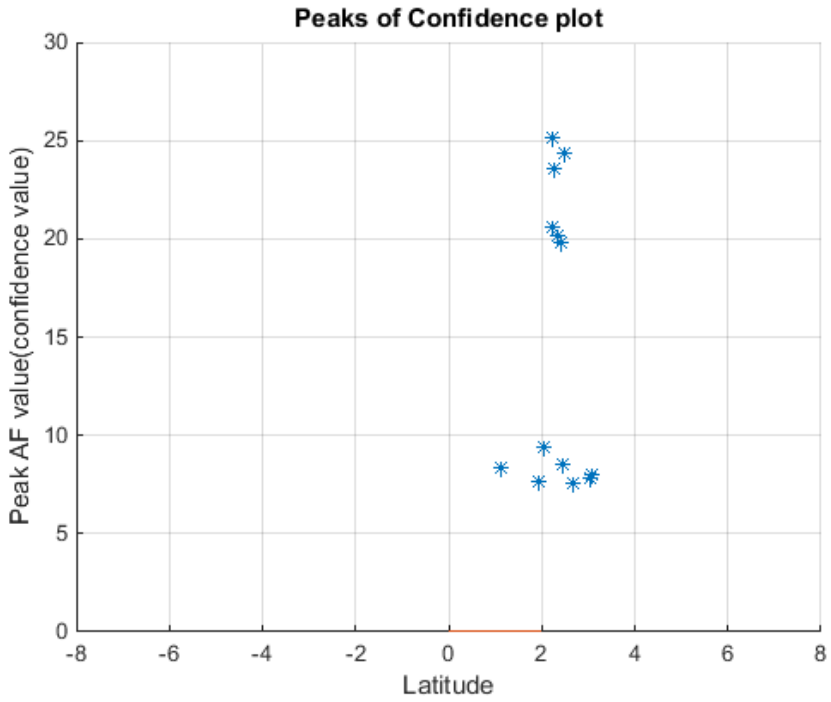

Figure 4.14 (b)

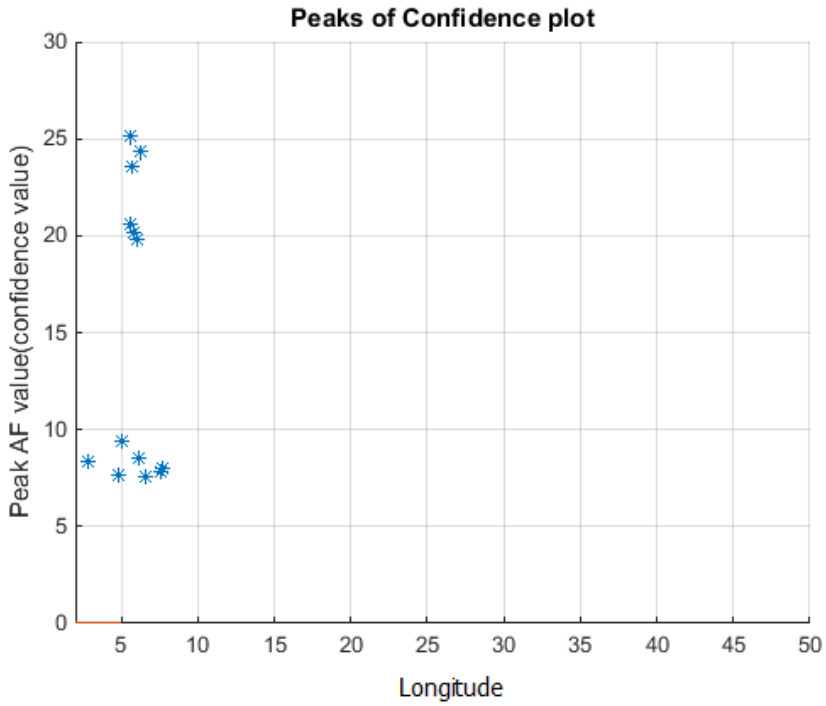

(c)

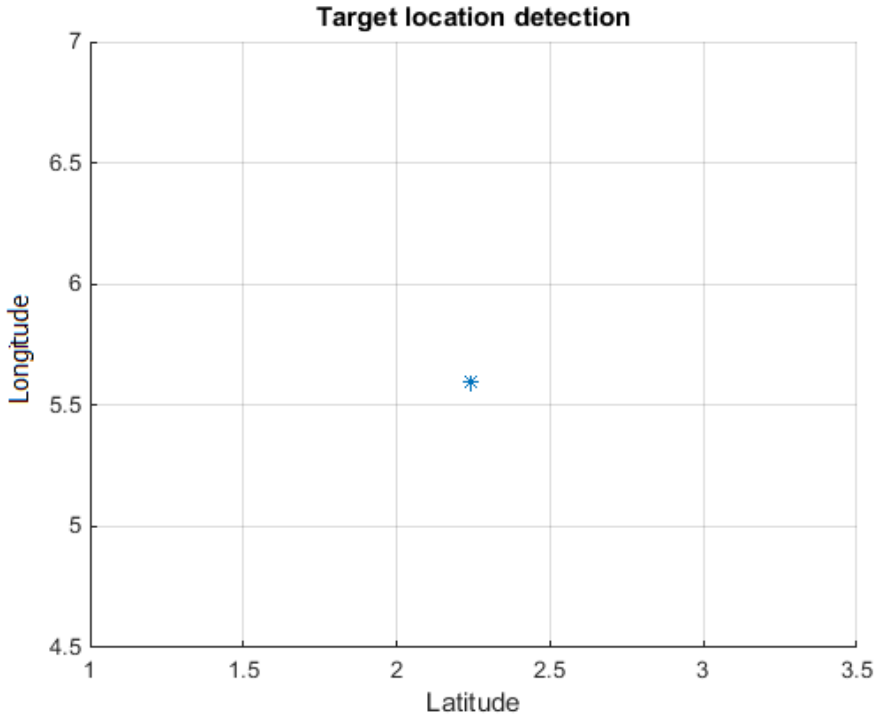

(d)

Figure 4.14: (a) The cumulative confidence values for a target at (2, 5), (b) A 2D view of latitude and cumulative confidence values, (c) A 2D view of longitude and cumulative confidence values and (d) Location of the peak in confidence value.

Figure 4.15 (a), (b) and (c) show the accumulation of confidence values after a threshold has been applied for a target at (8, 30) and the R-V line was used to sample ambiguity functions spread across the observation area at fixed intervals. Figure 4.15 (d) shows the peak of the confidence values detected to identify the target position of (8.03, 30.17). This results in a target position error of < 1% for each co-ordinate.

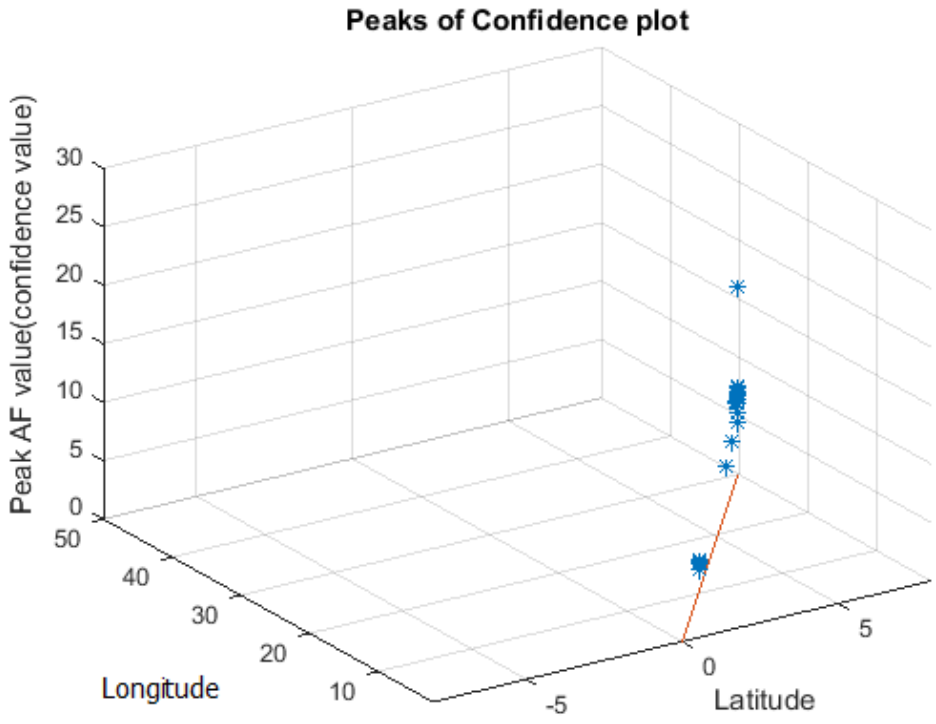

Figure 4.15 (a)

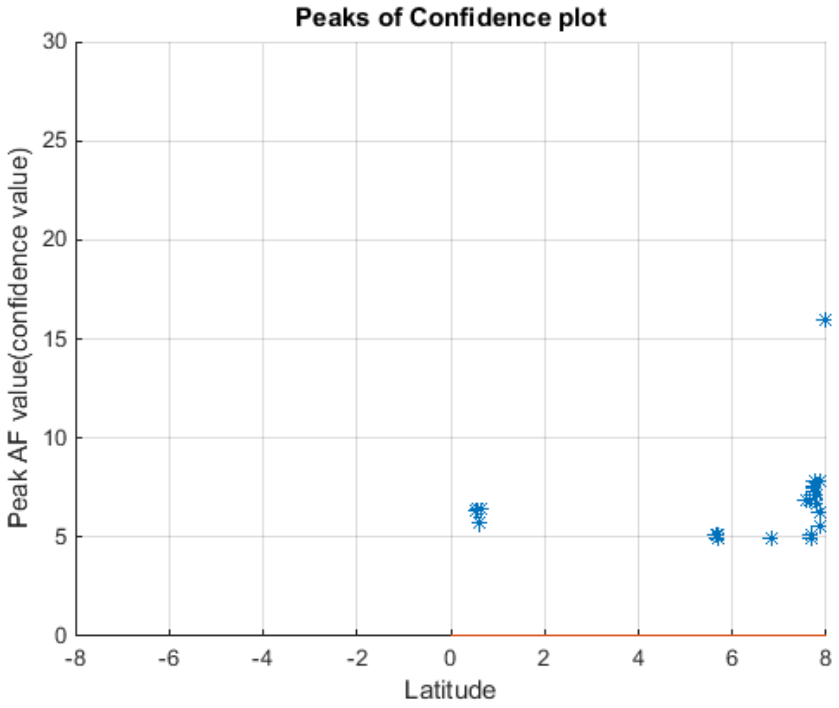

Figure 4.15 (b)

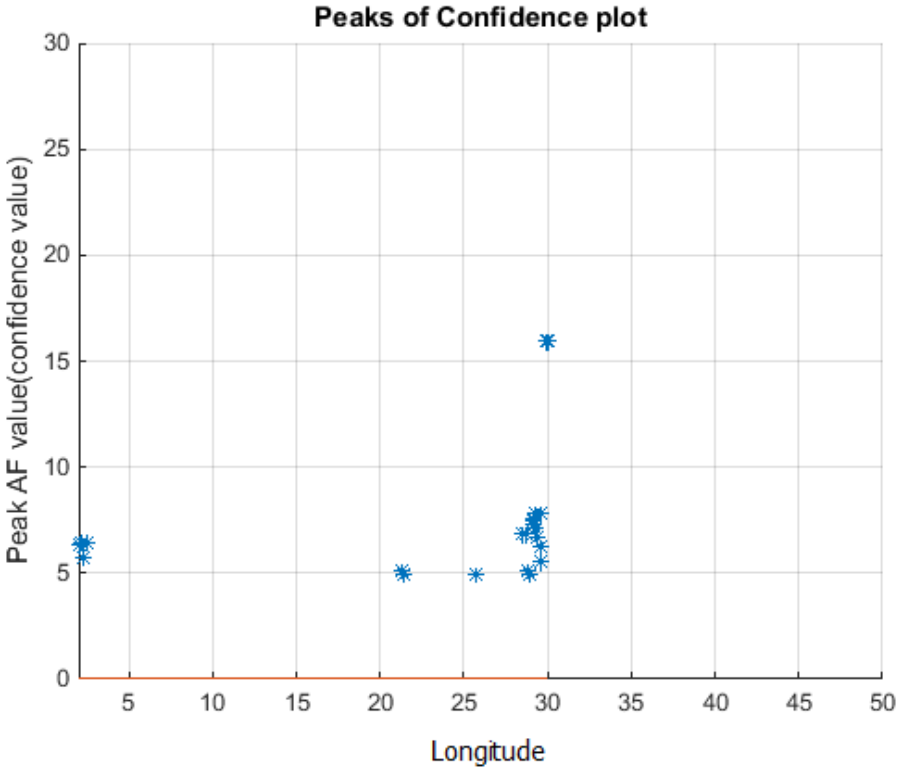

Figure 4.15 (c)

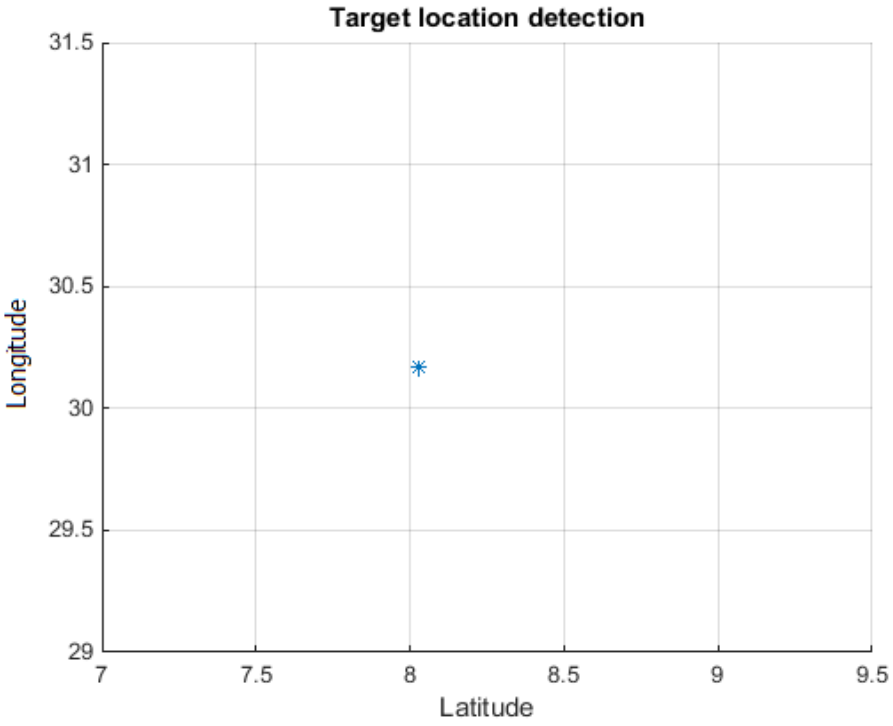

(d)

Figure 4.15: (a) The cumulative confidence values for a target at (8, 30), (b) A 2D view of latitude and cumulative confidence values, (c) A 2D view of longitude and cumulative confidence values and (d) Location of the peak in confidence value.

4.3.4 Building confidence plots for multiple targets

In a multi-target scenario, multiple R-V lines will be generated as a result of multiple frequency shifts received by the sensor. Here these multiple targets are also resolved using the technique described in the previous section for a single target. The confidence values obtained by sampling the ambiguity functions with multiple R-V lines are accumulated as shown in Figures 4.16 and 4.17. Figure 4.16 shows the accumulation of confidence values for three targets and Figure 4.17 for 10 targets.

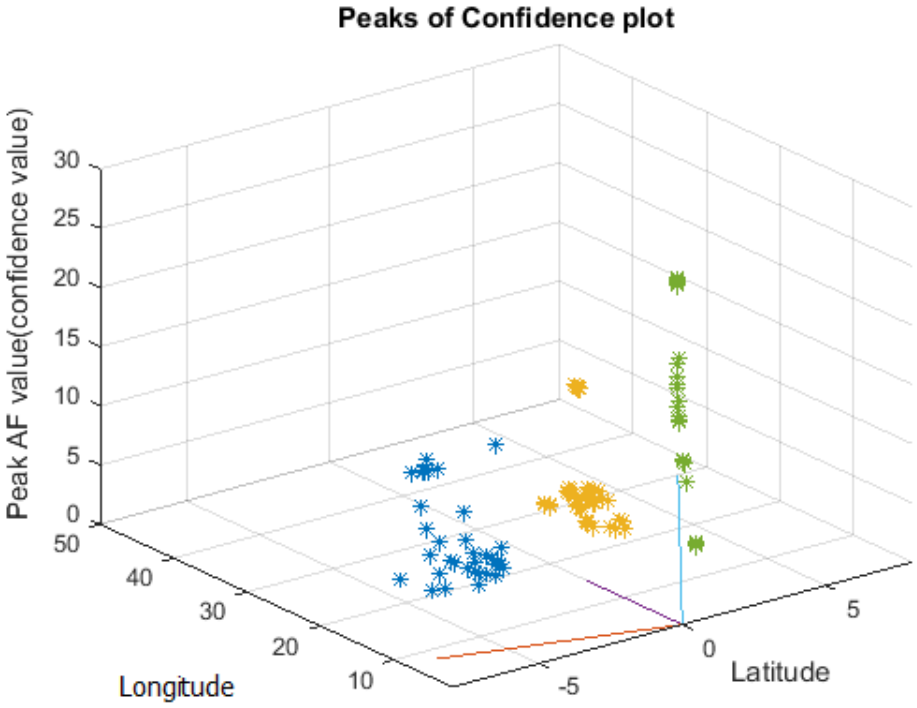

Figure 4.16 (a)

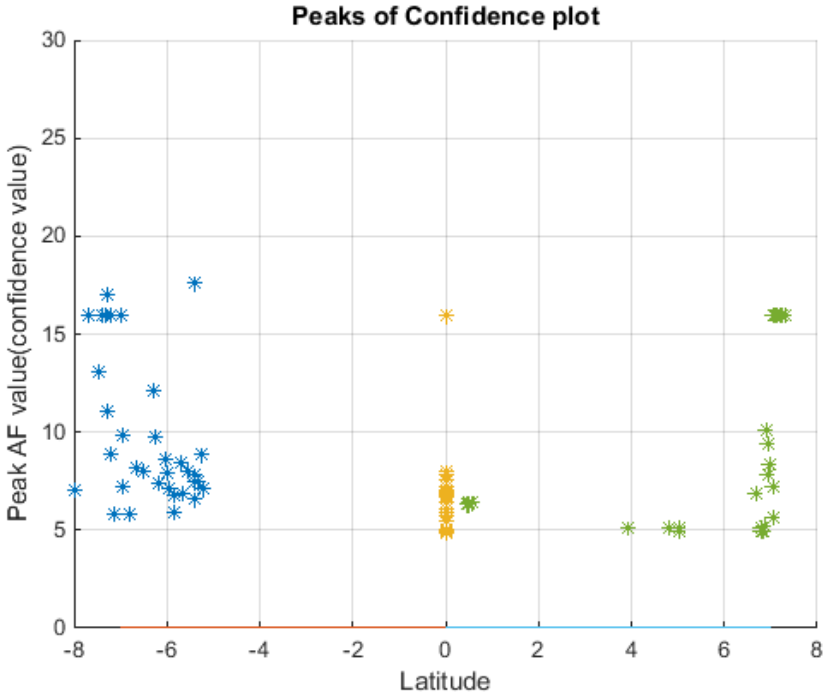

Figure 4.16 (b)

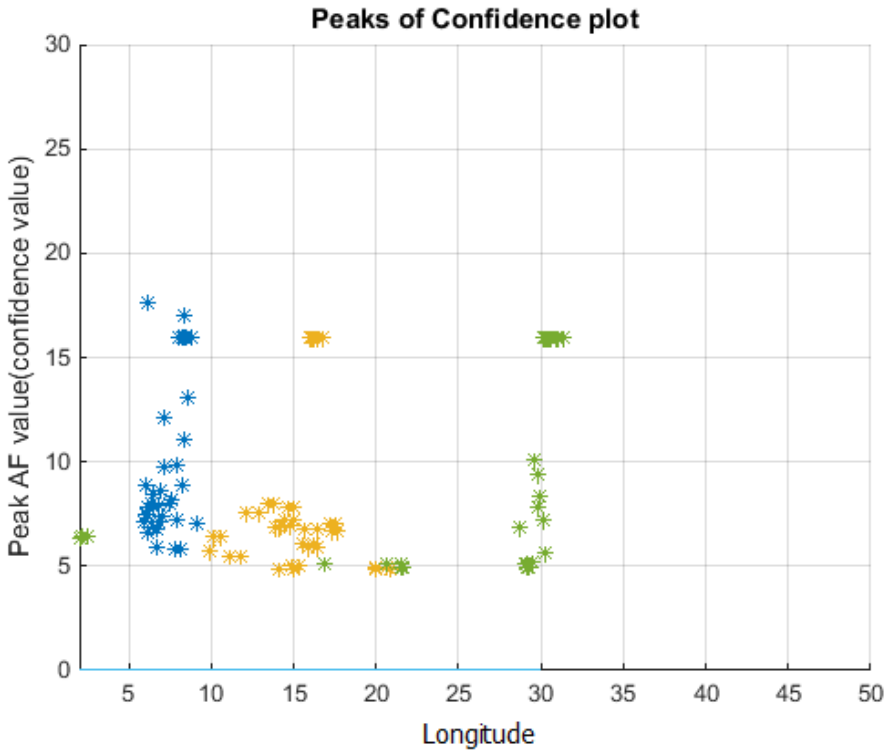

Figure 4.16 (c)

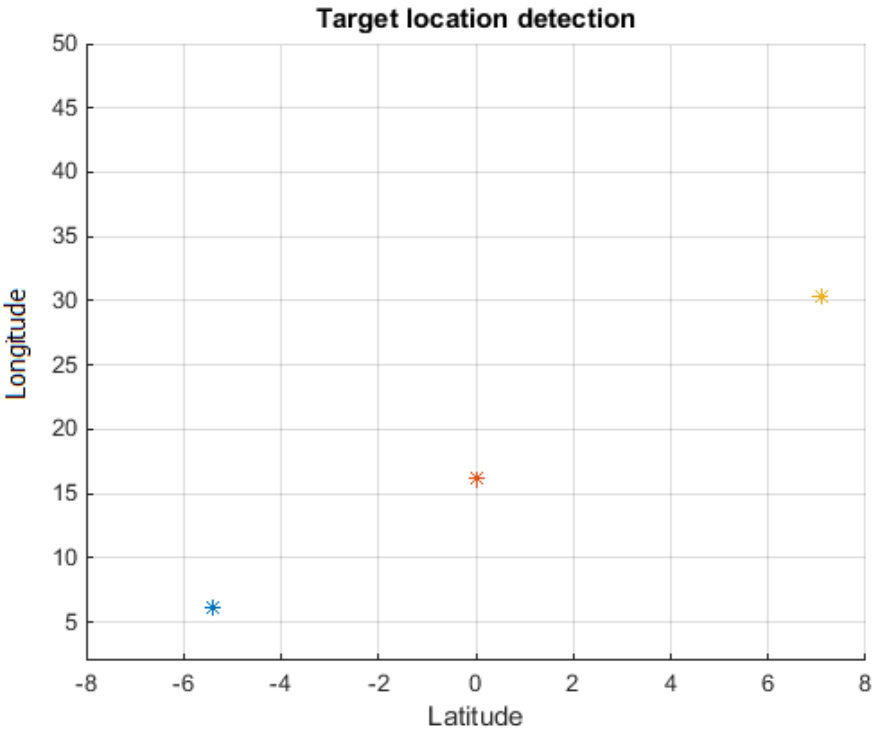

Figure 4.16 (d)

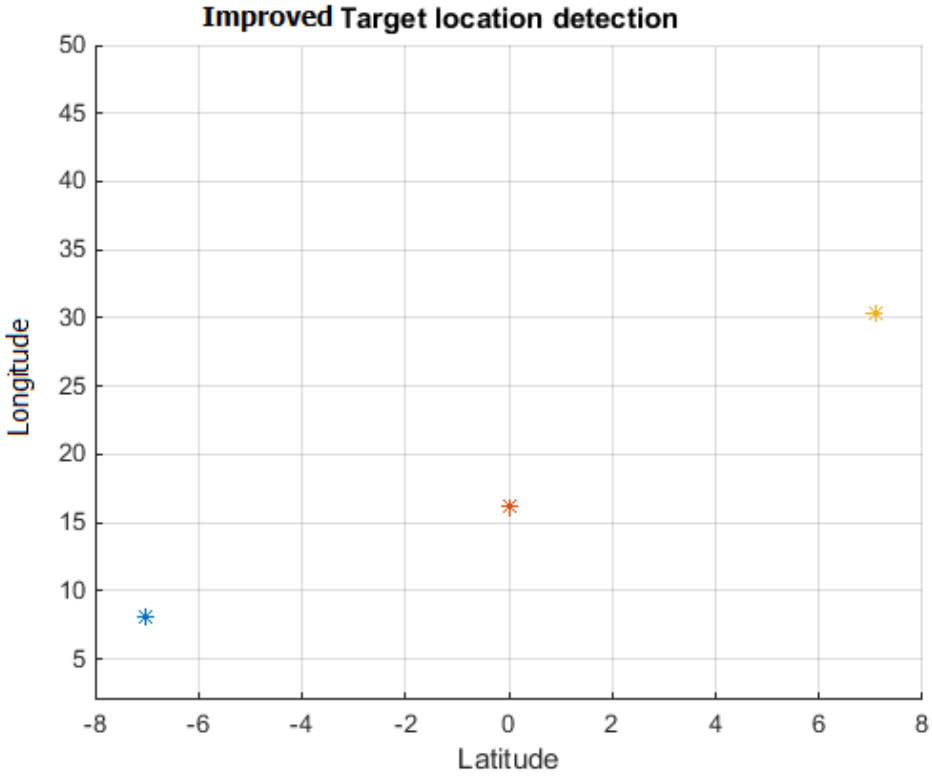

(e)

Figure 4.16: (a) Accumulated confidence values for three targets at (-7, 8), (0, 15) and (7, 30), (b) A 2D view of latitude and accumulated confidence values, (c) A 2D view of longitude and accumulated confidence values, (d) Location of the peaks of confidence values and (e) Improved target location after averaging.

Figure 4.16 (b) and (c) show the significant localized peaks for the targets, in blue; these peaks are not as distinct as the other two targets in yellow and green. An average of these significant localized peaks gives a better result, as shown in Figure 4.16 (d). The location is only improved for the blue target at (-7, 8) because the other two targets do not have multiple significant local peaks.

Figure 4.17 shows detection for 10 targets. The targets were at positions: (-8, 20), (-6, 8), (-4, 15), (-2, 5), (0, 7), (0, 30), (1, 15), (3, 10), (5, 25) and (6, 15). Figure 4.17 (b) and (c) shows that the target at (-6, 8) which is shown in yellow has significant local peaks. Figure 4.17 (d) shows the target position without averaging the local peaks and

Figure 4.17 (e) shows the target position for the same targets after averaging the local peaks. This improves target location at (-6, 8) whilst no significant change can be seen in the location of other targets.

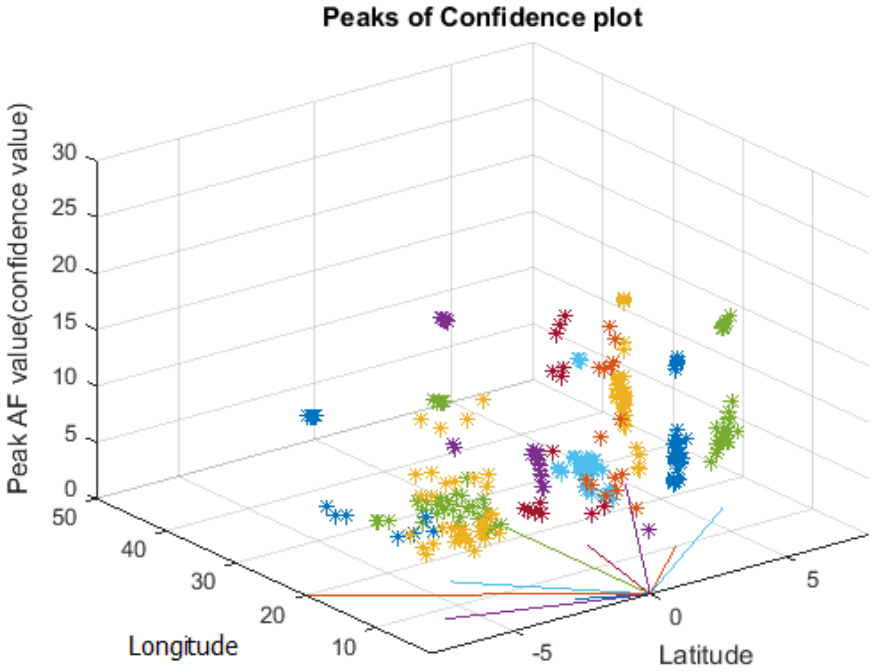

Figure 4.17 (a)

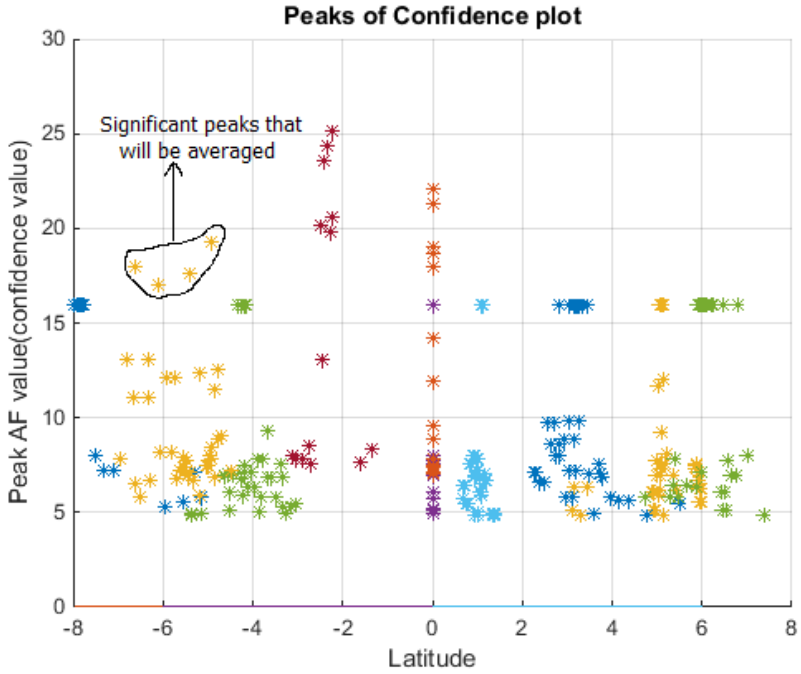

Figure 4.17 (b)

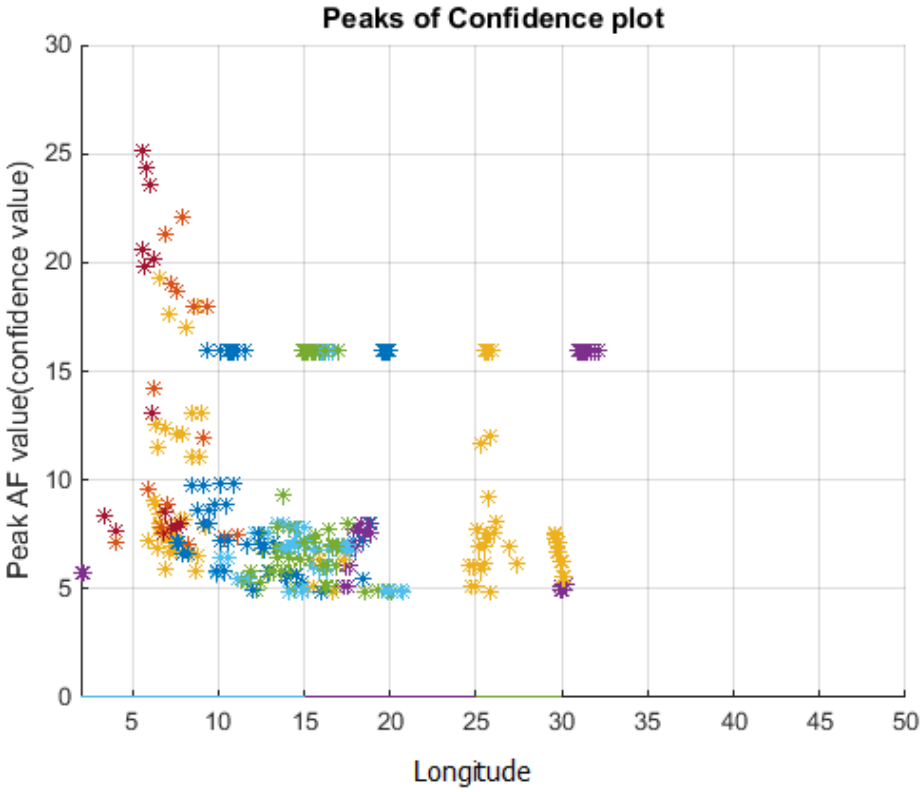

Figure 4.17 (c)

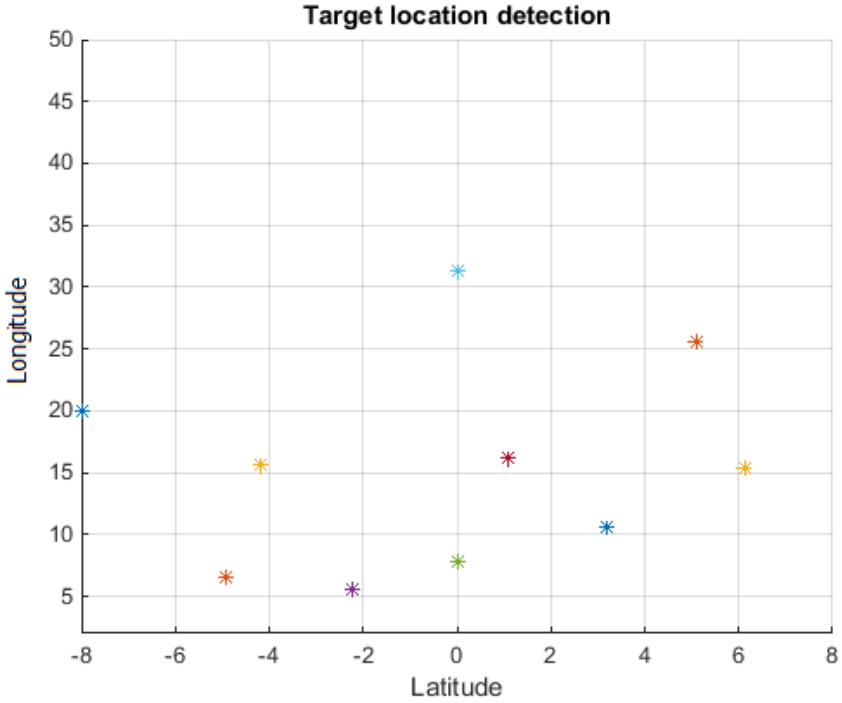

Figure 4.17 (d)

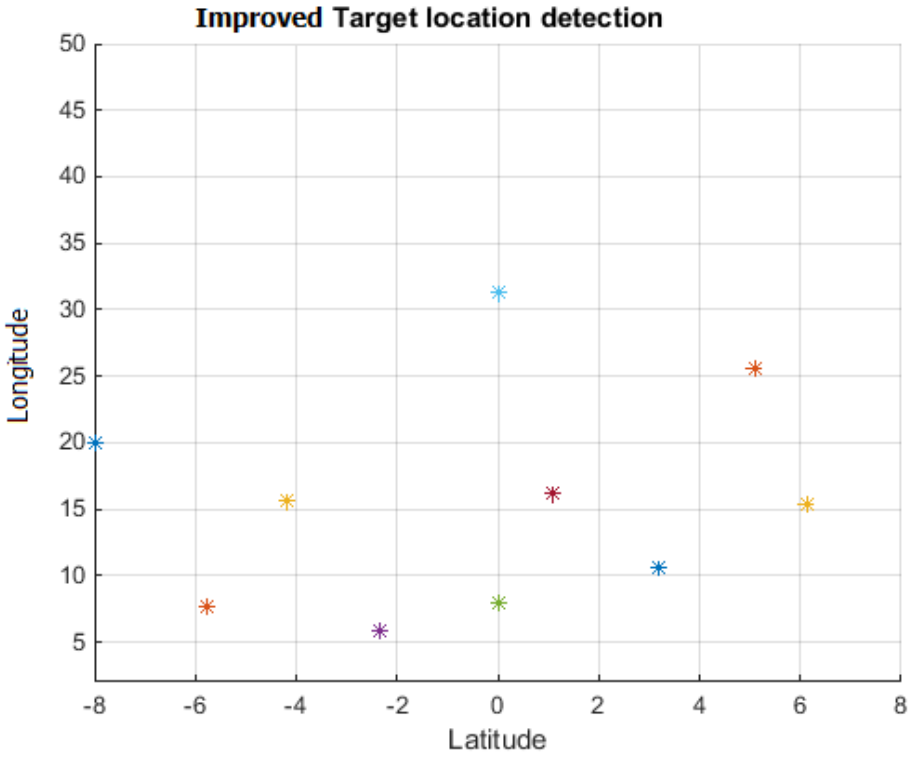

(e)

Figure 4.17: (a) Accumulated confidence values for ten targets, (b) A 2D view of latitude and accumulated confidence values, (c) A 2D view of longitude and accumulated confidence values, (d) Location of the peaks of confidence values and (e) Improved target location after averaging.

All the simulation results so far assumed a known constant target velocity; hence the focus was on estimating the target range. In the following simulation results velocity is allowed to change (within plausible limits) and both range and velocity are estimated.

4.4 Simulation results for changing target velocity

In the simulation results presented in this section the target velocity is allowed to change (within plausible limits).

4.4.1 Ambiguity function plots for changing target velocity

It has been shown in the preceding sections that the ambiguity function plot changes with the position of the target. This section shows how the ambiguity function plot is

affected by changes in the target velocity. The change in velocity could be due to the change in target speed and/or direction. This is manifest as a change in the targets' Doppler frequency. A change in the Doppler frequency affects the ambiguity function which depends on time-delay and Doppler frequency. Figure 4.18 shows how the ambiguity function changes for the same target position at different speeds in the same direction.

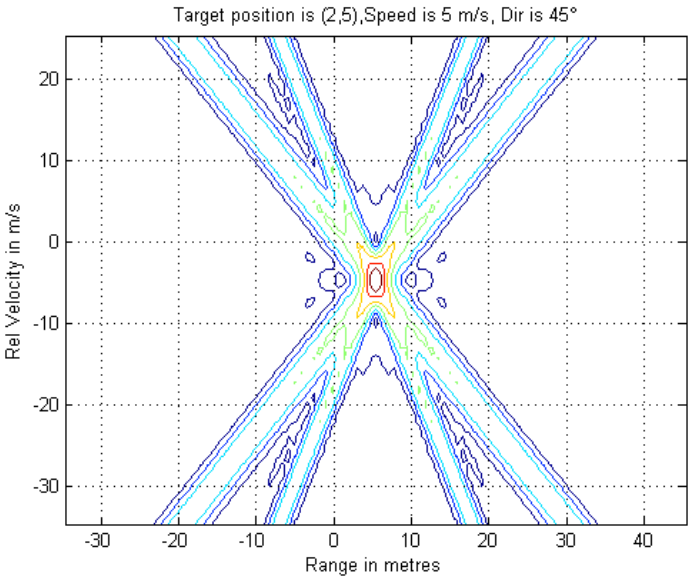

Figure 4.18 (a)

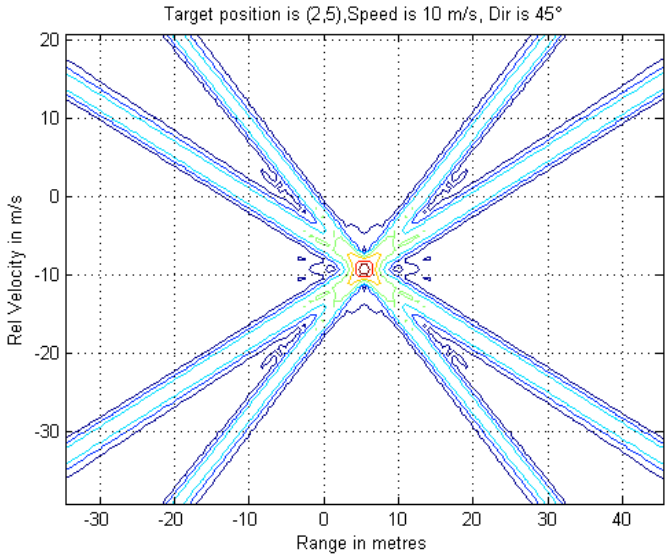

Figure 4.18 (b)

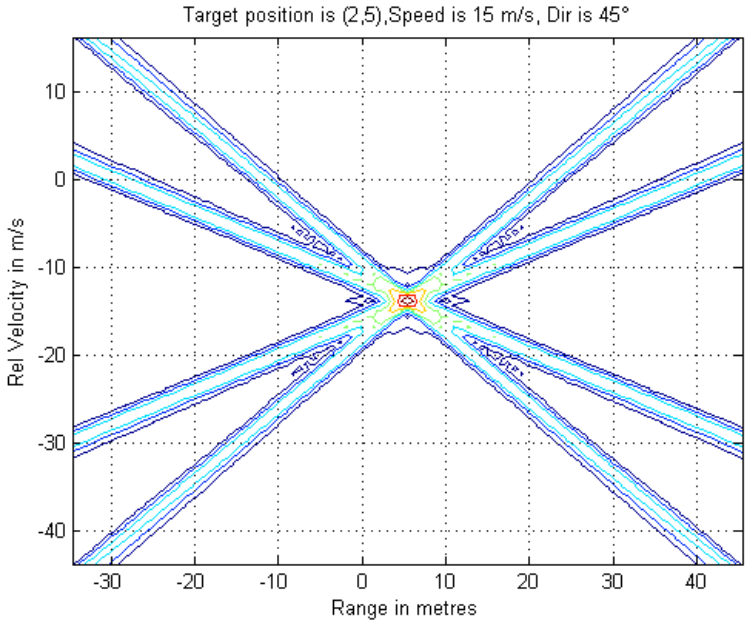

(c)

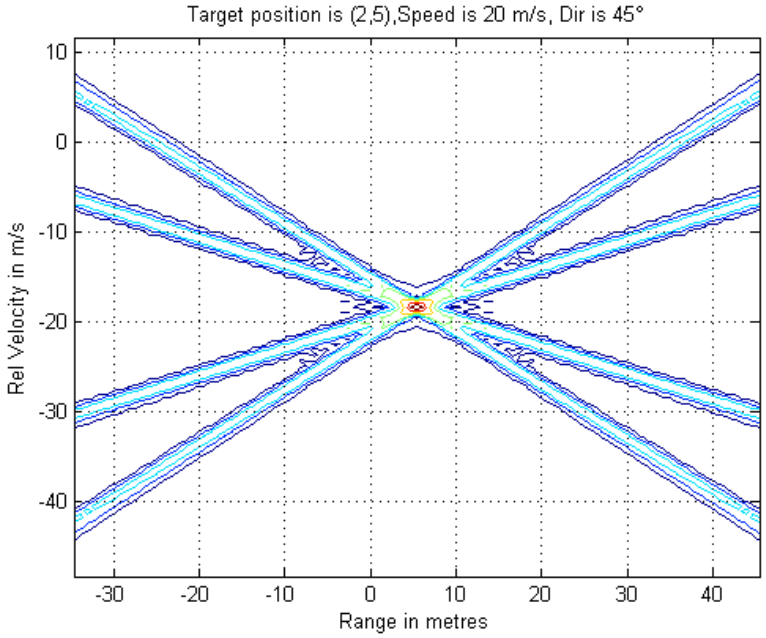

(d)

Figure 4.18: Ambiguity function plots for a target at position (2,5) and moving in a direction at an angle of 45^{o} CCW from the positive x-axis and at target speeds of: (a) 5 m/s, (b) 10 m/s, (c) 15 m/s and (d) 20 m/s.

Figure 4.19 shows how ambiguity function changes for the same target at the same speed when the direction of movement changes.

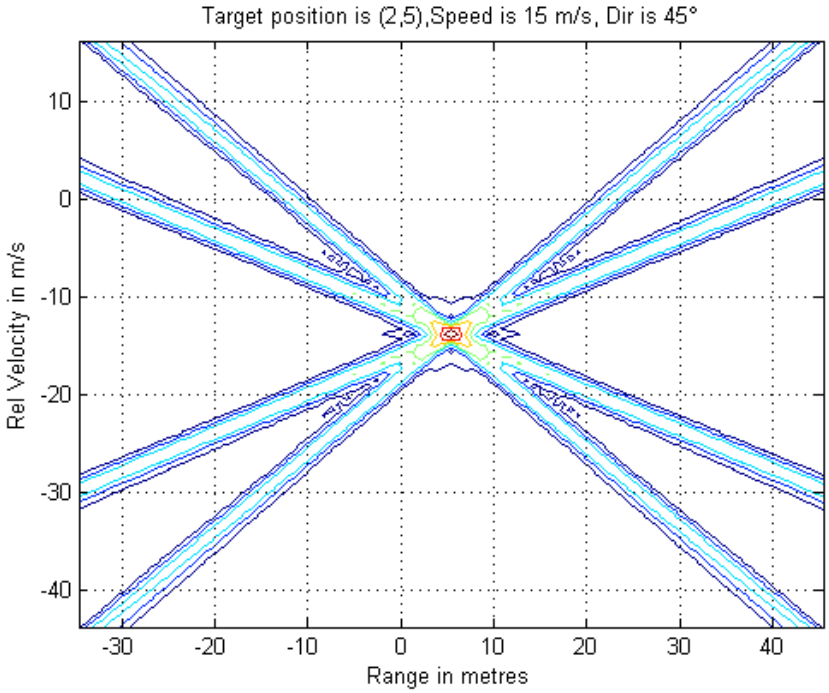

Figure 4.19 (a)

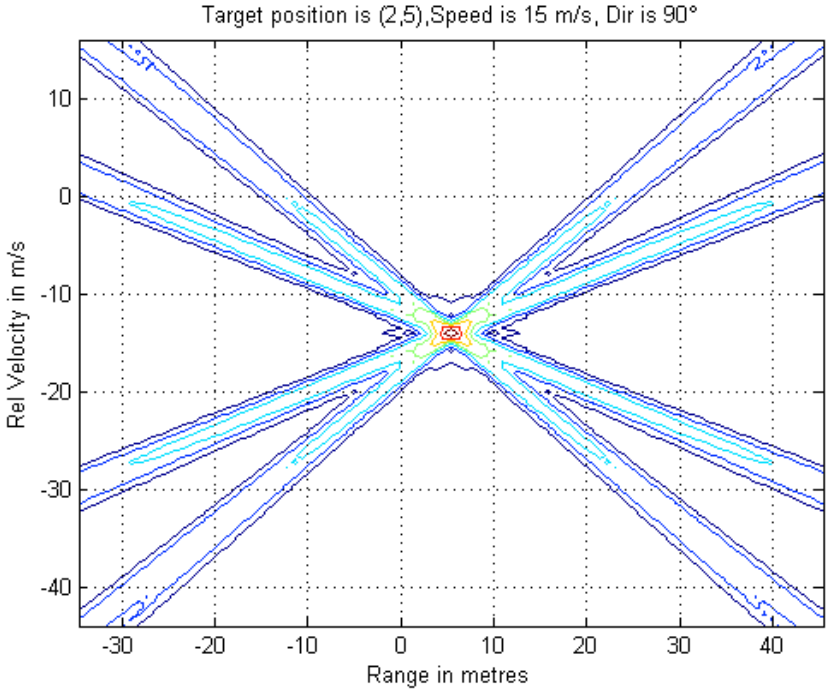

Figure 4.19 (b)

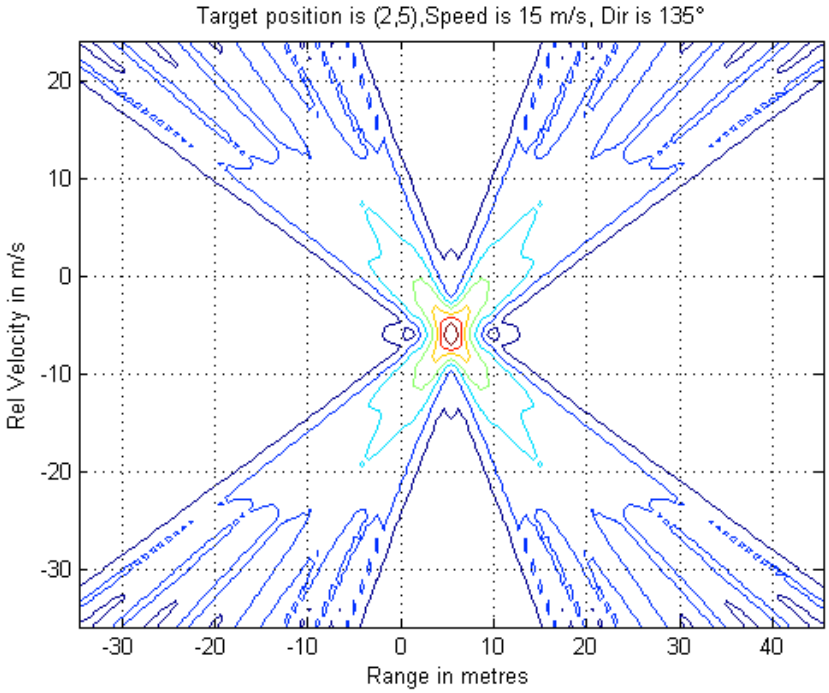

Figure 4.19 (c)

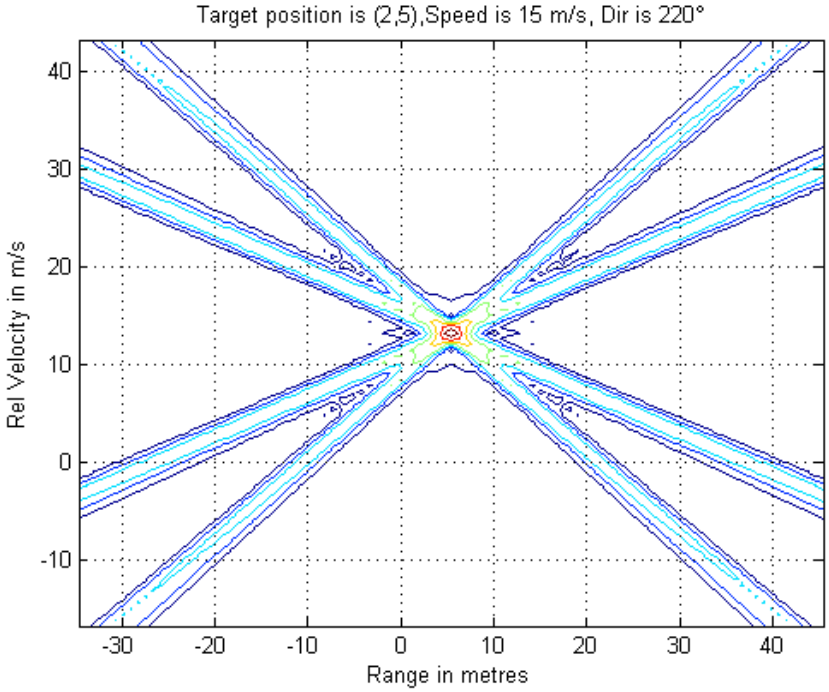

Figure 4.19 (d)

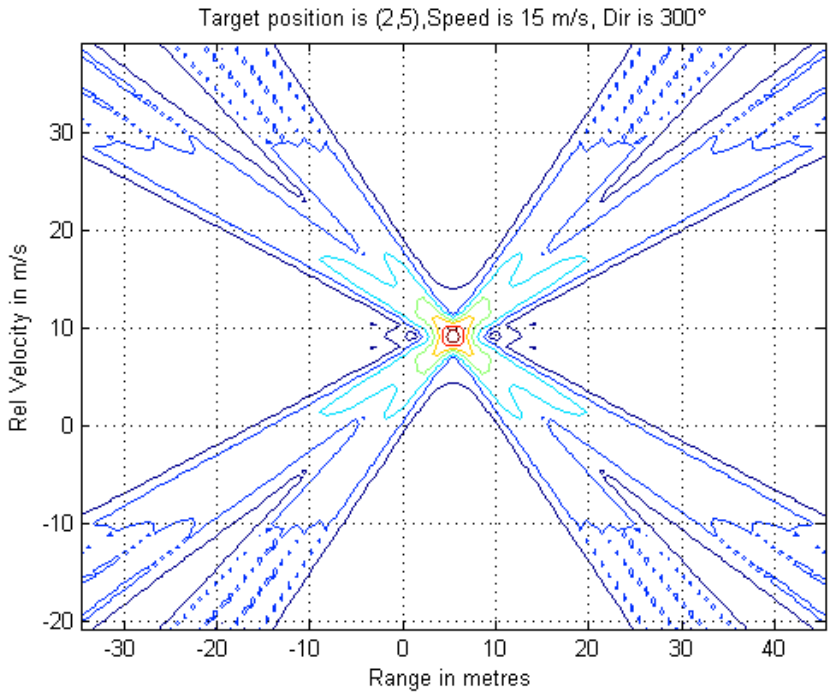

(e)

Figure 4.19: Ambiguity function plotted for a target at (2,5), moving with a speed of 15 m/s in a direction measured counter clockwise from the positive x-axis of (a) 45^o, (b) 90^o, (c) 135^o, (d) 220^o and (e) 300^o.

4.4.2 Detection of targets with changing velocity

It is clear from the above results that the ambiguity function changes both with target position and with target velocity. This means that a still greater number of ambiguity function plots must be considered in the proposed scheme of interpretation. The range detection procedure will be the same as for the previous cases but now the intersection of R-V lines will be with a greater number of ambiguity function plots. Each ambiguity function plot is now at a target position, speed and direction. The direction ranges from 0 to 360^o which includes any direction a target is moving in and the speed ranges only from 0 to 30 m/s. This is the velocity which is plausible on an urban road. The confidence values can be accumulated for intersections between the R-V lines and AF plots at the same range and radial velocity so that the range and radial velocity to each

sensor can be computed from the peaks in such confidence values. Figures 4.20 – 4.22 show the simulation results obtained for target detection in range and velocity direction for single and multiple target situations.

Figure 4.20 shows the peak in confidence values for a target at (-5, 10) moving with a speed of 30 m/s at an angle of 300^{o} in a direction measured CCW from positive x-axis.

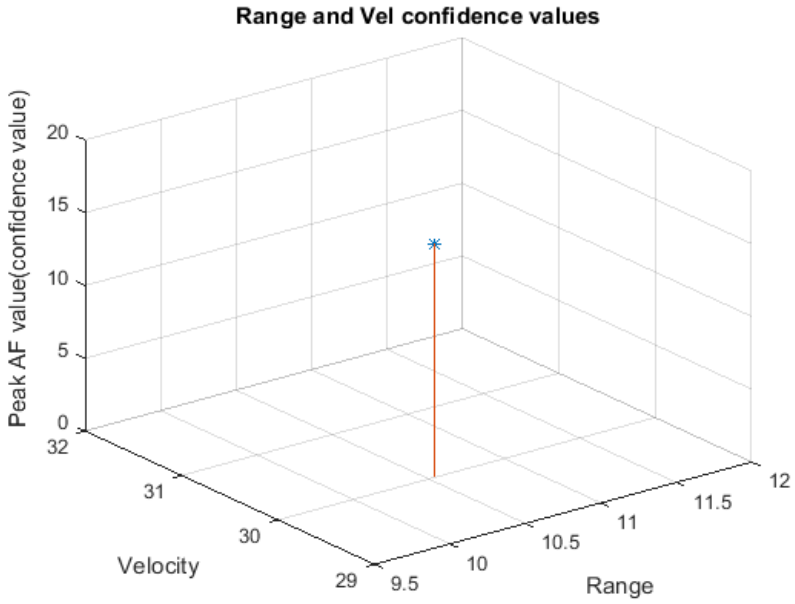

Figure 4.20 (a)

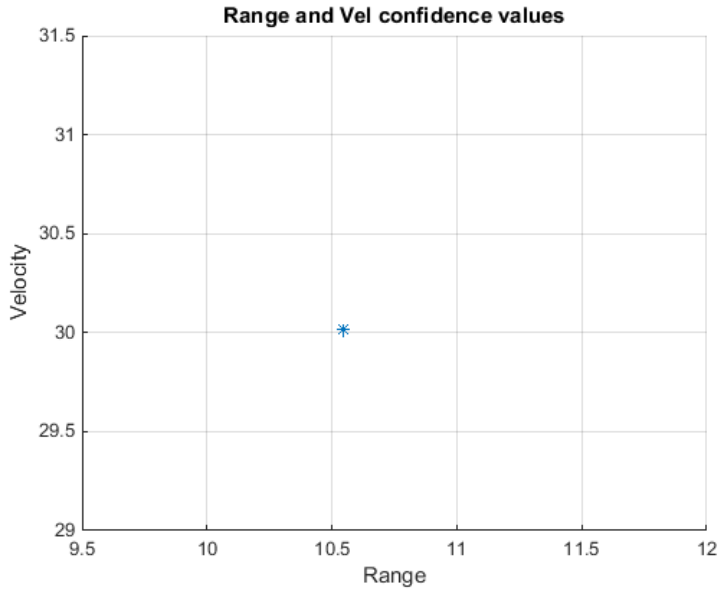

Figure 4.20 (b)

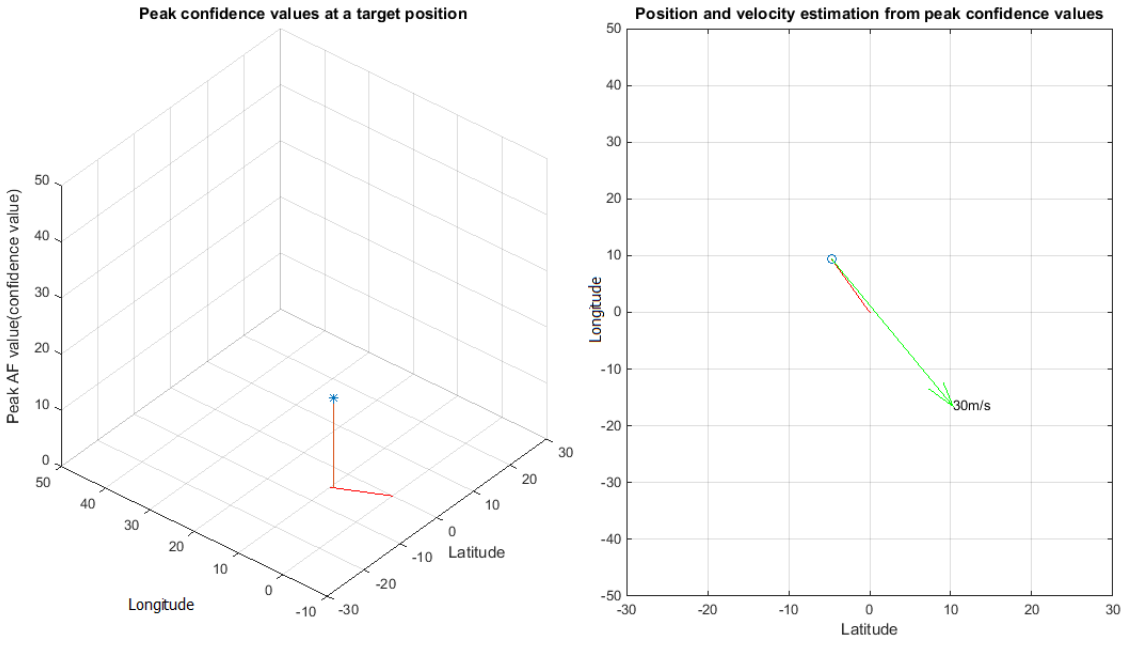

(c) (d)

Figure 4.20: (a) The peak confidence value in range and velocity, (b) A 2D plot of peak confidence value in range and velocity, (c) The peak confidence value at target co-ordinates and (d) Plot showing the detected target position (blue) and the velocity vector (green).

Figures 4.21 and 4.22 show the simulation results of peak confidence values in a multi target scenario.

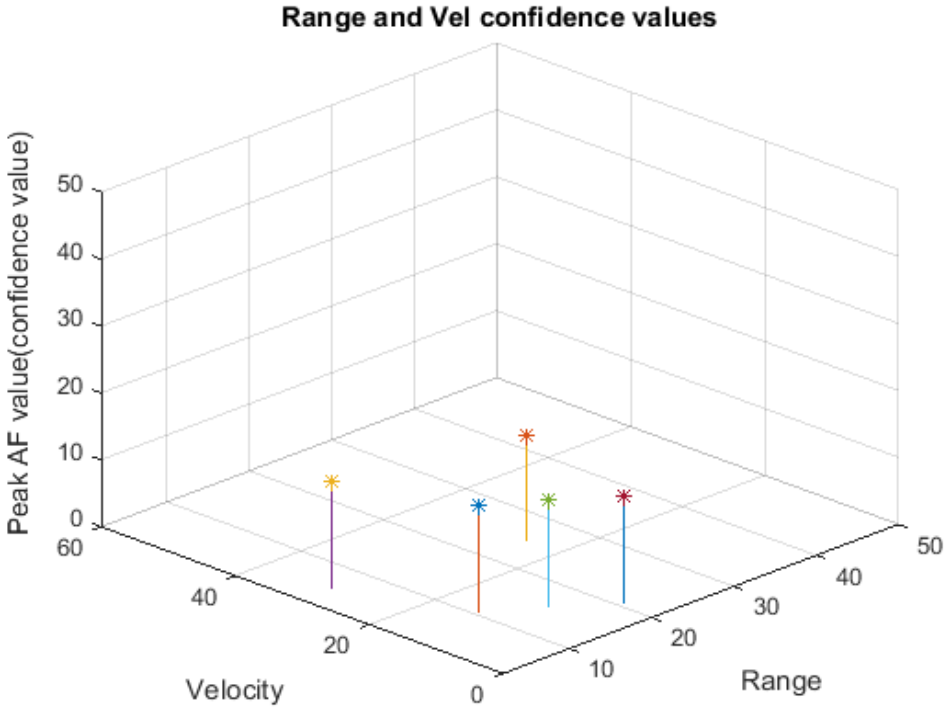

Figure 4.21 (a)

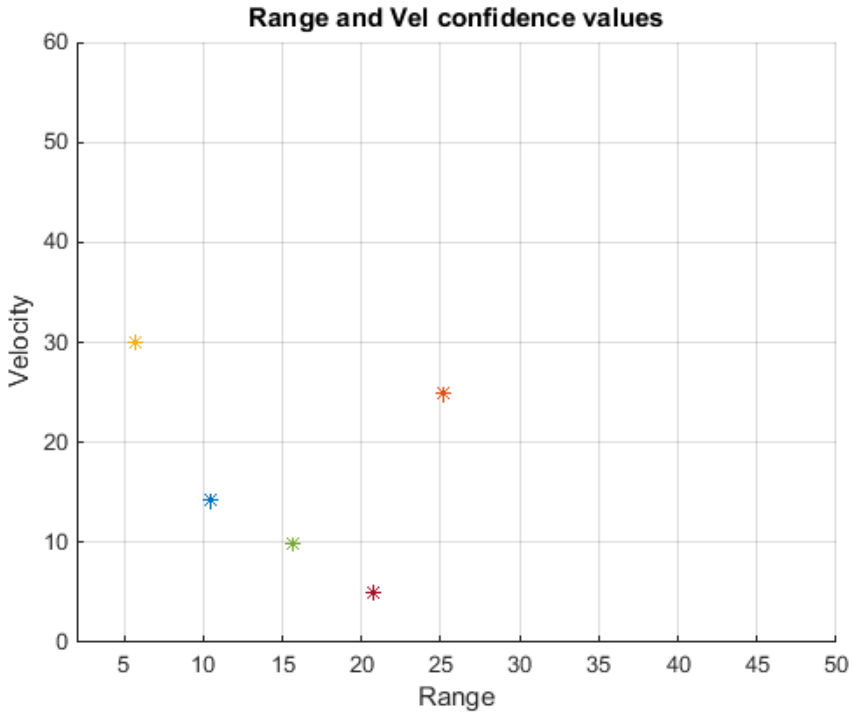

Figure 4.21 (b)

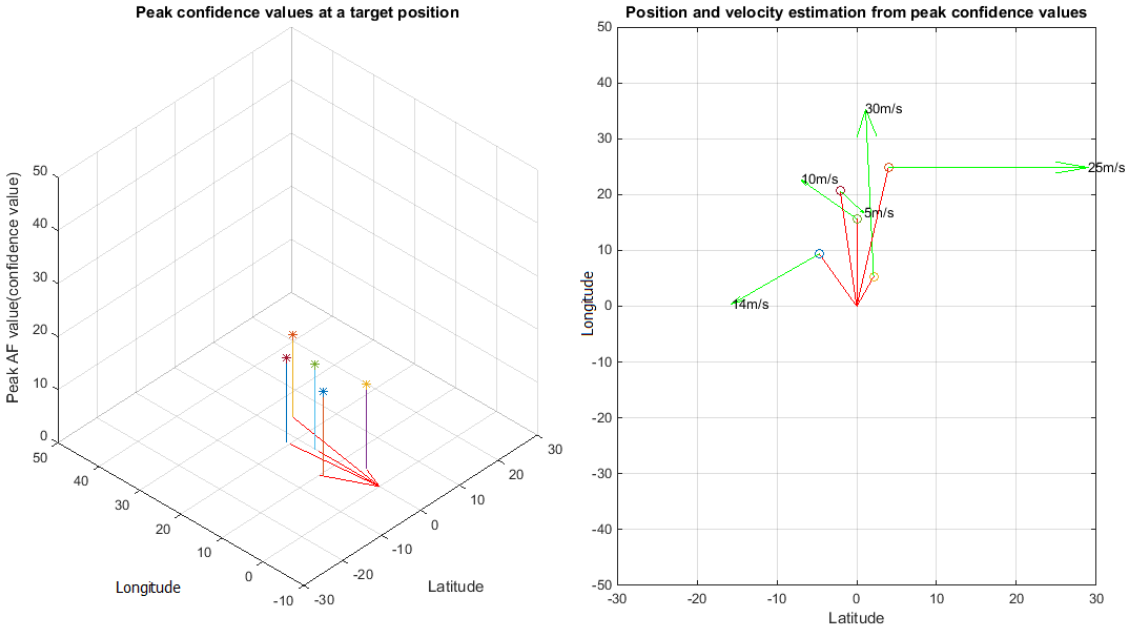

(c) (d)

Figure 4.21: (a) The peak confidence value in range and velocity, (b) A 2D plot of peak confidence value in range and velocity, (c) The peak confidence value at target co-ordinates and (d) Plot showing the detected target position (small circles) and the velocity vectors (green).

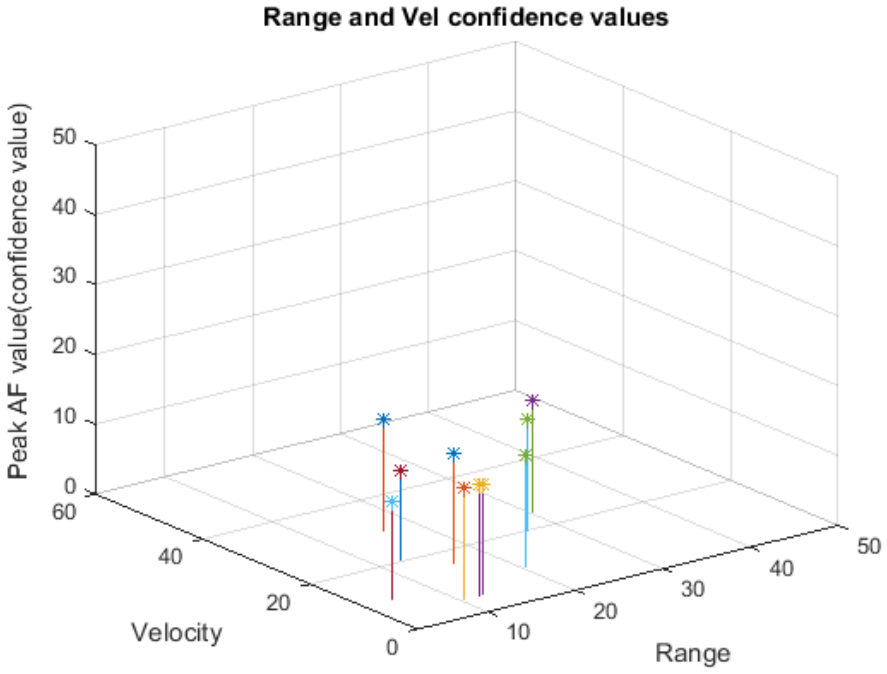

Figure 4.22 (a)

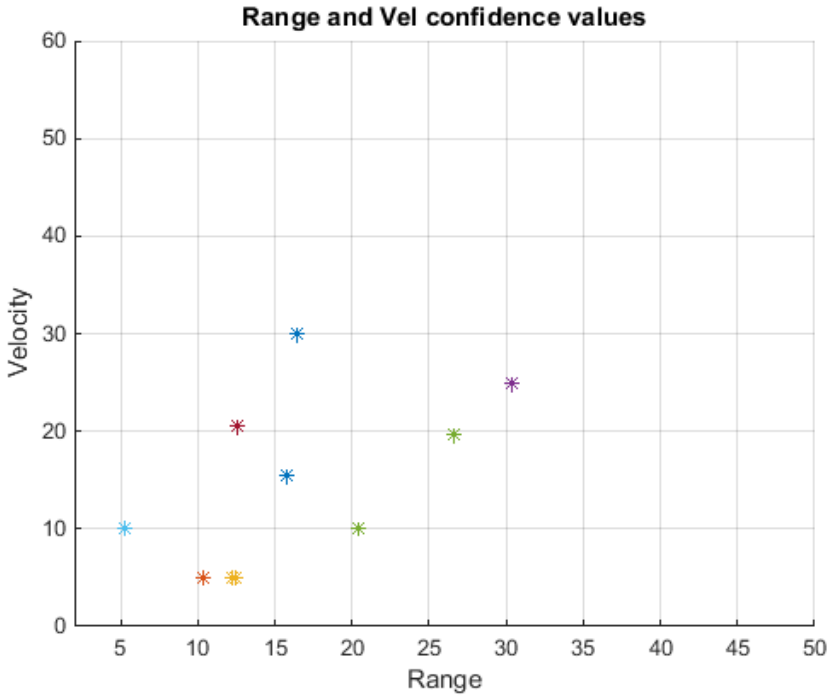

Figure 4.22 (b)

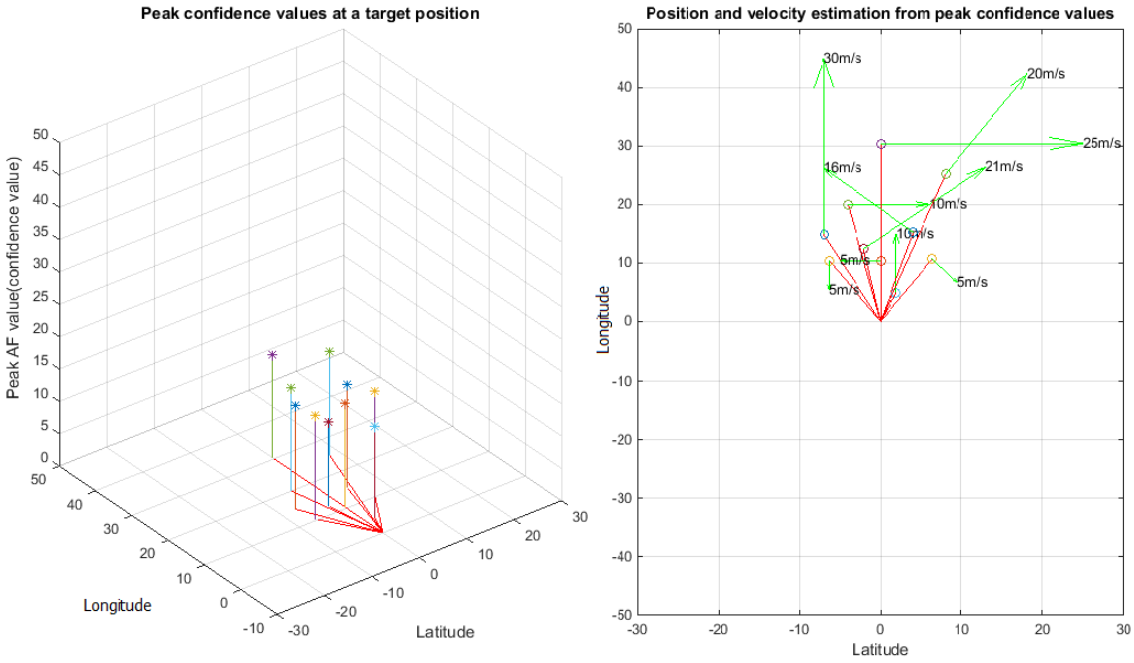

(c) (d)

Figure 4.22: (a) The peak confidence value in range and velocity, (b) A 2D plot of peak confidence value in range and velocity, (c) The peak confidence value at target co-ordinates and (d) Plot showing the detected target position (small circles) and the velocity vectors (green).

4.5 Comparison of results

The Table 4.2 below compares the results obtained in simulation using the novel strategy introduced in this thesis with the actual or expected values.

Table 4.2: Comparison of Range and Velocity Estimation.

Target No.	Expected Position	Estimated Position	Position Error %	Expected Rel.Velocity	Estimated Rel.Velocity	Rel.Velocity Error %
Target Position: (-7, 15), Velocity parameters: (30m/s, 90^o)						
1	(-7, 15)	(-6.96, 14.91)	< 1%	-27.19	-26.81	1.4%
Target Position: (-6, 10), Velocity parameters: (5m/s, 270^o)						
2	(-6, 10)	(-6.27, 10.45)	4.5%	4.29	4.61	7.5%
Target Position: (3, 8), Velocity parameters: (12 m/s, 105^o)						

3	(3, 8)	(2.8, 7.6)	6.6%, 5%	-9.76	-10.08	3.3%
Target Position: (7, 30), Velocity parameters: (5 m/s, 300^o)						
4	(7, 30)	(6.96, 29.83)	< 1%	3.65	3.88	6.3%
Target Position: (4,10), Velocity parameters: (18 m/s, 200^o)						
5	(4, 10)	(4.05, 10.13)	~1.3%	12.00	11.91	< 1%
Target position: (8, 25), Velocity parameters: (20m/s, 60^o)						
6	(8, 25)	(8.1, 25.3)	1.2%	-19.54	-18.46	5.5%

4.6 Discussion

This chapter shows simulation results for a novel strategy to detect range and velocity of a target in automotive applications on an urban road.

The parameters chosen for simulation form the basis for experimental method. These parameters can easily be varied for different contexts, vehicle type and permitted velocity. The radar operating frequency can also easily be changed in accordance with the licensed bands allocated in different countries.

A novel use of the ambiguity function has been made for the purpose of target detection. In a traditional method of target detection, the magnitude of the response depends on the range to the target and radar cross-section. This method overcomes the limitation of the existing traditional methods where applying a threshold to the power spectrum has the risk of eliminating weak responses from targets of low radar cross-section. The strategy proposed in this thesis does not eliminate responses based on their magnitude. All the responses, however big or small are used for further processing. The responses which do not accumulate as compared to rest of the responses during further

processing are eliminated as they do not contribute to building the confidence profile and hence indicate a very low probability of targets' presence.

The simulation results presented show that the accumulation of the confidence values actually takes place where the target is located. The precision with which the location of the target is estimated depends on various factors which are discussed in this section.

The simulation results presented were generated using ambiguity functions computed at fixed intervals of 2 m in latitude and 5 m in longitude. The ambiguity functions were computed for changes in speed of 5 m/s and angular changes of 20^{o}. Taking a greater number of ambiguity functions within the observation area will improve the precision with which the target is detected but this has a large computational overhead. One way to approach this is to obtain a rough estimate of the target position using less number of ambiguity functions within the physical search space. This estimate could be refined in a second round of simulation by considering closely spaced ambiguity functions in a smaller search space where the target is more likely to be present. The estimation of ambiguity function using Eq. (4.1) is computationally complex. Interpolation could be used as an alternative to using Eq. (4.1) to calculate ambiguity function at intermediate positions when considering closely spaced ambiguity functions. Appendix A briefly explains an interpolation technique that can be implemented to estimate ambiguity functions at intermediate positions.

The resolution of the steps in the simulation of ambiguity function is shown to be adequate to prevent sampling anomalies. This is important because if the density of the AF plot is not sufficient, incorrect values could be returned when the R-V line is used to sample the AF plot.

To evaluate the simulation, target positions and velocities at extreme values have also been considered. The errors are generally higher at extremes of target position and velocity because fewer AF plots are available for intersection with the R-V lines. This can be overcome by considering more AF plots for target positions and velocities which lie outside the boundary values. However, this will also result in a significant computational overhead.

The situations that would normally give rise to ghost targets are simulated and no ghost targets are detected. Tracking the targets in time can further reduce ghost targets as they will show unrealistic movement.

A target with low radar cross-section can be considered to have the same ambiguity function but scaled down in magnitude. The confidence plot will build up in the same way as it did before and the peaks will be obtained at positions where target is present but the magnitude of the peak will now be smaller. This does not result in target being missed.

There are some errors due to various limits of simulation. The numerical computation error is introduced while computing the AF and R-V line. The quantization of the AF plot and R-V line representation contributes to uncertainties in range and velocity estimation. The intersection of the two is discrete and does not match properly. An error due to the limited number of ambiguity functions considered for intersection with the R-V line also accumulates.

This approach is novel. A good amount of research has been performed in different areas of automotive radars, but the work presented in this thesis is based on a novel strategy and to the best of my knowledge no recent research has been found which uses

a similar strategy. Further investigation into this novel strategy is needed to reduce the errors and improve the efficiency of the system. This is addressed in Chapter 5.

Chapter 5

5 Conclusion and further work

5.1 Conclusion

The aim of this project was to resolve multiple targets as might be required in automotive applications such as collision avoidance. The short comings of existing methods that seek to address this issue were reviewed in Chapter 2. This is a current topic of research. In multi-target automotive contexts each radar target can produce multiple responses. This increases the total number of responses that must be processed within the observation area. The ranges and velocities that arise lead to high ambiguity which increases when multiple targets are present.

A novel method was adopted to detect targets and estimate their range and velocity without ambiguity even in multi-target situations [100], [101]. This method did not apply a threshold to the Fourier power spectrum of the responses to eliminate weaker responses. The novelty of the method adopted lay in using the radar ambiguity function in conjunction with the responses to an FMCW radar waveform and its equation.

Chapter 4 showed the simulation results obtained for each step of processing with this novel strategy. The results demonstrated that target position and velocity can be estimated precisely without ambiguity. No ghost targets were detected when simulating multiple targets with this novel strategy.

Some sources of error that affect the results were identified in Chapter 4. Further work to reduce these errors needs to be performed.

Practical experiments were beyond the scope of this project because further work is needed to refine the computational process and building a practical test system would require substantial effort.

5.2 Further work

The error introduced due to the limitation in the number of ambiguity functions that are considered for intersection with the R-V lines needs to be addressed. It is not appropriate to simply increase the number of ambiguity functions used. This is because the computation of ambiguity function at each position involves the repeated evaluation of the sinc function; this would be computationally burdensome and the volume of data to be held would also be prohibitively large. One approach to solving this problem would be to analyse the ambiguity function equation to identify an expression that would allow the AF plot at each position to be estimated with less computation. This could be achieved through theoretical study to express the ambiguity function in a way that makes explicit the dependence on time delay and Doppler frequency. Another way would be to interpolate ambiguity functions for the intermediate target positions. A method for this is described in Appendix A. The interpolation of the ambiguity functions between positions and with respect to target velocity is computationally less burdensome than the process by which the ambiguity function could be computed.

In addition to reduce the error rate of the reported method, further processing could be performed to yield better results. We know a single target can produce multiple responses, for example, from the body of the vehicle, the engine block and the vehicle body furniture (mirrors, etc.). All these responses would be classified as separate targets by the radar sensors although they are all responses from a single, composite object

target. To correctly recognise these responses as a single target a clustering constraint could be applied to group targets on the basis of proximity and velocity (direction and speed of movement). This is illustrated in Figure 5.1, where the targets within the cluster moving in another direction, shown in red, would be regarded as a ghost target and eliminated.

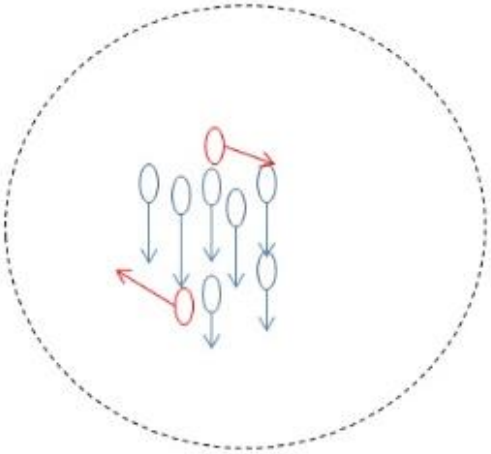

Figure 5.1: Clustering constraint

A temporal constraint could be applied to eliminate the ghost target, as illustrated in Figure 5.2, where the erratic change of position is shown in red. The position and velocity of the target could be tracked in time domain. Targets that changed position or trajectory in an abrupt manner would be eliminated from further consideration as breaking physical constraints for the movement of the objects being detected. Care would be needed to allow for all situations such as an accident involving the target being tracked.

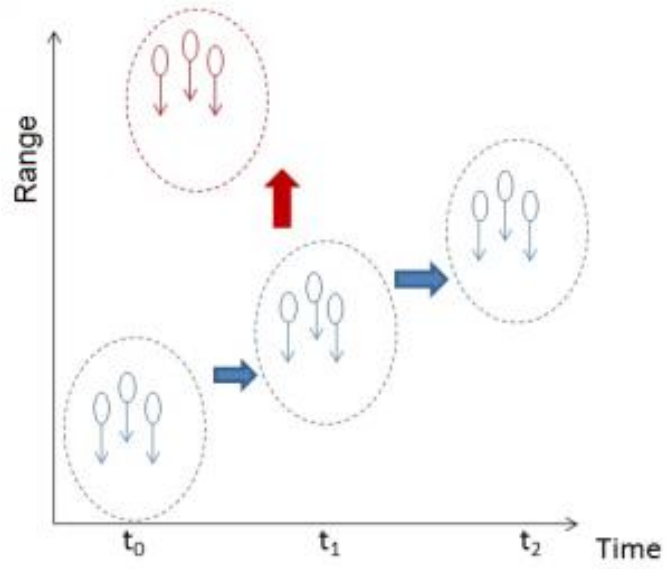

Figure 5.2: Temporal constraint

If all the further research is completed and implemented in the coming few years, automotive industry will see a more useful, effective and robust system for range and velocity detection.

Appendix A

A. Interpolation Method for Ambiguity Function

As the ambiguity function for a target changes with position, it is not feasible to precompute the ambiguity function at all the possible target positions due to its computational complexity. The storage requirment could be reduced by interpolating the ambiguity function from a relatively small set of precomputed ambiguity functions. To the best of my knowledge interpolation of the ambiguity function has not been considered to any depth previously. The method proposed for interpolation of the ambiguity function is described here.

Consider, the physical search space of the target is represented by Figure A.1. Within this search space there can be innumerable ambiguity functions at different target positions. It is impossible to precompute them all. For performance and feasibility reasons, a fair enough number of ambiguity functions have been computed which are used for processing the radar returns. However, if an ambiguity function for a target position which has not been precomputed is required, it can be interpolated using the information we already have.

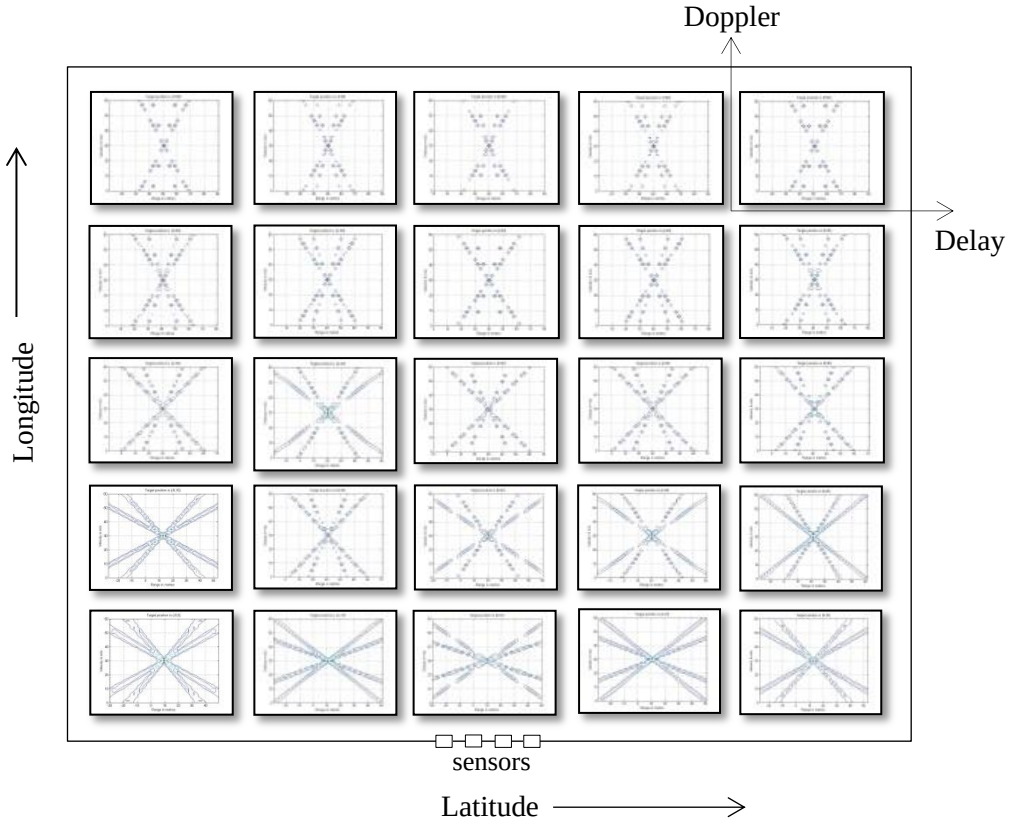

Figure A.1: Physical space and arrangement of radar sensors at the centre.

In Figure A.1, it is made clear that the physical search space has different axes compared to the axes of the amiguity function. The width and the orientation of each arm of the ambiguity function changes with the change in the target position. A direct bilinear interpolation of the ambiguity function without interpolating the ambiguity function arm width and orientation will not give appropriate results in all situations; it fails when the known ambiguity functions used for interpolation are widely spaced in position (and velocity). In such cases the width and orientation of the arms of the ambiguity function cannot be tracked by interpolation. Therefore, the following steps are used to interpolate the ambiguity function at any given target position:

1. Save the arm width and arm angle of known ambiguity functions for a number of target positions.
2. Sample along each arm of the known ambiguity functions and save their ambiguity function values.
3. Repeat step 2 along the width of each arm. Sampling along five lines for each arm width gives appropriate results.
4. Bi-linearly interpolate the arm width and arm angle for any given target position using the information from step 1.
5. Bi-linearly interpolate the ambiguity function value at any given target position using the information in step 2 and 3.
6. Plot the ambiguity function values obtained in step 5 at an arm angle and with an arm width obtained from step 4.

Bi-linear interpolation is a resampling method that uses the distance-weighted average of the four nearest pixel values to estimate a new pixel value. The bi-linear interpolation is actually quadratic rather than linear. It is a product of two linear interpolations. It is shown in Figure A.2.

Given the ambiguity function values at the four coordinates (x_1, y_1), (x_1, y_2), (x_2, y_1) and (x_2, y_2) the ambiguity function values at (x, y) can be found by first interpolating along one axis (x) and then along the other axis (y).

$$AF_{xy1} = \frac{x_2 - x}{x_2 - x_1} AF_{x1y1} + \frac{x_2 - x_1}{x_2 - x_1} AF_{x2y1} \tag{A.1}$$

$$AF_{xy2} = \frac{x_2 - x}{x_2 - x_1} AF_{x1y2} + \frac{x_2 - x_1}{x_2 - x_1} AF_{x2y2} \tag{A.2}$$

$$AF_{xy} = \frac{y_2 - y}{y_2 - y_1} AF_{xy1} + \frac{y_2 - y_1}{y_2 - y_1} AF_{xy2} \tag{A.3}$$

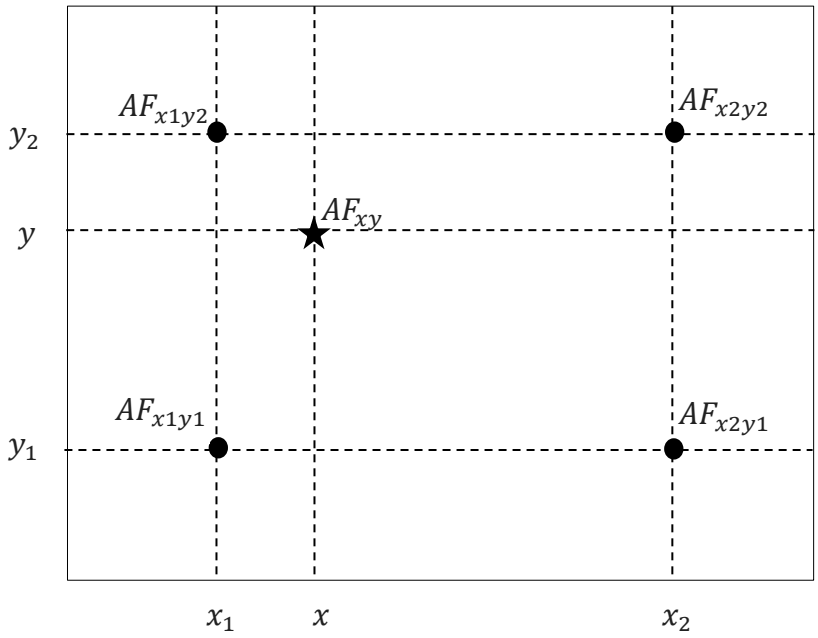

Figure A.2: Bilinear interpolation.

Similarly, the ambiguity function arm widths and orientations can be interpolated. Once all this information has been obtained the ambiguity function at any target position can be plotted using the arm width, arm angle and ambiguity function values at that target position. Figure A.3 compares the ambiguity function plot with its interpolated version.

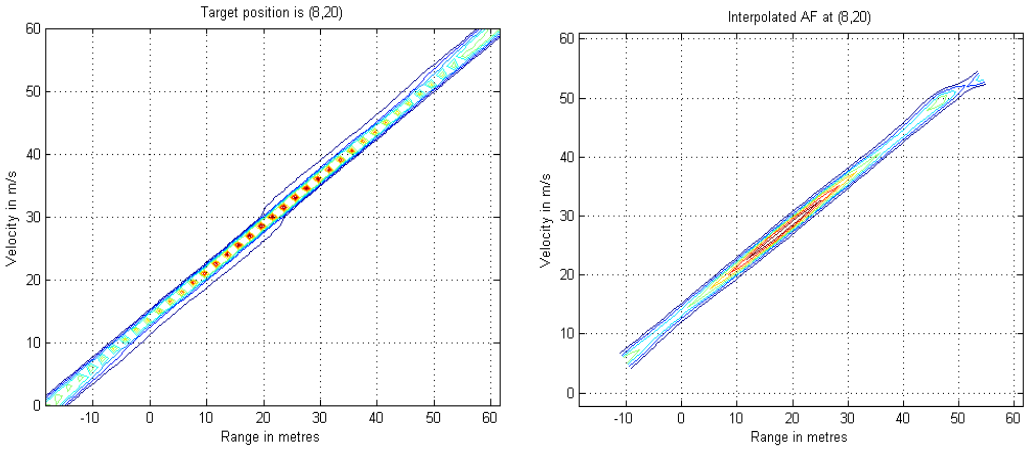

(a) (b)

Figure A.3: Comparison of the ambiguity function plot (a) actual and (b) interpolated.

References

[1] R. Rasshofer and K. Gresser, "Automotive radar and lidar systems for next generation driver assistance functions," *Advances in Radio Science*, vol. 3, pp. 205-209, 2005.

[2] P. Zador, S. Krawchuk, and R. Vocas, "Final Report–Automotive Collision Avoidance (ACAS) Program," Technical Report DOT HS 809 080, NHTSA, US DOT2000.

[3] R. Altendorfer, S. Wirkert, and S. Heinrichs-Bartscher, "Sensor fusion as an enabling technology for safety-critical driver assistance systems," *SAE International Journal of Passenger Cars-Electronic and Electrical Systems,* vol. 3, pp. 183-192, 2010.

[4] R. Mende and H. Rohling, "New automotive applications for smart radar systems," *Smart Microwave Sensors Report, www. smartmicro.de,* 2002.

[5] E. Lissel, H. Rohling, and W. Plagge, "Radar sensor for car applications," in *Vehicular Technology Conference, 1994 IEEE 44th*, 1994, pp. 438-442.

[6] H. Rohling, M.-M. Meinecke, M. Klotz, and R. Mende, "Experiences with an experimental car controlled by a 77 GHz radar sensor," in *International Radar Symposium, IRS98, München*, 1998, pp. 345-354.

[7] M. Klotz and H. Rohling, "A high range resolution radar system network for parking aid applications," in *Radar 99. International conference,* 1999.

[8] M.-M. Meinecke, T.-B. To, and J. Obermann, "A 24 GHz radar-based automotive pre-crash system," in *International Workshop on Intelligent Transportation, Hamburg/Germany*, 2004.

[9] W. Weidmann and D. Steinbuch, "A high resolution radar for short range automotive applications," in *Microwave Conference, 1998. 28th European*, 1998, pp. 590-594.

[10] M. Klotz and H. Rohling, "24 GHz radar sensors for automotive applications," in *13th International Conference on Microwaves, Radar and Wireless Communications. 2000. MIKON-2000.* , 2000, pp. 359-362.

[11] F. Kruse, F. Fölster, M. Ahrholdt, H. Rohling, M.-M. Meinecke, and T.-B. To, "Target classification based on near-distance radar sensors," in *Intelligent Vehicles Symposium, 2004 IEEE*, 2004, pp. 722-727.

[12] R. Zhang, J. Yang, and J. Xiong, "Novel method of parameter estimation for moving target in millimeter-wave short-range linear FMCW radar," in *7th International Conference on Signal Processing, 2004. Proceedings. ICSP'04. 2004* 2004, pp. 1985-1988.

[13] F. Fölster and H. Rohling, "Lateral velocity estimation based on automotive radar sensors," in *International Conference on Radar, 2006. CIE'06.* , 2006, pp. 1-4.

[14] D. Kellner, M. Barjenbruch, K. Dietmayer, J. Klappstein, and J. Dickmann, "Instantaneous lateral velocity estimation of a vehicle using doppler radar," in *16th International Conference on Information Fusion (FUSION), 2013* 2013, pp. 877-884.

[15] M. I. Skolnik, *Radar handbook*: McGraw-Hill, New York, 1970.

[16] J. Hasch, E. Topak, R. Schnabel, T. Zwick, R. Weigel, and C. Waldschmidt, "Millimeter-wave technology for automotive radar sensors in the 77 GHz

frequency band," *Microwave Theory and Techniques, IEEE Transactions on,* vol. 60, pp. 845-860, 2012.

[17] M. Schneider, "Automotive radar–status and trends," in *German microwave conference*, 2005, pp. 144-147.

[18] F. Fölster, H. Rohling, and U. Lübbert, "An automotive radar network based on 77 GHz FMCW sensors," in *Radar Conference, 2005 IEEE International*, 2005, pp. 871-876.

[19] C. Baker and H. Griffiths. (2004, 2 December 2013). *RADAR Systems and Waveforms*. Available: http://radar.det.unifi.it/radar/prin2007/Baker-Radar-Systems-and-Waveforms.pdf

[20] P. M. Woodward, "Radar ambiguity analysis," Technical note 731, Royal Radar Establishment ,Malvern, England, UK 1967.

[21] K. Simon and S. Quegan, "Understanding radar systems," *McGRAW-HILL1992,* 1992.

[22] B. R. Mahafza, *Radar Systems Analysis and Design Using MATLAB*, 2000.

[23] W. David, "Fmcw mmw radar for automotive longitudinal control," *California Partners for Advanced Transit and Highways (PATH),* 1997.

[24] D. G. C. Luck, *Frequency modulated radar*: McGraw-Hill, 1949.

[25] H. Griffiths, "New ideas in FM radar," *Electronics & Communication Engineering Journal*, vol. 2, pp. 185-194, 1990.

[26] A. G. Stove, "Linear FMCW radar techniques," in *IEE Proceedings F (Radar and Signal Processing)*, 1992, pp. 343-350.

[27] Radio frequency integrated circuit. (2004, 20 May 2014). *Radio Detection and Ranging*. Available: http://www.odyseus.nildram.co.uk/Systems_And_Devices_Files/radar_1.pdf

[28] J.-P. Artis and J.-F. Henrio, "Automotive radar development methodology," in *International Conference on Radar Systems, Brest, France*, 1999.

[29] H. Rohling and M.-M. Meinecke, "Waveform design principles for automotive radar systems," in *Radar, 2001 CIE International Conference on, Proceedings*, 2001, pp. 1-4.

[30] H. Rohling and C. Möller, "Radar waveform for automotive radar systems and applications," in *Radar Conference, 2008. RADAR'08. IEEE*, 2008, pp. 1-4.

[31] H. Rohling, "Some radar topics: waveform design, range CFAR and target recognition," in *Advances in Sensing with Security Applications*, ed: Springer, 2006, pp. 293-322.

[32] M.-M. Meinecke and H. Rohling, "Combination of FSK and LFMCW Modulation Principles for Automotive Radars," in *German Radar Symposium GRS*, 2000.

[33] H. Rohling, "Milestones in radar and the success story of automotive radar systems," in *Radar Symposium (IRS), 2010 11th International*, 2010, pp. 1-6.

[34] M. Jankiraman, *Design of multi-frequency CW radars*: SciTech Publishing, 2007.

[35] J. M. Weiss, "Continuous-wave stepped-frequency radar for target ranging and motion detection," in *Proceedings of MICS symposium*, 2009.

[36] A. Kajiwara, "Vehicular stepped-FM coded radar for collision avoidance," in *Vehicular Technology Conference, 1998. VTC 98. 48th IEEE*, 1998, pp. 2085-2089.

[37] M. I. Skolnik, *Introduction to Radar Systems*, 3rd ed.: McGRAW-HILL, 2001.

[38] B. Xin, "Du Jinsong," A new wave for range-velocity decoupling in automotive radar," in *2010 IEEE 2nd International Conference on Signal Processing Systems (ICSPS)*, 2010.

[39] H. Rohling and E. Lissel, "77 GHz radar sensor for car application," in *Radar Conference, 1995., Record of the IEEE 1995 International*, 1995, pp. 373-379.

[40] M. M. Meinecke and H. Rohling, "Waveform Design Principles for Automotive Radar Systems," in *German Radar Symposium*, 2000.

[41] V. Winkler, "Novel Waveform Generation Principle for short-range FMCW-Radars," in *German Microwave Conference, 2009*, 2009, pp. 1-4.

[42] W. K. Saunders, "CW and FM radar," *Radar Handbook*, pp. 16-21, 1990.

[43] A. Stove, "Modern FMCW radar-techniques and applications," in *Radar Conference, 2004. EURAD. First European*, 2004, pp. 149-152.

[44] G. M. Brooker, "Understanding millimetre wave fmcw radars," in *1st International Conference on Sensing Technology*, 2005, pp. 152-157.

[45] H. Rohling, "Radar CFAR thresholding in clutter and multiple target situations," *Aerospace and Electronic Systems, IEEE Transactions on*, pp. 608-621, 1983.

[46] U. Lübbert, "Target Position Estimation with a Continuous Wave Radar Network," Cuvillier Verlag, 2005.

[47] H. Rohling, "25 years Research in Range CFAR Techniques," in *Proc. IRS-2003, Germany*, 2003, pp. 363-368.

[48] R. Stolle and B. Schiek, "Multiple-target frequency-modulated continuous-wave ranging by evaluation of the impulse response phase," *Instrumentation and Measurement, IEEE Transactions on*, vol. 46, pp. 426-429, 1997.

[49] D. Bonacci, C. Mailhes, M. Chabert, and F. Castanié, "The impact of High Resolution Spectral Analysis methods on the performance and design of millimetre wave FMCW radars," *RADAR 2004*, 2004.

[50] I. Santamaria, C. Pantaleon, and J. Ibanez, "A comparative study of high-accuracy frequency estimation methods," *Mechanical Systems and Signal Processing*, vol. 14, pp. 819-834, 2000.

[51] W. Wang, J. Cai, and Y. Yang, "A novel method to identify multi-target by transformable periods LFM waveform," in *2005 International Conference on Communications, Circuits and Systems, 2005. Proceedings.* , 2005.

[52] W. Wang, "An approach for multiple moving targets detection and velocity estimation," in *IEEE Conference on Radar, 2006* 2006, pp. 749-753.

[53] L. Aifang, Z. Xiaohua, L. Jinhui, and L. Zhong, "The ISAR range profile compensation of fast-moving target using the dechirp method," in *Neural Networks and Signal Processing, 2003. Proceedings of the 2003 International Conference on*, 2003, pp. 1619-1623.

[54] V. Winkler, "Range Doppler detection for automotive FMCW radars," in *Microwave Conference, 2007. European*, 2007, pp. 1445-1448.

[55] S. Max, M. Vossiek, and P. Gulden, "Fusion of FMCW secondary radar signal beat frequency and phase estimations for high precision distance measurement," in *Radar Conference, 2008. EuRAD 2008. European*, 2008, pp. 124-127.

[56] S. Ayhan, M. Pauli, T. Kayser, S. Scherr, and T. Zwick, "FMCW radar system with additional phase evaluation for high accuracy range detection," in *European Radar Conference (EuRAD), 2011.*, 2011, pp. 117-120.

[57] E. Hyun, S.-D. Kim, C. Park, and J.-H. Lee, "Automotive FMCW radar with adaptive range resolution," in *2008 Second International Conference on Future Generation Communication and Networking Symposia*, 2008, pp. 130-133.

[58] E. Hyun and J.-H. Lee, "Method to improve range and velocity error using de-interleaving and frequency interpolation for automotive FMCW radars," *International Journal of Signal Processing, Image Processing and Pattern Recognition*, vol. 2, pp. 11-21, 2009.

[59] P. Stoica and R. L. Moses, *Introduction to spectral analysis* vol. 1: Prentice hall, Upper Saddle River NJ, 1997.

[60] M. Mitsumoto, T. Kirimoto, N. Uehara, and S. Inatsune, "FMCW automotive radars using only in-phase channel," SAE Technical Paper 1999.

[61] S. Miyahara, "New algorithm for multiple object detection in FM-CW radar," SAE Technical Paper 2004.

[62] M. Mitsumoto, N. Uehara, S. Inatsune, and T. Kirimoto, "Target distance and velocity measurement algorithm to reduce false targets in FMCW automotive radar," *IEICE transactions on communications*, vol. 83, pp. 1983-1989, 2000.

[63] E. Hyun and J.-H. Lee, "A method for multi-target range and velocity detection in automotive FMCW radar," in *12th International IEEE Conference on Intelligent Transportation Systems (ITSC 2009)*, 2009, pp. 7-11.

[64] E. Hyun, W. Oh, and J.-H. Lee, "Two-step moving target detection algorithm for automotive 77 ghz fmcw radar," in *Vehicular Technology Conference Fall (VTC 2010-Fall), 2010 IEEE 72nd*, 2010, pp. 1-5.

[65] E. Hyun, W. Oh, and J.-H. Lee, "Detection and tracking algorithm for 77Ghz automotive FMCW radar," in *3rd International Asia-Pacific Conference on Synthetic Aperture Radar (APSAR), 2011* 2011, pp. 1-4.

[66] E. Hyun, W. Oh, and J.-H. Lee, "Multi-target detection algorithm for FMCW radar," in *Radar Conference (RADAR), 2012 IEEE*, 2012, pp. 0338-0341.

[67] M. Song, J. Lim, and D.-J. Shin, "The velocity and range detection using the 2D-FFT scheme for automotive radars," in *Network Infrastructure and Digital Content (IC-NIDC), 2014 4th IEEE International Conference on*, 2014, pp. 507-510.

[68] B. Nagarajan, "Time frequency analysis–an application to fmcw radars," Ph. D. dissertation, University of Kansas, 2004.

[69] L. Su, H. S. Wu, and C.-K. C. Tzuang, "2-D FFT and time-frequency analysis techniques for multi-target recognition of FMCW radar signal," in *Microwave Conference Proceedings (APMC), 2011 Asia-Pacific*, 2011, pp. 1390-1393.

[70] N. J. Willis, "Bistatic Radar. Artech House," *Inc., Boston*, 1991.

[71] V. S. Chernyak, *Fundamentals of multisite radar systems: multistatic radars and multistatic radar systems*: CRC Press, 1998.

[72] C. Baker, A. Hume, and C. J. Baker, "Netted radar sensing," *Aerospace and Electronic Systems Magazine, IEEE*, vol. 18, pp. 3-6, 2003.

[73] S. R. Axelsson, "Estimation of target position and velocity using data from multiple radar stations," in *Geoscience and Remote Sensing Symposium, 2003. IGARSS'03. Proceedings. 2003 IEEE International*, 2003, pp. 4140-4143.

[74] C. Baker, "An introduction to multistatic radar," *NATO SET-136 Lecture Series" Multistatic Surveillance and Reconnaissance: Sensor, Signals and Data Fusion,* 2009.

[75] H. Rohling, A. Höß, U. Luebbert, and M. Schiementz, "Multistatic radar principles for automotive radarnet applications," in *2002 Germann Radar Symposium, Bonn, Germany*, 2002.

[76] M. Klotz, "An automotive short range high resolution pulse radar network," PhD dissertation, Department of Telecommunication, Technical University of Hamburg-Harburg, Hamburg, Germany, 2002.

[77] D. Oprişan and H. Rohling, "Tracking systems for automotive radar networks," in *RADAR 2002*, 2002, pp. 339-343.

[78] F. Fölster and H. Rohling, "Data association and tracking for automotive radar networks," *Intelligent Transportation Systems, IEEE Transactions on,* vol. 6, pp. 370-377, 2005.

[79] J. Van Kleef, J. Bergmans, L. Kester, and F. Groen, "Multiple-hypothesis trilateration and tracking with distributed radars," in *9th International Conference on Information Fusion, 2006* 2006, pp. 1-7.

[80] H. Rabe, E. Denicke, G. Armbrecht, T. Musch, and I. Rolfes, "Considerations on radar localization in multi-target environments," *Advances in Radio Science,* vol. 7, pp. 5-10, 2009.

[81] N. Levanon, "Radar principles," *New York, Wiley-Interscience, 1988, 320 p.*, vol. 1, 1988.

[82] N. Levanon and E. Mozeson, *Radar signals*: John Wiley & Sons, 2004.

[83] B. Mahafza, *Radar Systems Analysis and Processing Using MATLAB*: CRC Press, 2009.

[84] T.-C. Tsao, M. Slamani, P. Varshney, D. Weiner, and H. Schwarzlander, "Ambiguity function for a bistatic radar," *Aerospace and Electronic Systems, IEEE Transactions on,* vol. 33, pp. 1041-1051, 1997.

[85] P. Stinco, "Performance analysis of bistatic radar and optimization methodology in multistatic radar system," PhD thesis, University of Pisa, 2012.

[86] D. D. Weiner, M. C. Wicks, and G. T. Capraro, "Waveform diversity and sensors as robots in advanced military systems," in *1st International Waveform Diversity and Design Conference, Edinburgh, UK*, 2004.

[87] H. D. Griffiths and C. J. Baker, "Measurement and analysis of ambiguity functions of passive radar transmissions," in *Radar Conference, 2005 IEEE International*, 2005, pp. 321-325.

[88] I. Bradaric, G. T. Capraro, and M. C. Wicks, "Multistatic ambiguity function-A tool for waveform selection in distributed radar systems," in *Waveform Diversity and Design Conference, 2009 International*, 2009, pp. 40-44.

[89] T. Derham, "The design and calibration of a coherent multistatic radar system," PhD thesis, University College London, 2005.

[90] G. Capraro, I. Bradaric, D. Weiner, R. Day, J. Parretta, and M. Wicks, "Waveform diversity in multistatic radar," in *International Waveform Diversity and Design Conference, Lihue, HI*, 2006, pp. 1-2.

[91] I. Bradaric, G. Capraro, D. Weiner, and M. Wicks, "Multistatic radar systems signal processing," in *IEEE Radar Conference*, 2006, pp. 106-113.

[92] I. Bradaric, G. T. Capraro, M. C. Wicks, and P. Zulch, "Signal processing and waveform selection strategies in multistatic radar systems," in *Waveform Diversity and Design Conference, 2007. International*, 2007, pp. 307-311.

[93] I. Bradaric, G. Capraro, and M. Wicks, "Waveform diversity for different multistatic radar configurations," in *Forty-First Asilomar Conference in Signals, Systems and Computers, 2007. ACSSC 2007 (pp. 2038-2042). IEEE.*, 2007, pp. 2038-2042.

[94] I. Bradaric, G. Capraro, D. Weiner, and M. Wicks, "A framework for the analysis of multistatic radar systems with multiple transmitters," in *International Conference on Electromagnetics in Advanced Applications, ICEAA 2007.*, 2007, pp. 443-446.

[95] G. Capraro, I. Bradaric, and M. Wicks, "Waveform diversity and compatibility," in *General Assembly and Scientific Symposium, 2011 XXXth URSI*, 2011, pp. 1-4.

[96] I. Papoutsis, C. J. Baker, and H. D. Griffiths, "Netted radar and the ambiguity function," in *Radar Conference, 2005 IEEE International*, 2005, pp. 883-888.

[97] M. Adjrad and K. Woodbridge, "Analysis of the multistatic ambiguity function for coherent and incoherent detectors," in *Radar Conference (RADAR), 2011 IEEE*, 2011, pp. 1096-1099.

[98] T. Derham, S. Doughty, C. Baker, and K. Woodbridge, "Ambiguity functions for spatially coherent and incoherent multistatic radar," *Aerospace and Electronic Systems, IEEE Transactions on*, vol. 46, pp. 230-245, 2010.

[99] A. Hoess, "Multifunctional automotive radar network (RadarNet) final report," 2004.

[100] M. Nazir and D. Pycock, "Constraint-based range-velocity disambiguation," in *Radar Symposium (IRS), 2013 14th International*, 2013, pp. 708-713.

[101] M. Nazir and D. Pycock, "A novel strategy for interpreting multiple responses in vehicle radar: A novel consideration of the ambiguity function," in *Computer Science and Electronic Engineering Conference (CEEC), 2013 5th*, 2013, pp. 61-64.